Published for SISSA by Springer

Received: *April 17, 2025*
Revised: *December 31, 2025*
Accepted: *January 28, 2026*
Published: *April 14, 2026*

Combination and interpretation of differential Higgs boson production cross sections in proton-proton collisions at $\sqrt{s} = 13$ TeV

The CMS collaboration

Full author list at the end of the paper

E-mail: cms-publication-committee-chair@cern.ch

Abstract: Precision measurements of Higgs boson differential production cross sections are a key tool to probe the properties of the Higgs boson and test the standard model. New physics can affect both Higgs boson production and decay, leading to deviations from the distributions that are expected in the standard model. In this paper, combined measurements of differential spectra in a fiducial region matching the experimental selections are performed, based on analyses of four Higgs boson decay channels ($\gamma\gamma$, $ZZ^{(*)}$, $WW^{(*)}$, and $\tau\tau$) using proton-proton collision data recorded with the CMS detector at $\sqrt{s} = 13$ TeV, corresponding to an integrated luminosity of 138 fb^{-1}. The differential measurements are extrapolated to the full phase space and combined to provide the differential spectra. A measurement of the total Higgs boson production cross section is also performed using the $\gamma\gamma$ and ZZ decay channels, with a result of $53.4^{+2.9}_{-2.9}\,(\text{stat})^{+1.9}_{-1.8}\,(\text{syst})$ pb, consistent with the standard model prediction of 55.6 ± 2.5 pb. The fiducial measurements are used to compute limits on Higgs boson couplings using the κ-framework and the SM effective field theory.

Keywords: Higgs Production, Higgs Properties, SMEFT

ArXiv ePrint: 2504.13081

https://doi.org/10.1007/JHEP04(2026)093

Contents

1 Introduction

Since the discovery of the Higgs boson (H) by the CMS and ATLAS Collaborations in 2012 [1–3], extensive efforts have been devoted to investigating its properties and couplings, as well as to searching for possible deviations from the standard model (SM) predictions. The Higgs boson is produced in proton-proton (pp) collisions through four main mechanisms: gluon-gluon fusion (ggH), vector boson fusion (qqH), Higgs-strahlung (VH), and Higgs boson production associated with two top quarks ($t\bar{t}H$). Among these, the dominant production mechanism is ggH, which has a production cross section roughly one order of magnitude larger than the other mechanisms combined.

Differential fiducial measurements represent the most model-independent way to measure Higgs boson production cross sections. The term *fiducial* refers to the fact that measurements

JHEP04(2026)093

are performed in a specific region of the phase space, close to the detector acceptance. Whenever we mention differential cross sections in the rest of the paper, we are specifically referring to differential fiducial cross sections. The CMS Collaboration has measured differential Higgs boson production cross sections using data recorded during the years 2016–2018 at $\sqrt{s} = 13\,\text{TeV}$ (corresponding to an integrated luminosity of about $138\,\text{fb}^{-1}$ [4]) in a number of decay channels: $\text{H} \to \gamma\gamma$ [5], $\text{H} \to \text{ZZ}^{(*)} \to 4\ell$ [6], $\text{H} \to \text{WW}^{(*)} \to \text{e}^{\pm}\mu^{\mp}\nu_{\ell}\overline{\nu}_{\ell}$ [7], $\text{H} \to \tau^{+}\tau^{-}$ [8], and boosted $\text{H} \to \tau^{+}\tau^{-}$ [9]. In this paper we present combined measurements of differential cross sections, using the results above as input. The differential spectra are reported for the following observables: the Higgs boson transverse momentum p_{T}^{H}, the number of hadronic jets N_{jets}, the absolute value of the Higgs boson rapidity $|y_{\text{H}}|$, the transverse momentum of the leading hadronic jet $p_{\text{T}}^{\text{j}_1}$, the invariant mass of the dijet system containing the two leading-p_{T} jets m_{jj}, the absolute value of the difference in pseudorapidity between these two jets $|\Delta\eta_{\text{jj}}|$, and the variable $\tau_{\text{C}}^{\text{j}}$, defined in ref. [10], which is the jet p_{T} weighted by a function of its rapidity.

Differential distributions provide information on the Higgs boson couplings. When couplings to quarks, leptons and other bosons differ with respect to their SM values, distortions appear in the predicted differential cross section spectra, particularly noticeable in the p_{T}^{H} distribution.

Information is extracted by fitting parametrized spectra to a combination of differential cross sections in different decay channels. Several frameworks for parametrizing differential spectra exist. Two of these are the κ-framework [11, 12] and the standard model effective field theory (SMEFT) [13]: in the former, couplings are modified at the vertex level by scaling factors κ, while in the latter, the SM is extended by adding higher-dimensional operators to the Lagrangian. These operators may induce Higgs boson couplings with a different Lorentz structure than that present in the SM, and hence modify the kinematical properties of the Higgs boson. Therefore, the SMEFT language is considered more general than the κ-framework.

In the case of the κ-framework, we follow the same procedure as in ref. [14], which provides interpretations using data collected in 2016. The measured p_{T}^{H} spectra are parametrized in terms of Higgs boson couplings, with different sets studied simultaneously:

- the modifier of the Higgs boson coupling to the charm quark κ_{c} and the bottom quark κ_{b};
- the modifier of the Higgs boson coupling to the top quark κ_{t} and the coefficient c_{g} of the anomalous direct coupling to the gluon field in the heavy top mass limit;
- κ_{t} and κ_{b}.

In the context of the SMEFT, CP-even and CP-odd pairs of coefficients are extracted from the p_{T}^{H} and $\Delta\phi_{\text{jj}}$ spectra, the latter being defined as the signed difference in azimuthal angle (in radians) between the two highest p_{T} jets in the event.

In the main interpretation obtained in the SMEFT framework, given the complexity of the fit and the impossibility of constraining all the parameters of the effective theory, a principal component analysis (PCA) is performed to identify sensitive directions of the likelihood

JHEP04(2026)093

function in the parameter space. The linear combinations of the coefficients that have the largest eigenvalues are fitted, and constraints on these linear combinations are reported.

The results presented in this paper, tabulated and provided in the HEPData record for this analysis [15], constitute a step forward in the characterization of the properties of the Higgs boson and in the search for beyond-the-SM (BSM) physics: the combined spectra provide measurements of Higgs boson observables at the highest level of precision presently achievable; the interpretation in the κ-framework extends and improves the results obtained in ref. [14]. Interpretations of Higgs boson differential distributions in the SMEFT have been performed for the first time by the CMS Collaboration, providing complementary information to the results already published in refs. [16, 17].

This paper is organized as follows: Section 2 describes the CMS detector, with the measurements used as input to the combination presented in section 3. The statistical procedure used to combine the measurements and extract the results is described in section 4, and the systematic uncertainties are discussed in section 5. The combined differential spectra and the total Higgs boson production cross section measurement are presented in section 6, with the interpretations of the results in the κ and SMEFT frameworks presented in sections 7 and 8, respectively. Section 9 summarizes the results and presents the conclusions.

2 The CMS detector

The central feature of the CMS apparatus is a superconducting solenoid of 6 m internal diameter, providing a magnetic field of 3.8 T. Within the solenoid volume are a silicon pixel and strip tracker, a lead tungstate crystal electromagnetic calorimeter, and a brass and scintillator hadron calorimeter, each composed of a barrel and two endcap sections. Forward calorimeters extend the pseudorapidity (η) coverage provided by the barrel and endcap detectors. Muons are detected in gas-ionization chambers embedded in the steel flux-return yoke outside the solenoid. A more detailed description of the CMS detector, together with a definition of the coordinate system used and the relevant kinematic variables, can be found in [18].

3 Inputs to the combined analysis

The differential cross section measurements used as input to the combination, mentioned in the introduction, are $\mathrm{H} \to \gamma\gamma$, $\mathrm{H} \to \mathrm{ZZ}^{(*)} \to 4\ell$, $\mathrm{H} \to \mathrm{WW}^{(*)} \to \mathrm{e}^{\pm}\mu^{\mp}\nu_{\ell}\overline{\nu}_{\ell}$, $\mathrm{H} \to \tau^{+}\tau^{-}$, and Lorentz-boosted $\mathrm{H} \to \tau^{+}\tau^{-}$. The ggH production dominates in all the measurements considered. The inclusion of the $\mathrm{H} \to \tau^{+}\tau^{-}$ analyses provides better sensitivity at high $p_{\mathrm{T}}^{\mathrm{H}}$, where the three other channels are less sensitive.

A larger number of observables are measured compared with ref. [14]: $|\Delta\eta_{\mathrm{jj}}|$, m_{jj}, and $\tau_{\mathrm{C}}^{\mathrm{j}}$ are measured in addition to $p_{\mathrm{T}}^{\mathrm{H}}$, N_{jets}, $p_{\mathrm{T}}^{\mathrm{j}_1}$, and $|y_{\mathrm{H}}|$. Tables 1–7 show the bin boundaries used for each observable in each analysis. Table 8 reports the bin boundaries used for $|\Delta\phi_{\mathrm{jj}}|$ ($\mathrm{H} \to \gamma\gamma$, defined as in ref. [5]) and $\Delta\phi_{\mathrm{jj}}$ ($\mathrm{H} \to \mathrm{ZZ}^{(*)} \to 4\ell$, defined as in ref. [6]), which are used only to set limits on Wilson coefficients in the SMEFT interpretation.

JHEP04(2026)093

Each analysis is performed in a different fiducial phase space and applies a different event categorization. The fiducial phase spaces are defined by the selection criteria applied to the particles at generator level (i.e., before detector simulation).

In the $\mathrm{H} \to \gamma\gamma$ measurement [5], the leading (subleading) photon transverse momentum divided by the diphoton mass must be greater than 1/3 (1/4). The total hadronic energy in a cone of radius $\Delta R = 0.3$ around the photon candidate is required to be less than 10 GeV, with the angular distance between two particles i and j defined as $\Delta R(i,j) = \sqrt{(\Delta\eta_{i,j})^2 + (\Delta\phi_{i,j})^2}$, and only photons within $|\eta^{\gamma}| < 2.5$ are accepted.

In the case of $\mathrm{H} \to \mathrm{ZZ}^{(*)} \to 4\ell$ [6], leptons at the fiducial level are considered as *dressed*, i.e., final-state radiation (FSR) photons are collected within $\Delta R = 0.3$ from the lepton, and added to the lepton momentum. In the $\mathrm{H} \to \mathrm{ZZ}^{(*)} \to 4\ell$ analysis, FSR photons are identified by selecting all stable photons and then verifying, in simulation, whether the lepton to which the FSR recovery procedure is applied is a parent of those photons. Electrons (muons) are required to have $p_{\mathrm{T}} > 7$ (5) GeV and $|\eta| < 2.5$ (2.4). Pairs of same-flavor, opposite-charge leptons are used to form Z boson candidates, which are retained if the leading (subleading) dressed lepton has $p_{\mathrm{T}} > 20$ (10) GeV. To ensure the leptons are isolated, the scalar p_{T} sum of all stable particles within a cone of $\Delta R = 0.3$, with the exception of FSR photons and other leptons, must be less than 0.35 times the lepton p_{T}. Events passing these requirements are retained if they have at least two lepton pairs. The lepton pair with invariant mass closest to the true Z boson mass (Z_1) must have $40 < m_{\mathrm{Z}_1} < 120$ GeV. The second Z boson candidate (Z_2) must have $12 < m_{\mathrm{Z}_2} < 120$ GeV. Each lepton pair ℓ_i, ℓ_j must be separated by $\Delta R(\ell_i, \ell_j) > 0.02$, while any opposite-charge lepton pair must have $m_{\ell^+\ell'^-} > 4$ GeV.

In the case of $\mathrm{H} \to \mathrm{WW}^{(*)} \to \mathrm{e}^{\pm}\mu^{\mp}\nu_{\ell}\bar{\nu}_{\ell}$ [7], the leptons are dressed and must be either electrons or muons with opposite charge and $|\eta| < 2.5$ (2.4) for electrons (muons). The leading (subleading) lepton is required to have $p_{\mathrm{T}}^{\ell_1} > 25$ GeV ($p_{\mathrm{T}}^{\ell_2} > 13$ GeV). The dilepton system is required to have $m^{\ell\ell} > 12$ GeV and $p_{\mathrm{T}}^{\ell\ell} > 30$ GeV. Furthermore, the transverse mass of the subleading lepton must be $m_{\mathrm{T}}^{l_2} > 30$ GeV and the Higgs boson transverse mass must be greater than 60 GeV. Both these quantities are defined in ref. [7].

Electrons and muons are also dressed in the $\mathrm{H} \to \tau^+\tau^-$ analysis [8, 9]. In the $\mathrm{e}\tau_{\mathrm{h}}$ ($\mu\tau_{\mathrm{h}}$) final state, where τ_{h} denotes a hadronically decaying τ lepton, the electron (muon) is required to have $p_{\mathrm{T}} > 25$ (20) GeV and $|\eta| < 2.1$. The τ_{h} candidate must have a *visible* $p_{\mathrm{T}} > 30$ GeV and visible $|\eta| < 2.3$. Here, the term visible refers to the kinematic variables constructed from the momenta of the visible decay products of the τ leptons, thus excluding neutrinos. In addition, the transverse mass $m_{\mathrm{T}}(\mathrm{e}/\mu, \vec{p}_{\mathrm{T}}^{\,\mathrm{miss}})$, with $\vec{p}_{\mathrm{T}}^{\,\mathrm{miss}}$ computed by summing the p_{T} of the neutrinos, must be less than 50 GeV.

In the $\tau_{\mathrm{h}}\tau_{\mathrm{h}}$ final state, the visible p_{T} of both τ_{h} candidates must exceed 40 GeV, while their visible $|\eta|$ must be less than 2.1, and there must be at least one jet with $p_{\mathrm{T}} > 30$ GeV. In the $\mathrm{e}\mu$ final state, the leading (subleading) lepton must have $p_{\mathrm{T}} > 24$ (15) GeV, both leptons must have $|\eta| < 2.4$, and the m_{T} of the dilepton system and $\vec{p}_{\mathrm{T}}^{\,\mathrm{miss}}$ must be below 60 GeV.

SM predictions for the four main Higgs boson production modes (ggH, qqH, VH, $\mathrm{t\bar{t}H}$) are generated following the procedure described in ref. [5], using MadGraph5_aMC@NLO (version 2.6.5) at next-to-leading order (NLO) accuracy of the strong coupling constant α_{S} in perturbative quantum chromodynamics (QCD).

JHEP04(2026)093

Channel	$H \to \gamma\gamma$	$H \to ZZ^{(*)} \to 4\ell$	$H \to WW^{(*)} \to e^{\pm}\mu^{\mp}\nu_{\ell}\bar{\nu}_{\ell}$	$H \to \tau^{+}\tau^{-}$	$H \to \tau^{+}\tau^{-}$ boosted
p_{T}^{H} bin boundaries (GeV)	0–5	0–10	0–30	0–45	
	5–10				
	10–15	10–20			
	15–20				
	20–25	20–30			
	25–30				
	30–35	30–45	30–45		
	35–45				
	45–60	45–60	45–80	45–80	
	60–80	60–80			
	80–100	80–120	80–120	80–120	
	100–120				
	120–140			120–140	
	140–170	120–200	120–200	140–170	
	170–200			170–200	
	200–250			200–350	
	250–350				
	350–450	200–∞	200–∞	350–450	
	450–∞			450–∞	450–600
					600–∞

Table 1. The p_{T}^{H} bin boundaries used in the analyses that are input to the combination.

Channel	N_{jets} bins				
$H \to \gamma\gamma$	0	1	2	3	≥ 4
$H \to ZZ^{(*)} \to 4\ell$	0	1	2	3	≥ 4
$H \to WW^{(*)} \to e^{\pm}\mu^{\mp}\nu_{\ell}\bar{\nu}_{\ell}$	0	1	2	3	≥ 4
$H \to \tau^{+}\tau^{-}$	0	1	2	3	≥ 4

Table 2. The N_{jets} bins used in the analyses that are input to the combination.

Channel	$p_{T}^{j_1}$ bin boundaries (GeV)								
$H \to \gamma\gamma$	30–40	40–55	55–75	75–95	95–120	120–150	150–200	200–∞	
$H \to ZZ^{(*)} \to 4\ell$	30–55		55–95			95–200		200–∞	
$H \to \tau^{+}\tau^{-}$ boosted								450–600	600–∞

Table 3. The $p_{T}^{j_1}$ bin boundaries used in the analyses that are input to the combination.

Channel	$\lvert y_H \rvert$ bin boundaries (GeV)									
$H \to \gamma\gamma$	0.0–0.15	0.15–0.3	0.3–0.45	0.45–0.6	0.6–0.75	0.75–0.9	0.9–1.2	1.2–1.6	1.6–2.0	2.0–2.5
$H \to ZZ^{(*)} \to 4\ell$	0.0–0.15	0.15–0.3	0.3–0.45	0.45–0.6	0.6–0.75	0.75–0.9	0.9–1.2	1.2–1.6	1.6–2.5	

Table 4. The $|y_H|$ bin boundaries used in the analyses that are input to the combination.

JHEP04(2026)093

Channel	$\lvert\Delta\eta_{jj}\rvert$ bin boundaries				
$H \to \gamma\gamma$	0.0–0.7	0.7–1.6	1.6–3.0	3.0–5.0	5.0–∞
$H \to ZZ^{(*)} \to 4\ell$	0.0–1.6		1.6–3.0	3.0–∞	

Table 5. The $|\Delta\eta_{jj}|$ bin boundaries used in the analyses that are input to the combination.

Channel	m_{jj} bin boundaries (GeV)						
$H \to \gamma\gamma$	0–75	75–120	120–180	180–300	300–500	500–1000	1000–∞
$H \to ZZ^{(*)} \to 4\ell$	0–120		120–300			300–∞	

Table 6. The m_{jj} bin boundaries used in the analyses that are input to the combination.

Channel	τ_C^j bin boundaries				
$H \to \gamma\gamma$	15–20	20–30	30–50	50–80	80–∞
$H \to ZZ^{(*)} \to 4\ell$	15–20	20–30	30–50	50–80	80–∞

Table 7. The τ_C^j bin boundaries used in the analyses that are input to the combination.

Channel	$\lvert\Delta\phi_{jj}\rvert$, $\Delta\phi_{jj}$ bin boundaries					
$H \to \gamma\gamma$	0–0.5	0.5–0.9	0.9–1.3	1.3–1.7	1.7–2.5	2.5–π
$H \to ZZ^{(*)} \to 4\ell$	$(-\pi)$–$(-\pi/2)$	$(-\pi/2)$–0	0–$(\pi/2)$		$(\pi/2)$–π	

Table 8. The $|\Delta\phi_{jj}|$ ($H \to \gamma\gamma$, ref. [5]) and $\Delta\phi_{jj}$ ($H \to ZZ^{(*)} \to 4\ell$, ref. [6]) bin boundaries, used to set constraints on Wilson coefficients.

4 Statistical analysis

The parameters of interest are estimated through a simultaneous extended maximum likelihood fit in all the analysis categories of the following distributions:

- diphoton invariant mass in $H \to \gamma\gamma$;
- four-lepton invariant mass in $H \to ZZ^{(*)} \to 4\ell$;
- two-dimensional dilepton invariant mass and transverse mass in $H \to WW^{(*)} \to e^{\pm}\mu^{\mp}\nu_\ell\overline{\nu}_\ell$;
- di-τ invariant mass in $H \to \tau^+\tau^-$;
- output of the neural network used to distinguish signal from backgrounds in boosted $H \to \tau^+\tau^-$.

The numbers of expected events n^{exp} in a given reconstructed kinematic bin i, analysis category k, and decay channel m is written as:

$$n_i^{\text{exp},km}(\vec{\mu} \mid \vec{\nu}, \vec{\nu_{\text{th}}}) = n_i^{\text{sig},km}(\vec{\mu} \mid \vec{\nu}, \vec{\nu_{\text{th}}}) + n_i^{\text{bkg},km}(\vec{\nu}, \vec{\nu_{\text{th}}}), \tag{4.1}$$

JHEP04(2026)093

where $n_i^{\text{sig},\,km}$ and $n_i^{\text{bkg},\,km}$ are the expected number of signal and background events, respectively.

The signal component $n_i^{\text{sig},\,km}$ is explicitly written as:

$$n_i^{\text{sig},km}(\vec{\mu} \mid \vec{\nu}, \vec{\nu_{\text{th}}}) = \sum_{j=1}^{n_{\text{bins},k}^{\text{gen}}} \mu_j \sigma_j^{\text{SM}}(\vec{\nu_{\text{th}}}) A_j^{\text{SM},km}(\vec{\nu_{\text{th}}}) \varepsilon_{ji}^{\text{SM},km}(\vec{\nu}) L(\vec{\nu}) \mathcal{B}^{\text{SM},m}(\vec{\nu_{\text{th}}}) + n_{\text{OOA},i}^{km}(\vec{\nu}, \vec{\nu_{\text{th}}}), \tag{4.2}$$

where:

- $\vec{\mu}$ is the set of signal strength modifiers;
- $\vec{\nu}$ is the set of nuisance parameters associated with experimental uncertainties;
- $\vec{\nu_{\text{th}}}$ is the set of nuisance parameters associated with theoretical uncertainties;
- j is the index of a kinematic bin at the generator level;
- $n_{\text{bins},k}^{\text{gen}}$ is the number of bins at the generator level in analysis category k; for some observables (such as N_{jets}) it is the same for all decay channels, while this changes for other observables (such as p_{T}^{H});
- σ_j^{SM} is the SM cross section in generator-level bin j;
- $A_j^{\text{SM},km}$ is the SM expectation for the fiducial acceptance (fraction of the events in the fiducial region) in generator-level bin j for decay channel m and analysis category k;
- $\varepsilon_{ji}^{\text{SM},km}(\vec{\nu})$ is the efficiency with which events in generator-level bin j are reconstructed in the reconstructed bin i;
- L is the integrated luminosity of the data sets used in the analyses;
- $\mathcal{B}^{\text{SM},m}$ is the SM expectation for the branching fraction of the decay channel m;
- $n_{\text{OOA},i}^{km}$ is the number of events that originate from outside the fiducial region but are reconstructed within it.

Bin-to-bin migrations due to detector resolution effects are taken into account via a folding matrix. When performing the fits in the individual analyses, extracting the production cross sections in the corresponding fiducial phase space, the signal strength modifiers are defined as

$$\mu = \frac{\sigma \mathcal{B} A}{\sigma^{\text{SM}} \mathcal{B}^{\text{SM}} A^{\text{SM}}}, \tag{4.3}$$

where the indices of the quantities are omitted for simplicity. When performing combined fits, however, the cross sections in each decay channel are extrapolated to the full phase space, and the signal strength modifiers are defined as:

$$\mu = \frac{\sigma}{\sigma^{\text{SM}}}. \tag{4.4}$$

JHEP04(2026)093

It should be noted that the extrapolation procedure introduces theoretical uncertainties and an unavoidable model dependence in the results [19].

Using the terminology introduced in ref. [20], which we refer to for more details, this combination includes both parametric and template-based statistical models. Given a statistical model and a data set, a likelihood function is written as the product of the primary and auxiliary likelihoods, where $\mathcal{L}_{\text{primary}}$ is proportional to the probability of observing the event count in data for a given set of model parameters and $\mathcal{L}_{\text{auxiliary}}$ represents external constraints on the nuisance parameters. For the template-based models, the likelihood is written as

$$\mathcal{L} = \mathcal{L}_{\text{primary}}\,\mathcal{L}_{\text{auxiliary}} = \prod_{c=1}^{N_c}\prod_{b=1}^{N_b^c} \text{Pois}\left(n_{cb}; n_{cb}^{\text{exp}}(\vec{\mu},\vec{\nu})\right) \prod_{e=1}^{N_E} p_e\left(y_e;\nu_e\right), \tag{4.5}$$

where c runs over the channels, b over the bins, and e over the auxiliary measurements; N_c is the number of channels, N_b^c is the number of bins in channel c, N_E is the number of auxiliary measurements, n_{cb} is the observed number of events in bin b of channel c, n_{cb}^{exp} is the expected number of events in the same bin, y_e is the value of the auxiliary measurement e, and ν_e is the corresponding nuisance parameter. For parametric models, the (unbinned) likelihood is written as

$$\begin{aligned}\mathcal{L} &= \mathcal{L}_{\text{primary}}\,\mathcal{L}_{\text{auxiliary}} \\ &= \left(\prod_c \text{Pois}\left(n_{c,\,\text{tot}}^{\text{obs}}\,; n_{c,\,\text{tot}}^{\text{exp}}\,(\vec{\mu},\vec{\nu})\right) \prod_i^{n_{\text{bs}}^{\text{obs}}} \sum_p f_{cp}^{\text{exp}}\,\text{pdf}_{cp}\left(\vec{x}_i;\vec{\mu},\vec{\nu}\right)\right) \prod_e^{N_E} p_e\left(y_e;\nu_e\right),\end{aligned} \tag{4.6}$$

where c runs over the channels (as in the binned case), i runs over the events, $n_{c,\,\text{tot}}^{\text{exp}}$ is the total number of expected events in channel c, pdf_{cp} is the probability density function of the process p in channel c, and f_{cp}^{exp} is the fraction of the total number of expected events in channel c that originate from process p, $f_{cp} = n_{cp}/\sum_p n_{cp}$. It should be noted that, in the case of parametric models, the likelihood function can be either binned or unbinned.

When combining the likelihoods from different analyses, the likelihood function is the product of the likelihood functions of the individual analyses, both binned and unbinned:

$$\mathcal{L}_{\text{combined}} = \mathcal{L}_{\text{primary}}\,\mathcal{L}_{\text{auxiliary}} = \left(\prod_{c_{\text{template}}} \mathcal{L}_{\text{primary}}^{c_{\text{template}}}\right)\left(\prod_{c_{\text{parametric}}} \mathcal{L}_{\text{primary}}^{c_{\text{parametric}}}\right)\mathcal{L}_{\text{auxiliary}}\,, \tag{4.7}$$

where c_{template} runs over the analyses that adopt template-based models (i.e., $\text{H} \to \text{WW}^{(*)} \to \text{e}^{\pm}\mu^{\mp}\nu_\ell\bar{\nu}_\ell$, $\text{H} \to \tau^+\tau^-$, and boosted $\text{H} \to \tau^+\tau^-$), and $c_{\text{parametric}}$ runs over the analyses that adopt parametric models (i.e., $\text{H} \to \gamma\gamma$ and $\text{H} \to \text{ZZ}^{(*)} \to 4\ell$).

The test statistic q is defined as

$$q(\vec{\mu}) = -2\ln\left(\frac{\mathcal{L}\left(\vec{\mu} \mid \hat{\hat{\nu}}_{\vec{\mu}}\right)}{\mathcal{L}(\hat{\vec{\mu}} \mid \hat{\vec{\nu}})}\right) \tag{4.8}$$

and is used to set confidence intervals on the signal strength modifiers μ [20]. The quantities $\hat{\vec{\mu}}$ and $\hat{\vec{\nu}}$ are the unconditional maximum likelihood estimates for the parameters $\vec{\mu}$ and

JHEP04(2026)093

$\vec{\nu}$, respectively, while $\hat{\vec{\nu}}_{\vec{\mu}}$ denotes the maximum likelihood estimate for $\vec{\nu}$ conditional on the values of $\vec{\mu}$.

5 Systematic uncertainties

The experimental systematic uncertainties from the input analyses are incorporated in the combination as nuisance parameters, which are profiled in the maximum likelihood fit. Detailed descriptions of the systematic uncertainties can be found in the papers describing the individual analyses [5–8]. Systematic uncertainties that affect different decay channels are correlated when building the likelihood function: this happens for the integrated luminosity, pileup, jet energy scale and resolution, and b tagging uncertainties. Some analyses employ a more detailed nuisance parameter scheme (e.g., different nuisance parameters for different eras, final states, etc.); in this case the uncertainties are not correlated between the input analyses. This happens in the case of the τ energy scales and lepton efficiencies, including electrons, muons, and hadronic taus.

Since the combined spectra are extrapolated to the full phase space, studies have been performed to assess the impact of scale and parton distribution function (PDF) variations on the acceptance of each observable and decay channel. Scale variations show a nonnegligible impact on the acceptance in most of the observables and decay channels. Therefore, two additional nuisance parameters are introduced in the combined fit to account for the renormalization and factorization scale uncertainties in the extrapolation to the full phase space. The probability density function of the number of expected events as a function of these parameters is an asymmetric log-normal distribution with the $+1\sigma$ (-1σ) variation obtained by taking the ratio between the acceptance computed with a scale parameter of 2 (0.5) and the nominal acceptance (scale parameter equal to 1). When the renormalization scale is varied, the factorization scale is set to 1 and vice versa. These additional uncertainties are also correlated across all decay channels. In the case of PDF variations, the impact on the acceptance is negligible and no additional nuisance parameters are introduced.

In the interpretation using the κ-framework, theoretical uncertainties are implemented following the procedure described in ref. [14]. Since only the ggH contribution is parametrized, the other contributions are set to their SM predictions. A 2.1% uncertainty, determined in ref. [19], is applied to all contributions other than ggH.

6 Combination of differential spectra and total cross section measurement

In this section we present the combined unfolded differential cross section measurements for the observables $p_{\mathrm{T}}^{\mathrm{H}}$, $p_{\mathrm{T}}^{\mathrm{j}_1}$, N_{jets}, $|y_{\mathrm{H}}|$, $|\Delta\eta_{\mathrm{jj}}|$, m_{jj}, and $\tau_{\mathrm{C}}^{\mathrm{j}}$. The differential cross section measurements are performed by assigning a parameter of interest μ to scale predictions for each generator-level bin, as discussed in section 4. The difference in generator-level binning and, therefore, the difference in the number of parameters of interest across the channels entering the combination, are accounted for with the following procedure. First, a set of bins in which measurements are provided is chosen. The binning of the $\mathrm{H} \to \gamma\gamma$ analysis is employed for this (see tables 1–7), as this provides better sensitivity to various regions of the differential phase space. Then, the contributions of processes that have a coarser

JHEP04(2026)093

binning at the generator level are rescaled with a linear combination of the finer parameters of interest contained in the coarser bin. The weights used in this rescaling are the ratio of the SM cross section in each bin to the sum over bins. As an example, one can consider the bins at very low $p_{\mathrm{T}}^{\mathrm{H}}$: the choice of parameters of interest is (μ_{0-5}, μ_{5-10}), as in the $\mathrm{H} \to \gamma\gamma$ measurement. In the $\mathrm{H} \to \mathrm{ZZ}^{(*)} \to 4\ell$ analysis, only one generator-level bin is used in the range 0–10 GeV. A weighted sum of the chosen parameters of interest is needed to scale this bin in the $\mathrm{H} \to \mathrm{ZZ}^{(*)} \to 4\ell$ analysis:

$$\mu_{0-10}^{ZZ} = w_{0-5}\mu_{0-5} + w_{5-10}\mu_{5-10}. \tag{6.1}$$

The weights do not include the contributions of efficiency and acceptance, which are assumed not to vary within the bin. Tests have been performed to assess the validity of this assumption. In particular, the deviation from a constant acceptance has been tested in the 0–45 GeV bin of the $p_{\mathrm{T}}^{\mathrm{H}}$ spectrum in the $\mathrm{H} \to \tau^{+}\tau^{-}$ analysis, which includes nine generator-level bins. For all the bins, the deviation from a constant acceptance is less than 2%.

The unfolded differential cross sections for the observables $p_{\mathrm{T}}^{\mathrm{H}}$, $p_{\mathrm{T}}^{\mathrm{j}_1}$, N_{jets}, $|y_{\mathrm{H}}|$, $|\Delta\eta_{\mathrm{jj}}|$, m_{jj}, and $\tau_{\mathrm{C}}^{\mathrm{j}}$ are shown in figures 1 and 2. Numerical results are given in tables 11–17, available in appendix A. The correlation matrices for the unfolded differential cross sections are shown in figures 16 and 17, appendix B. Each figure compares the measurement with three theoretical predictions. The predicted cross section for the ggH production mode is taken from the MadGraph5_aMC@NLO (version 2.6.5) simulation, generated at NLO accuracy, and the POWHEG (version 2) event generator [21–24]. The events produced with MadGraph5_aMC@NLO are weighted as a function of the Higgs boson p_{T} and the number of jets in the event, to match the prediction from the next-to-NLO including parton showering event generator (NNLOPS) program [25–27]. The sum of the production cross sections of the other (non-ggH) production modes is taken from the MadGraph5_aMC@NLO (version 2.6.5) simulation; this non-ggH prediction is common to the different SM calculations that are shown. The uncertainty in the theoretical predictions takes into account variations in the predicted differential cross section spectra from varying the set of PDF replicas, the renormalization and factorization scales, and α_{S}. The uncertainty on the total cross section value, taken from ref. [19], is included by summing it in quadrature with the shape uncertainties. Overall, no significant deviations from the SM predictions are observed. For all the measurements, nuisance parameters are introduced to account for the scale variations in the acceptance for the extrapolation to the full phase space, as described in section 5. Statistical uncertainties form the dominant source of uncertainty at low p_{T} in the $p_{\mathrm{T}}^{\mathrm{H}}$ measurement, while at high p_{T} the statistical and systematic uncertainties are comparable. In the case of the N_{jets} measurement, systematic uncertainties dominate, while for the other spectra the statistical uncertainties are the most important. It should be noted that the differential cross section measurements are not defined to be positive in every bin, and negative values can occur as a result of small event samples and possible anticorrelations between bins.

The same spectra, along with the measurements from the individual channels, are shown in figures 3 and 4. In the case of the $p_{\mathrm{T}}^{\mathrm{H}}$ spectrum (figure 3, upper left), the sensitivity is driven by the $\mathrm{H} \to \gamma\gamma$ and $\mathrm{H} \to \mathrm{ZZ}^{(*)} \to 4\ell$ analyses. A comparison with the $\mathrm{H} \to \gamma\gamma$ measurement alone shows that the decrease in uncertainty achieved by the combination is

JHEP04(2026)093

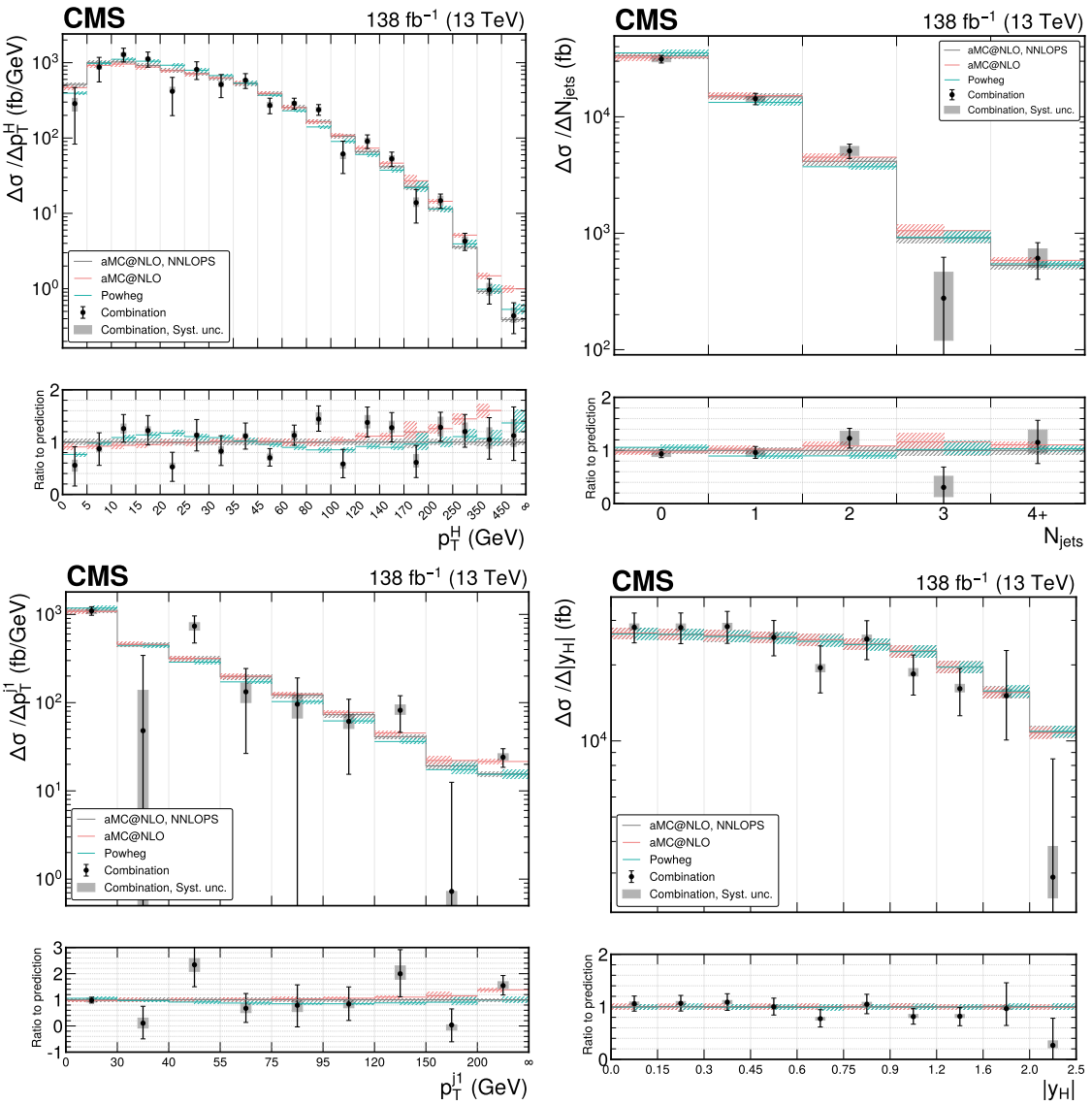

Figure 1. Measurement of the total differential cross section as a function of $p_{\mathrm{T}}^{\mathrm{H}}$ (upper left), N_{jets} (upper right), $p_{\mathrm{T}}^{\mathrm{j}_1}$ (lower left), and $|y_{\mathrm{H}}|$ (lower right). For $p_{\mathrm{T}}^{\mathrm{j}_1}$, the first bin comprises all events with less than one jet, for which $p_{\mathrm{T}}^{\mathrm{j}_1}$ is undefined. The combined spectrum is shown as black points with error bars indicating the 68% confidence interval. The systematic component of the uncertainty is shown in gray. The SM prediction is reported for different generators. The hatched areas show the uncertainties in the shapes of the theoretical predictions from varying the PDFs, the value of α_{S}, and the renormalization and factorization scales. The uncertainty on the total cross section value, taken from ref. [19], is also included in the hatched areas by summing it in quadrature with the shape uncertainties. In the case of $p_{\mathrm{T}}^{\mathrm{H}}$ and $p_{\mathrm{T}}^{\mathrm{j}_1}$, the rightmost bins of the distributions are overflow bins, and their width is assumed equal to the last but one bin when computing the differential cross section. In cases where the systematic uncertainty band covers only one side of the data point, the systematic uncertainty on the other side is negligible. The ratio between the measurements and the MadGraph5_aMC@NLO NNLOPS-reweighted SM predictions is shown in the lower panel of each plot.

JHEP04(2026)093

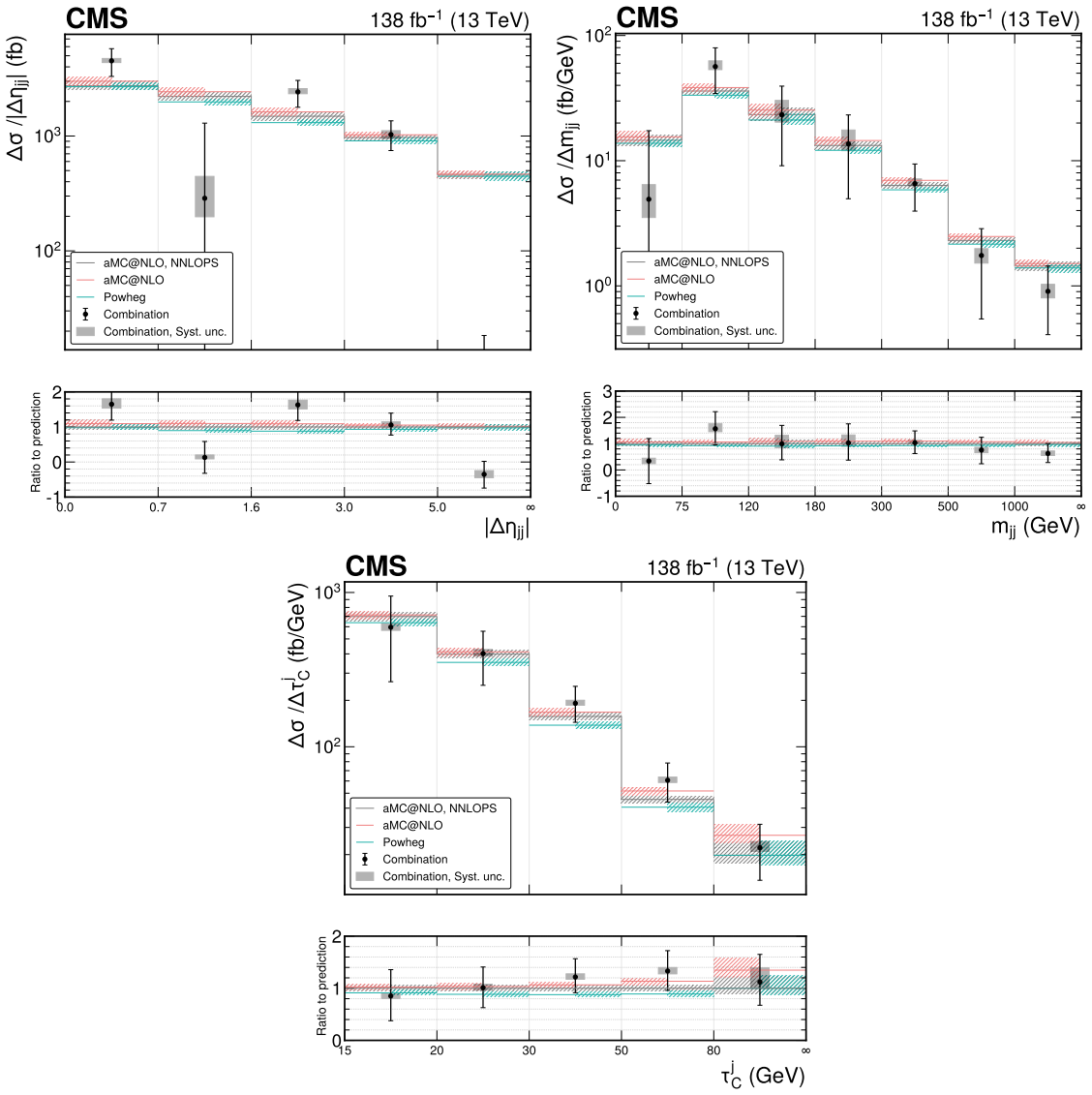

Figure 2. Measurement of the total differential cross section as a function of $|\Delta\eta_{jj}|$ (upper left), m_{jj} (upper right), and τ_C^j (lower). The combined spectrum is shown as black points with error bars indicating the 68% confidence interval. The systematic component of the uncertainty is shown in gray. The SM prediction is reported for different generators. The hatched areas show the uncertainties in the shape of the theoretical predictions from varying the PDFs, the value of α_S, and the renormalization and factorization scales. The uncertainty on the total cross section value, taken from ref. [19], is also included in the hatched areas by summing it in quadrature with the shape uncertainties. The rightmost bins of the distributions are overflow bins, and their width is assumed equal to the last but one bin when computing the differential cross section. The ratio between the measurements and the MadGraph5_aMC@NLO NNLOPS-reweighted SM predictions is shown in the lower panel of each plot.

JHEP04(2026)093

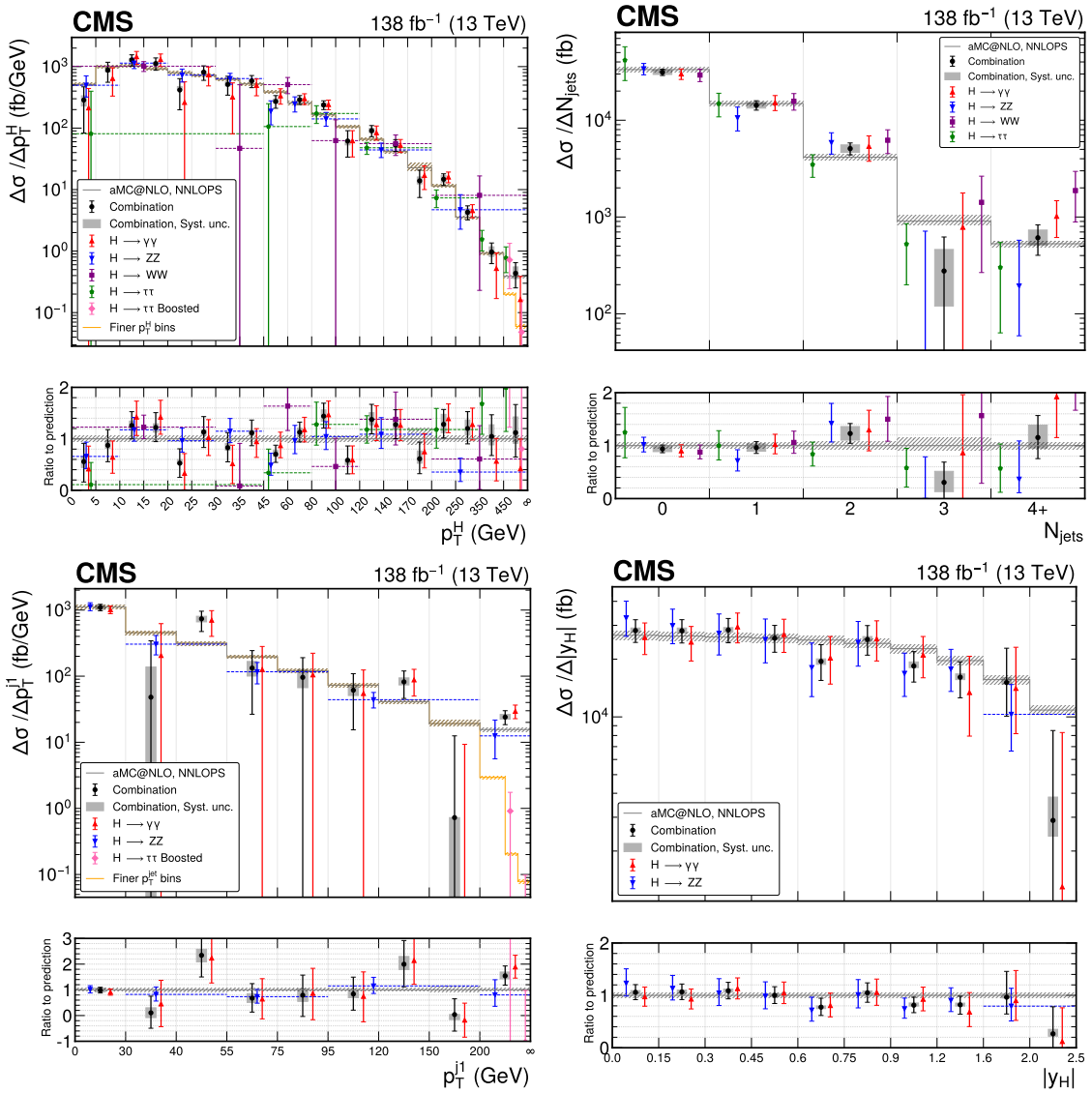

Figure 3. Measurement of the total differential cross section as a function of p_T^H (upper left), N_{jets} (upper right), $p_T^{j_1}$ (lower left), and $|y_H|$ (lower right). The combined spectrum is shown in black points with error bars indicating the 68% interval. The systematic component of the uncertainty is shown in gray. The spectra for the analyses in $H \to \gamma\gamma$, $H \to ZZ^{(*)} \to 4\ell$, $H \to WW^{(*)} \to e^{\pm}\mu^{\mp}\nu_\ell\bar{\nu}_\ell$, $H \to \tau^+\tau^-$, and $H \to \tau^+\tau^-$ boosted are shown in red, blue, purple, green, and pink respectively. The SM prediction is reported in light gray for MadGraph5_aMC@NLO NNLOPS. In the case of p_T^H and $p_T^{j_1}$, the rightmost bins of the distributions are overflow bins, and their width is assumed equal to the last but one bin when computing the differential cross section. Measurements or predictions with different binnings can be directly compared only in the ratio panels of the figures. In cases where individual contributions have finer bins than the combination, such as the last bin of the p_T^H and $p_T^{j_1}$ spectra, a second, finer, SM prediction is shown in the upper panel.

most notable in the very low and very high p_T^H regions, with an average reduction of 23%. In four out of the nineteen bins, the relative uncertainty does not decrease with respect to the $H \to \gamma\gamma$ measurement alone.

JHEP04(2026)093

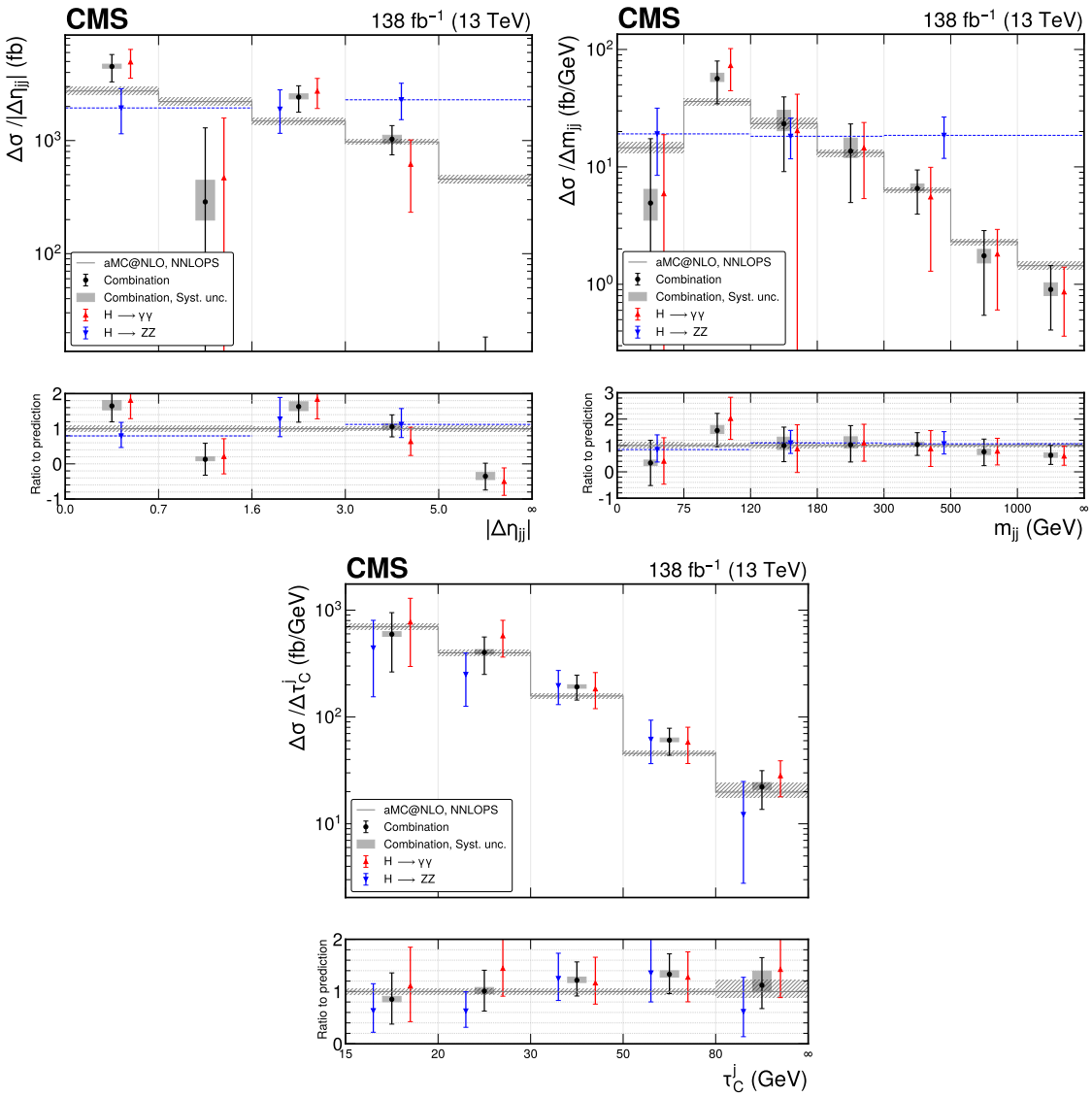

Figure 4. Measurement of the total differential cross section as a function of $|\Delta\eta_{jj}|$ (upper left), m_{jj} (upper right), and τ_C^j (lower). The combined spectrum is shown in black points with error bars indicating the 68% interval. The systematic component of the uncertainty is shown in gray. The spectra for the analyses in $H \to \gamma\gamma$ and $H \to ZZ^{(*)} \to 4\ell$ are shown in red and blue, respectively. The SM prediction is reported in light gray for MadGraph5_aMC@NLO NNLOPS. The rightmost bins of the distributions are overflow bins, and their width is assumed equal to the last but one bin when computing the differential cross section. Measurements or predictions with different binnings can be directly compared only in the ratio panels of the figures.

JHEP04(2026)093

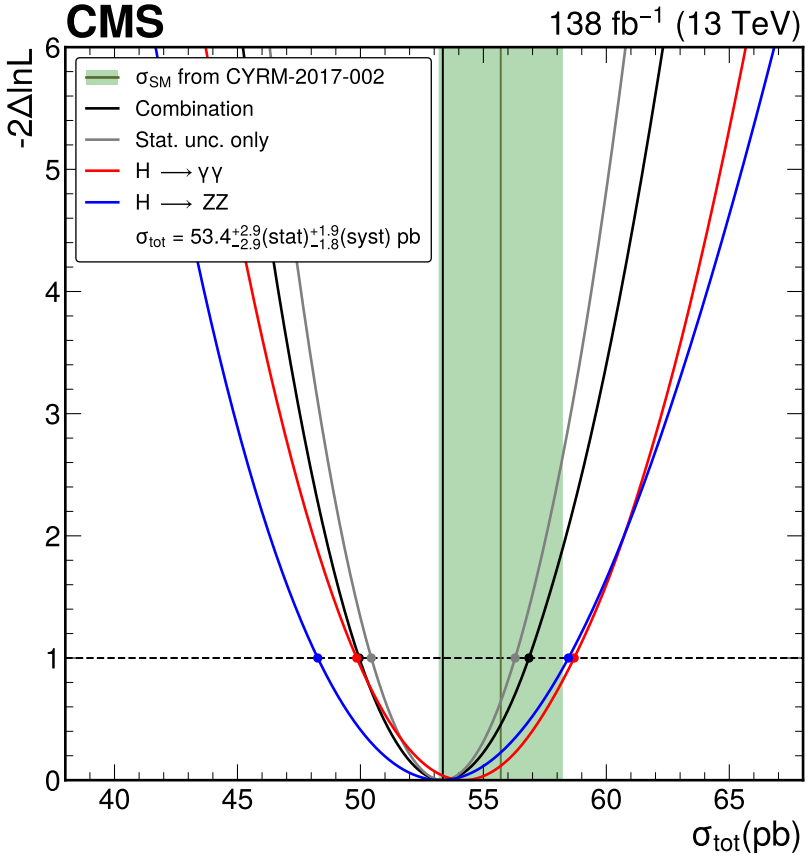

Figure 5. Negative log-likelihood scan of the total Higgs boson production cross section σ_{tot} for the $\mathrm{H} \to \gamma\gamma$, $\mathrm{H} \to \mathrm{ZZ}^{(*)} \to 4\ell$, and combined analyses. The markers indicate the 68% confidence interval. The label *CYRM-2017-002* in the legend denotes ref. [19].

The total cross section for Higgs boson production, based on a combination of the $\mathrm{H} \to \gamma\gamma$ and $\mathrm{H} \to \mathrm{ZZ}^{(*)} \to 4\ell$ channels, is measured to be $53.4^{+3.5}_{-3.4}$ pb, obtained by applying the statistical treatment described in section 4 (i.e., with a single bin, both at generator and reconstruction levels). The measured total cross sections from the individual channels are $54.2^{+4.5}_{-4.3}$ pb for $\mathrm{H} \to \gamma\gamma$ and $53.3^{+5.2}_{-5.0}$ pb for $\mathrm{H} \to \mathrm{ZZ}^{(*)} \to 4\ell$; the combination thus improves the precision by 21% with respect to the $\mathrm{H} \to \gamma\gamma$ channel alone. The likelihood scans for the individual decay channels and their combination are shown in figure 5. The combined result agrees with the SM value of 55.6 ± 2.5 pb [19].

JHEP04(2026)093

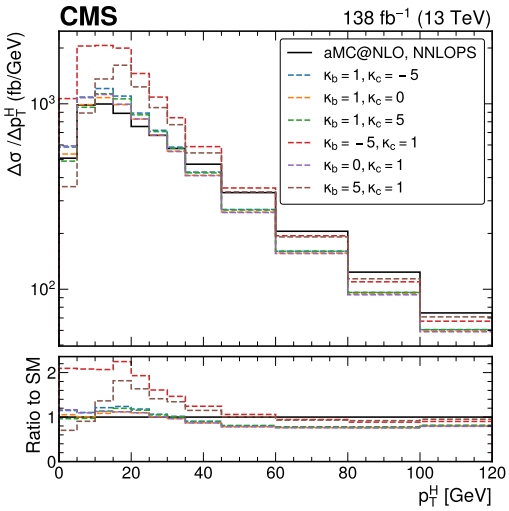

Figure 6. The $p_{\mathrm{T}}^{\mathrm{H}}$ spectrum, for different values of κ_{b} and κ_{c}, as predicted by the κ_{b}–κ_{c} model. The MadGraph5_aMC@NLO NNLOPS-reweighted SM prediction is shown in black. The $\mathrm{H} \to \gamma\gamma$ binning is used.

7 κ-framework interpretation

Differential cross section measurements can be used to constrain the couplings of the Higgs boson to other particles. For Higgs boson production via ggH, variations of the Higgs boson couplings mostly manifest themselves through distortions of the $p_{\mathrm{T}}^{\mathrm{H}}$ spectrum. The κ-framework has been developed [11] to study the coupling structure of the Higgs boson. Following the procedure described in ref. [14], two models are used to interpret the $p_{\mathrm{T}}^{\mathrm{H}}$ spectrum for ggH: one, referred to as κ_{b}–κ_{c} [28], which takes into account the effects of heavy quarks in the ggH loop, and one, referred to as κ_{b}–κ_{t}–c_{g} [29, 30], tailored to top and bottom quarks and the effective Higgs boson coupling to gluons, sensitive to effects at high $p_{\mathrm{T}}^{\mathrm{H}}$. The coupling modifiers are defined as:

$$\kappa_i = \frac{y_i}{y_i^{\mathrm{SM}}}, \tag{7.1}$$

where y_i is the Higgs boson coupling to particle i. In the SM, the values of all κ_i are equal to 1.

In the κ_{b}–κ_{c} model, only the differential ggH cross section is affected by variations of κ_{b} and κ_{c}: in this paper, the most recent parametrization [6] is used. These variations are parametrized using a quadratic polynomial for each bin of the differential production cross section. It is important to note that since these parametrizations address the low range of the $p_{\mathrm{T}}^{\mathrm{H}}$ spectrum, they are available only up to 120 GeV. The $\mathrm{H} \to \tau^+\tau^-$ boosted analysis is therefore not included in this interpretation. Moreover, the $\mathrm{H} \to \mathrm{WW}^{(*)} \to \mathrm{e}^{\pm}\mu^{\mp}\nu_{\ell}\overline{\nu}_{\ell}$ analysis is excluded from this interpretation, as for that analysis the signal predictions are only available inclusively and not separating the ggH contribution from the other production modes. The $p_{\mathrm{T}}^{\mathrm{H}}$ spectrum, for different values of κ_{b} and κ_{c}, as predicted by this model is shown in figure 6.

The κ_{b}–κ_{t}–c_{g} model, which produces simultaneous variations of κ_t, c_g, and κ_b, has been derived in ref. [29] by adding dimension-6 operators to the SM Lagrangian. The $p_{\mathrm{T}}^{\mathrm{H}}$ spectrum is computed at next-to-next-to-leading order (NNLO) accuracy with an analytic resummation

JHEP04(2026)093

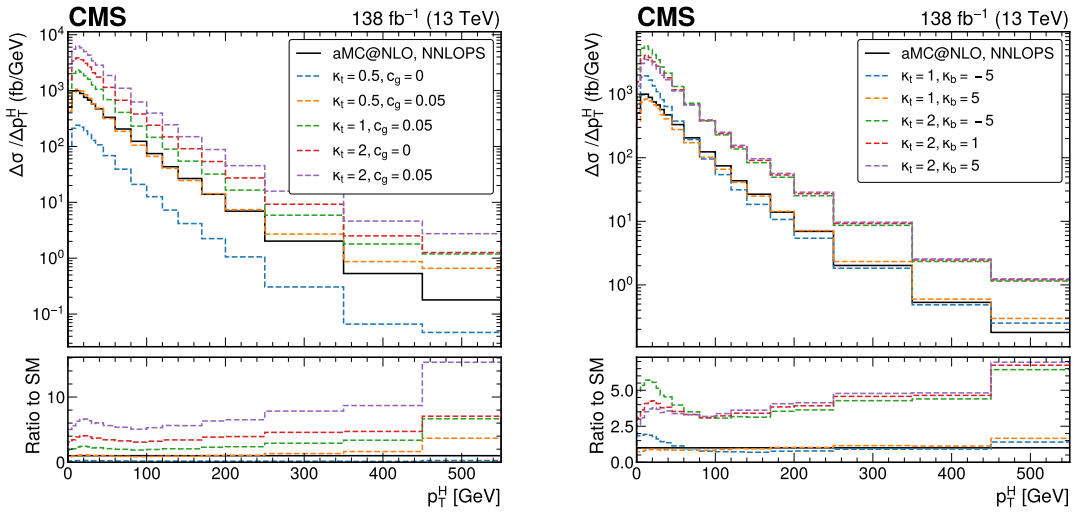

Figure 7. The p_T^H spectrum, for different values of κ_t and c_g (left) and of κ_t and κ_b (right), as predicted by the κ_b–κ_t–c_g model. The third coupling is set to its SM value. The MadGraph5_aMC@NLO NNLOPS-reweighted SM prediction is shown in black. The $H \to \gamma\gamma$ binning is used. The width of the overflow bin is assumed equal to the last but one bin when computing the differential cross section.

performed up to next-to-next-to-leading-logarithmic (NNLL) accuracy. This is achieved by rescaling the SM prediction at NNLL+NNLO accuracy by a BSM correction factor computed as the ratio of the SMEFT to SM predictions at next-to-leading-logarithmic (NLL)+NLO accuracy; this approach allows bottom and top quark mass effects to be approximately included at NNLL+NNLO. The dimension-6 operator corresponding to the coefficient c_g models a direct coupling of the Higgs field to the gluon field with the same underlying tensor structure as in the heavy top quark limit. The value of c_g equals 0 in the SM. The introduction of c_g in the effective Lagrangian is detailed in ref. [30]. The inclusive cross section is parametrized as $\sigma \simeq |12c_g + \kappa_t|^2 \sigma^{SM}$. Two other operators are included in the Lagrangian to describe modifications of the top quark and bottom quark Yukawa couplings, having coefficients κ_t and κ_b, respectively. Simultaneous variations of κ_t and c_g and of κ_t and κ_b are considered. In this result, all the decay channels apart from $H \to WW^{(*)} \to e^{\pm}\mu^{\mp}\nu_\ell\bar{\nu}_\ell$ are included. The p_T^H spectrum, for different values of κ_t and c_g (left) and of κ_t and κ_b (right), as predicted by this model is shown in figure 7. In both cases, the third coupling is set to its SM value.

It should be noted that the vector of signal strength modifiers includes one parameter per bin per decay channel, hence the procedure exemplified in eq. (6.1) is not necessary in this case. Since the parametrizations are derived in the full phase space, the acceptance term is not included in the signal strength modifiers. These considerations lead to the following form for the vector of signal strength modifiers:

$$\begin{aligned}\vec{\mu} &= \left(\vec{\mu}_{H\to\gamma\gamma}, \vec{\mu}_{H\to ZZ^{(*)}\to 4\ell}, \dots\right) \\ &= \left(\mu_{H\to\gamma\gamma,0-5}, \dots, \mu_{H\to ZZ^{(*)}\to 4\ell,0-10}, \dots\right) \\ &= \left(\frac{\sigma_{0-5}(\vec{\kappa})\mathcal{B}_{H\to\gamma\gamma}(\vec{\kappa})}{\sigma^{SM}_{0-5}\mathcal{B}^{SM}_{H\to\gamma\gamma}}, \dots, \frac{\sigma_{0-10}(\vec{\kappa})\mathcal{B}_{H\to ZZ^{(*)}\to 4\ell}(\vec{\kappa})}{\sigma^{SM}_{0-10}\mathcal{B}^{SM}_{H\to ZZ^{(*)}\to 4\ell}}, \dots\right).\end{aligned} \tag{7.2}$$

JHEP04(2026)093

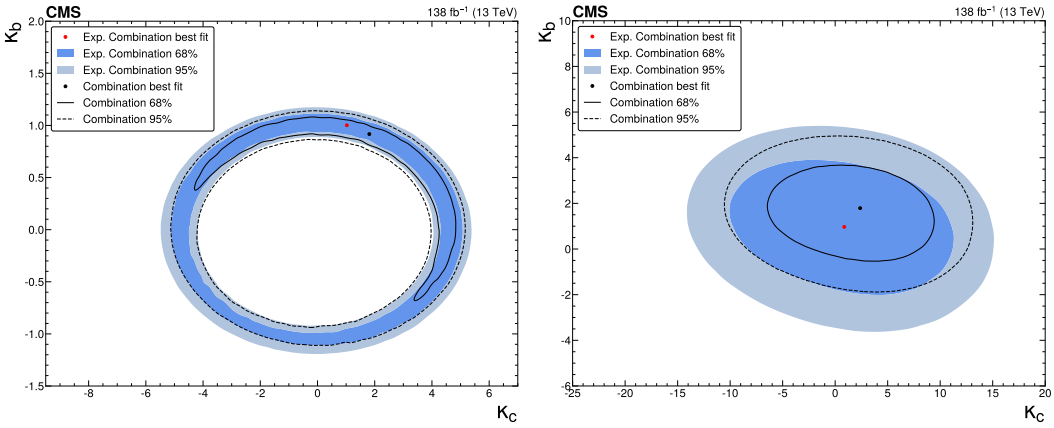

Figure 8. Observed and expected simultaneous fits for κ_b and κ_c, including the coupling dependence of the branching fractions (left) and with the branching fractions of the decay channels entering the combination implemented as nuisance parameters with no dependence on the couplings (right). The 68% and 95% CL contours are shown in solid and dashed lines for the observed data, with the expected contours indicated in blue.

Figure 8 shows the constraints on κ_b and κ_c when including the coupling dependence of the branching fraction (left) and when implemented as nuisance parameters with no branching-fraction dependence on the couplings and no prior constraint, i.e., floating (right). The shapes of the constraints are similar to the ones obtained in ref. [14]. They are in agreement with the SM at 68% confidence level (CL).

The observed and expected two-dimensional confidence intervals for κ_t and c_g are shown in figure 9. For the case of coupling dependence of the branching fractions, the normalization of the spectrum is, by construction, equal to the SM normalization for the set of coefficients satisfying $12c_g + \kappa_t \simeq 1$. The shape of the parametrized spectrum, s, is calculated by normalizing the differential cross section to 1:

$$s_i(\kappa_t, c_g) = \frac{\sigma_i(\kappa_t, c_g)}{\sum_j \sigma_j(\kappa_t, c_g)}, \tag{7.3}$$

where σ_i is the parametrization in bin i. Inserting the expected parabolic dependence of $\sigma_i(\kappa_t, c_g)$ reveals that the shape of the parametrization for κ_t and c_g variations becomes a function only of the ratio of the two couplings, $s_i(c_g/\kappa_t)$. Thus, the dependence of the likelihood on the radial distance $\sqrt{\kappa_t^2 + c_g^2}$ stems from the constraints on the overall normalization, while the dependence on the slope c_g/κ_t is due to the shape of the distribution. The dependence of the likelihood on the slope becomes apparent in figure 9 (right), where the branching fractions are implemented as nuisance parameters with no prior constraint. Except at small values of the couplings, the constraint on the couplings comes from their ratio. The two symmetric sets of contours are due to a symmetry of the parametrization under $(\kappa_t, c_g) \to (-\kappa_t, -c_g)$. In both scenarios, the results are consistent with the SM at the 68% CL. The shapes of the constrained regions are in agreement with those in ref. [14], once scaled for the increase in the data sample size and the number of decay channels included in the combination.

JHEP04(2026)093

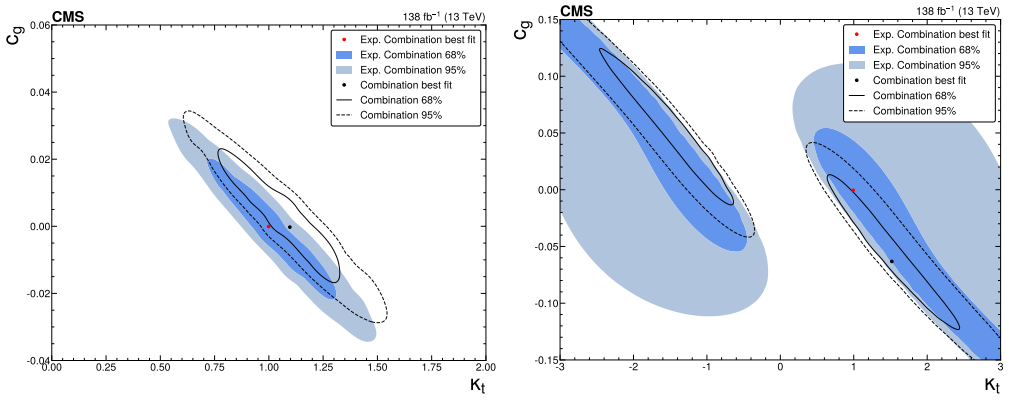

Figure 9. Simultaneous fit for κ_t and c_g, observed and expected, including the coupling dependence of the branching fractions (left) and with the branching fractions of the decay channels entering the combination implemented as nuisance parameters with no dependence on the couplings (right). The 68% and 95% CL contours are shown in solid and dashed lines for observed data, the expected contours are indicated by the blue shaded areas. In the fit with the branching fractions implemented as nuisance parameters, the best fit point is shown in the region with positive κ_t, but a second degenerate best fit point exists for negative κ_t.

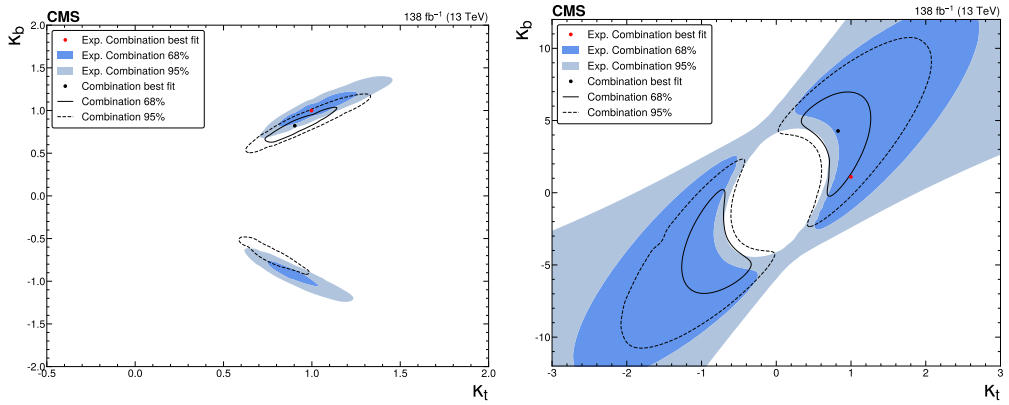

Figure 10. Simultaneous fit for κ_t and κ_b, observed and expected, including the coupling dependence of the branching fractions (left) and with the branching fractions of the decay channels entering the combination implemented as nuisance parameters with no dependence on the couplings (right). The 68% and 95% CL contours are indicated by the solid and dashed lines for the observed data, the expected contours are indicated by the blue shaded regions. In the fit with the branching fractions implemented as nuisance parameters, the best fit point is shown in the region with positive κ_t, but a second degenerate best fit point exists for negative κ_t.

The observed and expected two-dimensional likelihood scans for κ_t and κ_b are shown in figure 10. For the branching fractions implemented as nuisance parameters with no prior constraint, the parametrization is symmetric under $(\kappa_t, \kappa_b) \to (-\kappa_t, -\kappa_b)$, hence the two sets of contours are symmetric. In both scenarios, the results are consistent with the SM at the 68% confidence level. The shapes of the likelihoods are in agreement with those in ref. [14], once scaled for the increase in the size of the data sample and the number of decay channels included.

JHEP04(2026)093

8 SMEFT interpretation

The effective field theory (EFT) approach aims to constrain BSM physics in a model-agnostic way. Assuming the existence of a yet unknown phenomenon at an energy scale Λ above the energy scale that our experiment can reach directly, effects of BSM physics may manifest themselves through effective interactions between SM fields. The effective Lagrangian is written as:

$$\mathcal{L}_{\text{SMEFT}} = \mathcal{L}_{\text{SM}} + \sum_{i=5}^{\infty} \sum_{j=0}^{N_i} \frac{c_j^{(i)}}{\Lambda^{i-4}} O_j^{(i)}, \tag{8.1}$$

where i runs over the number of dimensions, j runs over the number of operators of dimension i, $\mathcal{L}_{\text{SM}}$ is of dimension 4, the operators $O_j^{(i)}$ have dimensions of i, $c_j^{(i)}$ are dimensionless Wilson coefficients (WCs) that correspond to the strength of the interaction, and Λ is the above-mentioned energy scale. Dimension-five operators are related to the neutrino sector and lepton number violation, and are not studied in this paper. The leading contributions are then from dimension-six operators and eq. (8.1) can be written as:

$$\mathcal{L}_{\text{SMEFT}} = \mathcal{L}_{\text{SM}} + \sum_{j=0}^{N_{(6)}} \frac{c_j^{(6)}}{\Lambda^2} O_j^{(6)}, \tag{8.2}$$

where the number of independent operators $N_{(6)}$ in this basis can be reduced to 59 (barring flavor structure and Hermitian conjugations), divided into eight classes, following the scheme introduced in ref. [13].

8.1 SMEFT model details

The two main packages used to generate events within MadGraph5_aMC@NLO are SMEFTsim3.0 [31] and SMEFT@NLO [32]. The FeynRules model used is topU3l, which implements $\text{U}(2)^3_{\text{q,u,d}}$ and $\text{U}(3)^2_{\ell,\text{e}}$ flavor symmetry. Light quarks (u, d, s, c) and heavy quarks (b, t) have separate WCs, while all leptons share the same WCs. The input parameter scheme is $\{G_F, m_Z, m_W\}$. The value of the parameter Λ is set to 1 TeV, which is the scale at which the SMEFT operators are assumed to be valid. Several differences exist between SMEFTsim3.0 and SMEFT@NLO. SMEFTsim3.0 includes leading order (LO) corrections, while SMEFT@NLO includes NLO corrections in QCD: this translates to a higher accuracy in the calculation of coefficients affecting ggH production in the latter case. Another important difference is that SMEFT@NLO does not include CP-odd operators, while SMEFTsim3.0 does. For the different interpretations provided in this paper, three input configurations are used to derive the parametrizations, exploiting the strengths of both packages. The differences are related to the model used to derive the parameterizations of ggH production and of the $\text{H} \to \gamma\gamma$ decay width: the first configuration, adopted to produce the results for (c_{HG}, $\tilde{c}_{\text{HG}}$) in section 8.3, uses SMEFTsim3.0 to derive both the ggH parametrization and the $\text{H} \to \gamma\gamma$ decay width parameterization; the second configuration, adopted to produce the results for the pairs (c_{HB}, $\tilde{c}_{\text{HB}}$), (c_{HW}, $\tilde{c}_{\text{HW}}$) and (c_{HWB}, $\tilde{c}_{\text{HWB}}$) in section 8.3, uses SMEFT@NLO to derive the ggH parametrization and SMEFTsim3.0 to derive the $\text{H} \to \gamma\gamma$ decay width parameterization; the last configuration, adopted to produce the results shown in section 8.4,

JHEP04(2026)093

uses SMEFT@NLO to derive the ggH parametrization and the NLO theoretical predictions provided in ref. [33] for the parametrization of the $H \to \gamma\gamma$ decay width. Production modes other than ggH and decay modes other than $H \to \gamma\gamma$ are parametrized using SMEFTsim3.0 and are the same for all the configurations.

8.2 Derivation of the parametrizations

When working within an EFT framework, the amplitude for each Higgs boson production and decay process can be described as:

$$|\mathcal{M}_{\text{SMEFT}}|^2 = |\mathcal{M}_{\text{SM}} + \mathcal{M}_{\text{BSM}}|^2 = |\mathcal{M}_{\text{SM}}|^2 + 2\,\text{Re}\left\{\mathcal{M}_{\text{SM}}\mathcal{M}_{\text{BSM}}^{\dagger}\right\} + |\mathcal{M}_{\text{BSM}}|^2\,, \tag{8.3}$$

where $\mathcal{M}_{\text{SM}}$ and $\mathcal{M}_{\text{BSM}}$ are the matrix elements originating from the SM and BSM Lagrangians, respectively. The SM-BSM interference term is suppressed by a factor of $1/\Lambda^2$ and the purely-BSM term is suppressed by a factor of $1/\Lambda^4$. If the BSM contributions are restricted to diagrams with a single insertion of a BSM vertex, then $\mathcal{M}_{\text{BSM}}$ is linear in the WCs c_i. Thus, using the fact that $\sigma \propto |\mathcal{M}|^2$, the production cross section in a bin i can be written as:

$$\sigma^i_{\text{SMEFT}} = \sigma^i_{\text{SM}} + \sigma^i_{\text{int}} + \sigma^i_{\text{BSM}}, \tag{8.4}$$

and a scaling function quadratic in the WCs can be derived as:

$$\mu^i_{\text{prod}}(\vec{c}) = \frac{\sigma^i_{\text{SMEFT}}}{\sigma^i_{\text{SM}}} = 1 + \sum_j A^i_j c_i + \sum_{jk} B^i_{jk} c_j c_k. \tag{8.5}$$

The A^i_j and B^i_{jk} constants encode the impact of the WCs on the production cross section in bin i: A^i_j are the linear terms, B^i_{jj} are the quadratic terms, and B^i_{jk} for $j \neq k$ are the cross terms. This procedure also applies to both partial and total decay widths, meaning the scaling function of the branching fraction to a given final state f can be written as:

$$\mu^f_{\text{decay}}(\vec{c}) = \frac{\mathcal{B}^f_{\text{SMEFT}}}{\mathcal{B}^f_{\text{SM}}} = \frac{\Gamma^f_{\text{SMEFT}}/\Gamma^f_{\text{SM}}}{\Gamma^H_{\text{SMEFT}}/\Gamma^H_{\text{SM}}} = \frac{1 + \sum_j A^f_j c_j + \sum_{jk} B^f_{jk} c_j c_k}{1 + \sum_j A^H_j c_j + \sum_{jk} B^H_{jk} c_j c_k}. \tag{8.6}$$

Introducing the narrow width approximation, the total scaling function for a given bin i and final state f is then:

$$\mu^{i,f}(\vec{c}) = \frac{(\sigma\mathcal{B})^{i,\text{H}\to f}}{(\sigma\mathcal{B})^{i,\text{H}\to f}_{\text{SM}}} = \mu^i_{\text{prod}}\,(\vec{c})\mu^f_{\text{decay}}\,(\vec{c}). \tag{8.7}$$

The terms A_j and B_{jk} are derived either analytically at higher orders than possible with current Monte Carlo tools, or using the EFT2Obs tool [34], which wraps and interfaces widely-used packages to facilitate the process of deriving an EFT parametrization. It utilizes MadGraph5_aMC@NLO [35] (version 2.6.7) for simulation and Pythia 8 [36] (version 8.2) for parton showering and hadronization. Fiducial selections and histograms of observables are defined in the Rivet [37] (version 3.0.1) framework. Through the use of Rivet, acceptance effects, which are crucial in the case of differential fiducial cross sections, are taken into account.

An important note concerning the parametrization of the production terms is that most of the analyses are not sufficiently sensitive to measure different production modes

JHEP04(2026)093

separately, hence a weighted parametrization, scaling the expected inclusive cross section in each observable bin, is applied:

$$\mu_i = \sum_j \frac{\sigma_{ij}^{\mathrm{MG5}} \frac{\sigma_j^{\mathrm{YR}}}{\sigma_j^{\mathrm{MG5}}}}{\sum_k \sigma_{ik}^{\mathrm{MG5}} \frac{\sigma_k^{\mathrm{YR}}}{\sigma_k^{\mathrm{MG5}}}} \mu_{ij}, \tag{8.8}$$

where:

- i and j refer to observable bin and production mode, respectively;
- σ_j^{YR} is the SM cross section for production mode j (taken from ref. [11]);
- σ_j^{MG5} is the full cross section for production mode j before the application of fiducial selections;
- σ_{ij}^{MG5} is the cross section in bin i for production mode j after the application of fiducial selections.

8.3 Constraints on CP-even and CP-odd pairs of Wilson coefficients

A particularly relevant group of operators is the group X^2H^2, listed in table 9. For each process shown, the first operator conserves CP while the second violates it. The coefficients c_{HG} and $\tilde{c}_{\mathrm{HG}}$ mainly affect ggH production, while the others affect qqH and VH production along with the Higgs boson decay.

Confidence regions are obtained for the following pairs:

- c_{HG}-$\tilde{c}_{\mathrm{HG}}$;
- c_{HB}-$\tilde{c}_{\mathrm{HB}}$;
- c_{HW}-$\tilde{c}_{\mathrm{HW}}$;
- c_{HWB}-$\tilde{c}_{\mathrm{HWB}}$.

When a pair is studied, all the other WCs are set to their SM values (i.e., 0). Two-dimensional constraints, obtained using Wilks theorem and by combining the $p_{\mathrm{T}}^{\mathrm{H}}$ spectra of all the input analyses, are shown in figure 11. The results are consistent with the SM at the 68% CL. Constraints in this configuration have also been set by the ATLAS Collaboration [16], using only the $\mathrm{H} \to \gamma\gamma$ decay channel. The contour plots presented in this paper are in agreement with the results obtained by the ATLAS Collaboration, but the constraints presented in this paper are tighter because of the use of a larger number of decay channels.

Constraints on the same coefficients are set using the $\Delta\phi_{\mathrm{jj}}$ spectra of the $\mathrm{H} \to \gamma\gamma$ and $\mathrm{H} \to \mathrm{ZZ}^{(*)} \to 4\ell$ decay channels. The results, shown in figure 18 in appendix C, are consistent with the SM at the 68% CL and provide less stringent constraints than the ones obtained using the $p_{\mathrm{T}}^{\mathrm{H}}$ spectra. However, since the observable is CP-even, it can only be used to constrain CP-odd operators in conjunction with CP-even operators, and not to determine if the Wilson coefficients of CP-odd operators are nonzero.

JHEP04(2026)093

Class	Operator	Wilson coefficient	Example process
$\mathcal{L}_6^{(4)} - X^2H^2$	$H^\dagger H G^a_{\mu\nu} G^{a\mu\nu}$	$c_{\rm HG}$	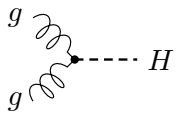
	$H^\dagger H \tilde{G}^a_{\mu\nu} G^{a\mu\nu}$	$\tilde{c}_{\rm HG}$	
	$H^\dagger H B_{\mu\nu} B^{\mu\nu}$	$c_{\rm HB}$	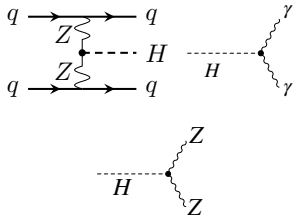
	$H^\dagger H \tilde{B}_{\mu\nu} B^{\mu\nu}$	$\tilde{c}_{\rm HB}$	
	$H^\dagger H W^i_{\mu\nu} W^{i\mu\nu}$	$c_{\rm HW}$	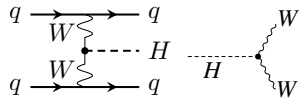
	$H^\dagger H \tilde{W}^i_{\mu\nu} W^{i\mu\nu}$	$\tilde{c}_{\rm HW}$	
	$H^\dagger \sigma^i H W^i_{\mu\nu} B^{i\mu\nu}$	$c_{\rm HWB}$	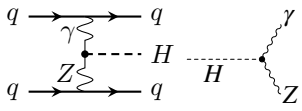
	$H^\dagger \sigma^i H \tilde{W}^i_{\mu\nu} B^{i\mu\nu}$	$\tilde{c}_{\rm HWB}$	

Table 9. List of X^2H^2 operators and corresponding Wilson coefficients. Example Feynman diagrams of the processes affected by the operators are shown in the rightmost column. The notation used is based on ref. [31].

8.4 Constraints on linear combinations of Wilson coefficients

The available data do not contain enough information to simultaneously constrain all coefficients c_i. Many degrees of freedom are left unconstrained by the data, manifesting as flat directions of the likelihood in the parameter space. One way to get insights into the values of the WCs is to use techniques such as principal component analysis. Performing an eigenvector decomposition of the Fisher information matrix provides linear combinations of the original coefficients c_i with an indication of their constraining power (the eigenvalues): the ones with the largest constraining power are left floating in the fit, while the remaining directions are fixed to their SM value (i.e., 0).

In the case of a single measurement, taking as example $\mathrm{H} \to \gamma\gamma$, the PCA is performed as follows. Under the Gaussian approximation, the following equality holds:

$$\mathcal{I}_{\gamma\gamma,\mathrm{diff}} = \mathcal{H}_{\gamma\gamma,\mathrm{diff}} = C^{-1}_{\gamma\gamma,\mathrm{diff}}, \tag{8.9}$$

where, referring to the $\mathrm{H} \to \gamma\gamma$ differential cross section measurement, $\mathcal{I}_{\gamma\gamma,\mathrm{diff}}$ and $\mathcal{H}_{\gamma\gamma,\mathrm{diff}}$ are the Fisher information matrix and the Hessian of the likelihood built with parameters of interest and nuisances of the analysis parametrized with the cross section modifiers μ_i, while $C^{-1}_{\gamma\gamma,\mathrm{diff}}$ is the inverse of the covariance matrix between the parameters of interest. To obtain $C^{-1}_{\gamma\gamma,\mathrm{diff}}$, a fit to the Asimov data set [38] is performed in the original analysis. To move to a WC basis, one can build a matrix $P^{\gamma\gamma}$ by expanding eq. (8.7) to only include

JHEP04(2026)093

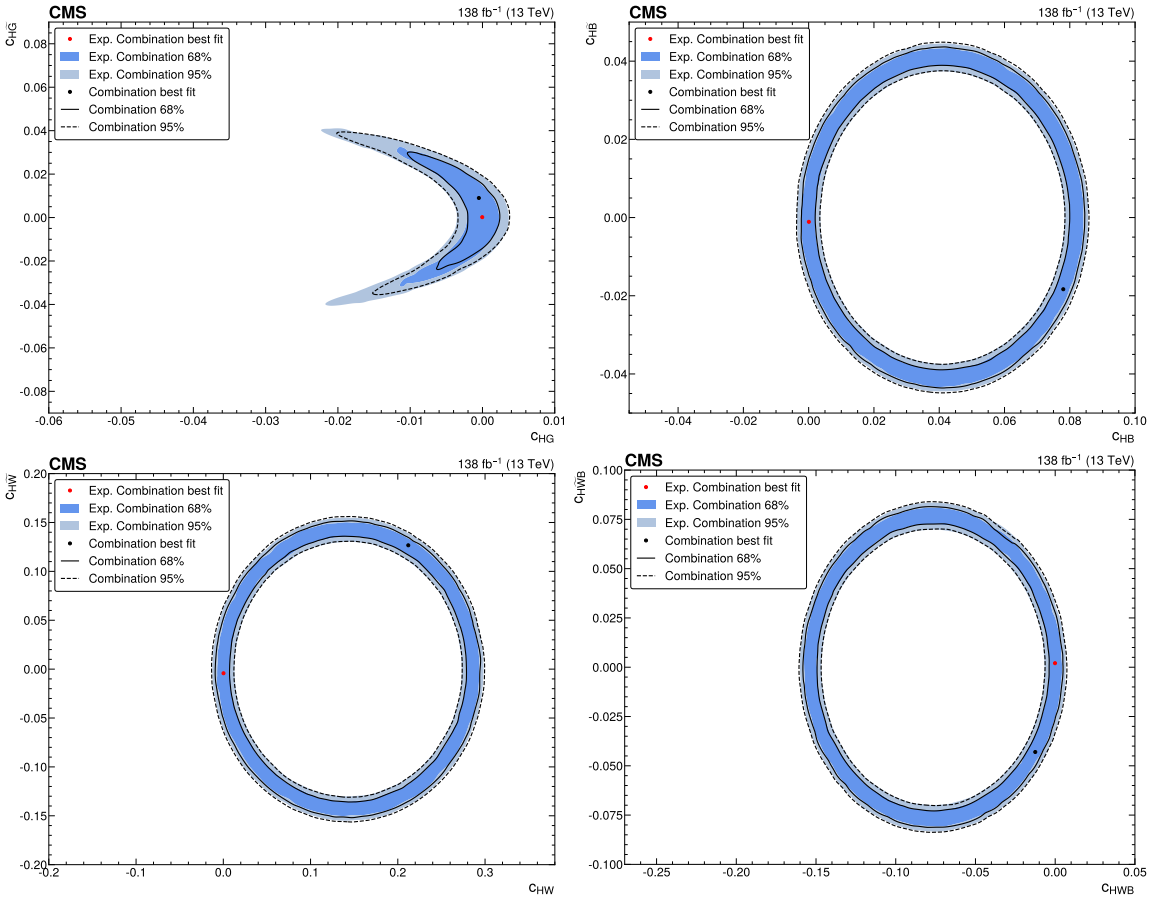

Figure 11. Observed and expected two-dimensional scans for the c_{HG}-$\tilde{c}_{\mathrm{HG}}$ (upper left), c_{HB}-$\tilde{c}_{\mathrm{HB}}$ (upper right), c_{HW}-$\tilde{c}_{\mathrm{HW}}$ (lower left), and c_{HWB}-$\tilde{c}_{\mathrm{HWB}}$ (lower right) pairs with $p_{\mathrm{T}}^{\mathrm{H}}$ spectra in all decay channels.

terms linear in the WCs:

$$P_{ij}^{\gamma\gamma} = A_{ij}^{\mathrm{gg\to H}} + A_{j}^{\mathrm{H}\to\gamma\gamma} - A_{j}^{H}, \tag{8.10}$$

where the index i runs over the generator level bins in $\mathrm{H}\to\gamma\gamma$, the index j runs over the WCs, and A_j^{H} refers to the linear term for the total Higgs boson decay width. The inverse of the covariance matrix in the new basis is then obtained through:

$$C^{-1}_{\gamma\gamma,\mathrm{SMEFT}} = P^{\gamma\gamma T} C^{-1}_{\gamma\gamma,\mathrm{diff}} P^{\gamma\gamma}\ . \tag{8.11}$$

By performing the eigenvector decomposition of $C^{-1}_{\gamma\gamma,\mathrm{SMEFT}}$ one can obtain a matrix $EV_{\gamma\gamma}$ whose columns are the eigenvectors of $C^{-1}_{\gamma\gamma,\mathrm{SMEFT}}$ and a diagonal matrix $\Lambda_{\gamma\gamma}$ whose elements are the eigenvalues of $C^{-1}_{\gamma\gamma,\mathrm{SMEFT}}$ so that:

$$C^{-1}_{\gamma\gamma,\mathrm{SMEFT}} = (EV_{\gamma\gamma})\Lambda_{\gamma\gamma}(EV_{\gamma\gamma})^{-1}. \tag{8.12}$$

The coefficients in $(EV)^{-1}$ are used to write linear combinations of the WCs. The last step consists of rewriting the scaling equations in the newly defined linear combinations. From

JHEP04(2026)093

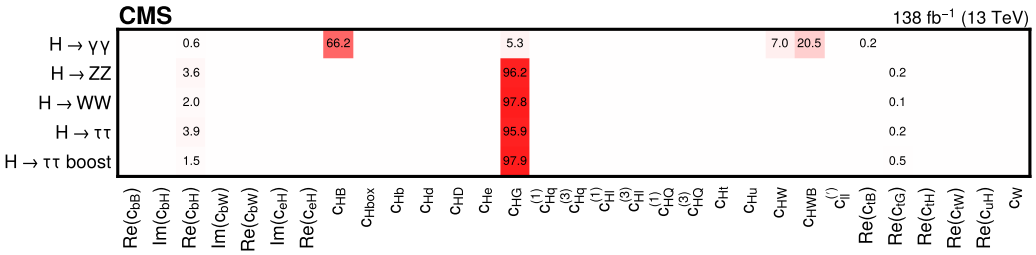

Figure 12. The values of the diagonal entries of the Fisher information matrix, presented as rows, for each decay channel. The normalization is such that the sum of the entries associated with each decay channel is equal to 100.

the description above and in particular from eq. (8.10), one can see that only linear terms (up to $1/\Lambda^2$) are used to build the new basis.

The procedure to perform a PCA in the case of a combination of a set of differential cross section measurements follows the same steps as in the case of a single measurement, with two main differences:

- the Fisher information matrix $\mathcal{I}_{\text{diff}}$ is built as a block-diagonal matrix by concatenating the matrices from individual measurements, since no correlation is assumed between the measurements;
- the new P matrix is built by concatenating the P matrices from individual measurements along the rows, since each bin at generator level is considered independently and the number of WCs (i.e., the number of columns of P) remains the same.

Figure 12 displays the values of the diagonal entries of the Fisher information matrix, separated by decay channel. The normalization is such that the sum of the entries associated with each decay channel is equal to 100. In this way, it is possible to see, within each decay channel, which WCs are the most constrained (the higher the value, the more constrained the coefficient is by the data). In all the decay channels except $\mathrm{H} \to \gamma\gamma$, the sensitivity is dominated by c_{HG}: this is because, in these cases, the correction in production is two orders of magnitude larger than the correction in the decay. This, combined with the fact that differential fiducial cross section measurements are mostly sensitive to ggH production, leads to these channels being sensitive almost exclusively to c_{HG}. The case of $\mathrm{H} \to \gamma\gamma$ is different: the production and decay contributions are comparable (both at one SM loop), hence the sensitivity is also high for c_{HB}, c_{HW}, and c_{HWB}, which affect the decay. To justify the proportions between c_{HG}, c_{HB}, c_{HW}, and c_{HWB}, as defined in SMEFTsim3.0, one has to consider the linear terms A entering the scaling equations, since these terms are used to build the rotation matrix P. The linear terms for c_{HB}, c_{HW}, and c_{HWB} in the decay scaling equation are higher than the ones for c_{HG} in the production scaling formula, leading to the observed proportions. This comes from the fact that the linear terms are proportional to the ratio between the interference term and the SM term, and the SM term contains α_{S} while the interference term contains α_{EM}.

The WCs chosen as input to the PCA are selected from the initial set used to derive the parametrizations, based on a threshold on the A coefficients. The selected subset is reported

JHEP04(2026)093

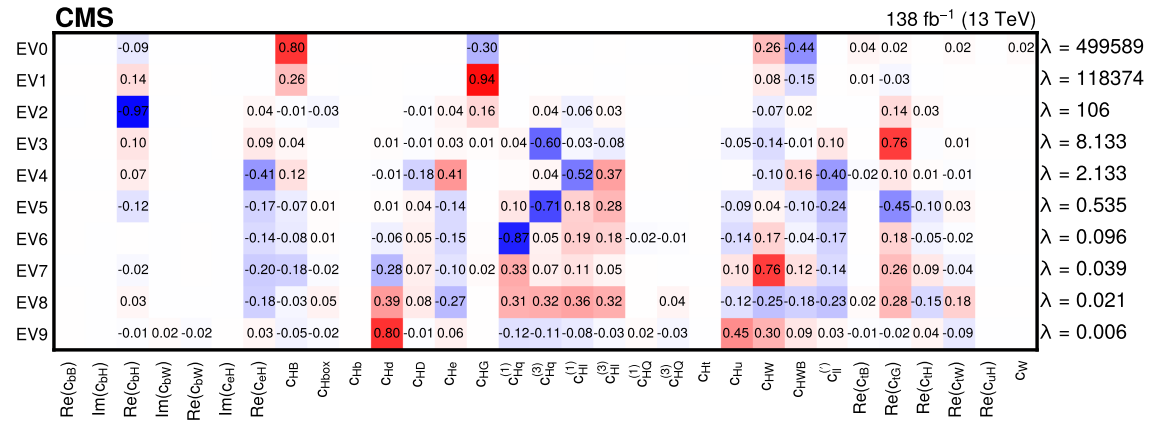

Figure 13. Graphical representation of the ten eigenvectors with the highest eigenvalues λ of the expected combined Fisher information matrix in the SMEFT basis. Values lower than 10^{-3} are not shown. The intensity of the color represents the absolute value of the coefficient, going from -1 (blue) to 1 (red).

in table 10. The rotation matrix EV^{-1}, shown in figure 13, is then used to derive linear combinations of the WCs. The absolute values of the coefficients shown in figure 13 provide an idea of the weight that each WC has in the linear combination. The larger the weight of a WC in a linear combination with large eigenvalues, the more constrained it is by the data. As an example, one can see that the first two linear combinations are dominated by c_{HG}, c_{HB}, c_{HW}, and c_{HWB}, which are the most constrained WCs in the analysis and also dominate in figure 12.

Observed and expected results for the ten eigenvectors with the largest eigenvalues are shown in figure 14. The corresponding one-dimensional scans, obtained profiling the other nine eigenvectors, are shown in figures 19, 20, and 21 in appendix D. The results are consistent with the SM within two standard deviations. The largest tension with the SM is observed in the sixth eigenvector, where the best fit value is $\mathrm{EV}_5 = 2.71^{+1.33}_{-1.39}$. The p-value corresponding to this tension is 3.6%. As shown in figure 13, the WC with the highest weight in EV_5 is $c^{(3)}_{\mathrm{Hq}}$.

The correlation matrix of the linear combinations of WCs is shown in figure 15. Some level of correlation is present between the eigenvectors (up to 18% in the worst cases). This can be explained by the fact that the eigenvectors are obtained by diagonalizing the expected Fisher information matrix, and not the observed one, hence a perfect level of decorrelation is not to be expected.

JHEP04(2026)093

Class	Operator	Wilson coefficient
$\mathcal{L}_6^{(1)} - X^3$	$\varepsilon^{ijk} W_\mu^{i\nu} W_\nu^{j\rho} W_\rho^{k\mu}$	$c_{\rm W}$
$\mathcal{L}_6^{(3)} - H^4 D^2$	$(D^\mu H^\dagger H)(H^\dagger D_\mu H)$	$c_{\rm HD}$
	$(H^\dagger H)\Box(H^\dagger H)$	$c_{\rm H\Box}$
$\mathcal{L}_6^{(4)} - X^2 H^2$	$H^\dagger H G^a_{\mu\nu} G^{a\mu\nu}$	$c_{\rm HG}$
	$H^\dagger H B_{\mu\nu} B^{\mu\nu}$	$c_{\rm HB}$
	$H^\dagger H W^i_{\mu\nu} W^{i\mu\nu}$	$c_{\rm HW}$
	$H^\dagger \sigma^i H W^i_{\mu\nu} B^{i\mu\nu}$	$c_{\rm HWB}$
$\mathcal{L}_6^{(5)} - \psi^2 H^3$	$(H^\dagger H)(\bar{Q} H b)$	$\mathrm{Re}(c_{\rm bH})$
		$\mathrm{Im}(c_{\rm bH})$
	$(H^\dagger H)(\bar{Q} H t)$	$\mathrm{Re}(c_{\rm tH})$
	$(H^\dagger H)(\bar{l}_p e_r H)$	$\mathrm{Re}(c_{\rm eH})$
		$\mathrm{Im}(c_{\rm eH})$
	$(H^\dagger H)(\bar{q} Y_u^\dagger u \tilde{H})$	$\mathrm{Re}(c_{\rm uH})$
$\mathcal{L}_6^{(6)} - \psi^2 X H$	$(\bar{Q}\sigma^{\mu\nu} T^a t)\tilde{H} G^a_{\mu\nu}$	$\mathrm{Re}(c_{\rm tG})$
	$(\bar{Q}\sigma^{\mu\nu} b) H B_{\mu\nu}$	$\mathrm{Re}(c_{\rm bB})$
	$(\bar{Q}\sigma^{\mu\nu} t) H B_{\mu\nu}$	$\mathrm{Re}(c_{\rm tB})$
	$(\bar{Q}\sigma^{\mu\nu} b)\sigma^i H W^i_{\mu\nu}$	$\mathrm{Re}(c_{\rm bW})$
		$\mathrm{Im}(c_{\rm bW})$
	$(\bar{Q}\sigma^{\mu\nu} t)\sigma^i \tilde{H} W^i_{\mu\nu}$	$\mathrm{Re}(c_{\rm tW})$
$\mathcal{L}_6^{(7)} - \psi^2 H^2 D$	$(H^\dagger i \overleftrightarrow{D}_\mu H)(\bar{l}_p \gamma^\mu l_r)$	$c_{\rm Hl}^{(1)}$
	$(H^\dagger i \overleftrightarrow{D}^i_\mu H)(\bar{l}_p \sigma^i \gamma^\mu l_r)$	$c_{\rm Hl}^{(3)}$
	$(H^\dagger i \overleftrightarrow{D}_\mu H)(\bar{q}_p \gamma^\mu q_r)$	$c_{\rm Hq}^{(1)}$
	$(H^\dagger i \overleftrightarrow{D}^i_\mu H)(\bar{q}_p \sigma^i \gamma^\mu q_r)$	$c_{\rm Hq}^{(3)}$
	$(H^\dagger i \overleftrightarrow{D}_\mu H)(\bar{Q}_p \gamma^\mu Q_r)$	$c_{\rm HQ}^{(1)}$
	$(H^\dagger i \overleftrightarrow{D}^i_\mu H)(\bar{Q}_p \sigma^i \gamma^\mu Q_r)$	$c_{\rm HQ}^{(3)}$
	$(H^\dagger i \overleftrightarrow{D}_\mu H)(\bar{u}_p \gamma^\mu u_r)$	$c_{\rm Hu}$
	$(H^\dagger i \overleftrightarrow{D}_\mu H)(\bar{d}_p \gamma^\mu d_r)$	$c_{\rm Hd}$
	$(H^\dagger i \overleftrightarrow{D}_\mu H)(\bar{e}_p \gamma^\mu e_r)$	$c_{\rm He}$
	$(H^\dagger i \overleftrightarrow{D}_\mu H)(\bar{b} \gamma^\mu b)$	$c_{\rm Hb}$
	$(H^\dagger i \overleftrightarrow{D}_\mu H)(\bar{t} \gamma^\mu t)$	$c_{\rm Ht}$
$\mathcal{L}_6^{(8a)} - (\bar{L}L)(\bar{L}L)$	$(\bar{l}_p \gamma_\mu l_r)(\bar{l}_s \gamma^\mu l_t)$	$c'_{\rm ll}$

Table 10. Wilson coefficients used as input to the SMEFT interpretation (right column). In the left and center columns the class they belong to and the corresponding operator are reported. The notation used is based on ref. [31].

JHEP04(2026)093

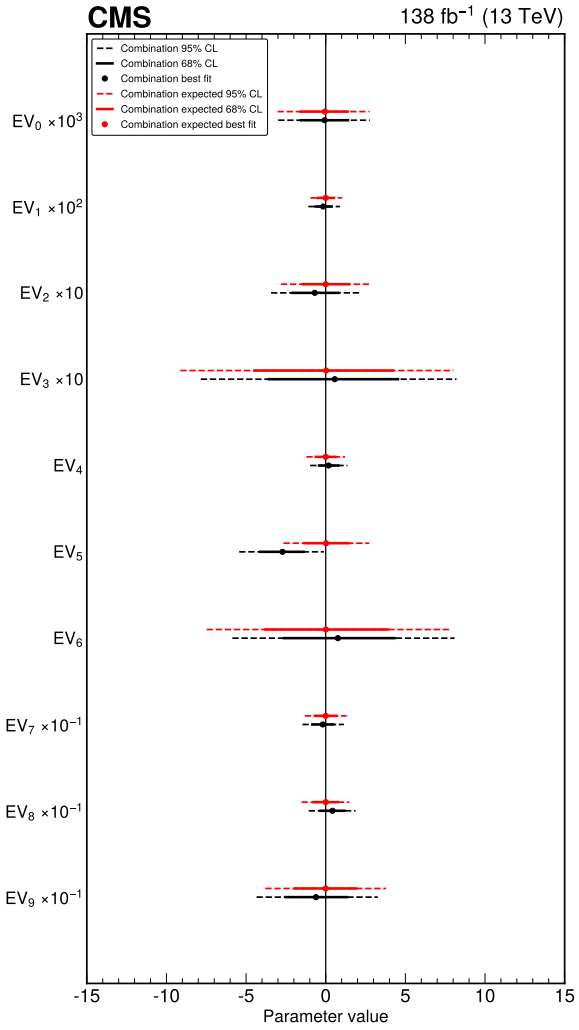

Figure 14. Summary of observed and expected confidence intervals at 68% and 95% confidence level for the first ten eigenvectors. On the y-axis, the quantity being displayed is multiplied by the corresponding power of ten. The eigenvectors are ordered by decreasing eigenvalue.

JHEP04(2026)093

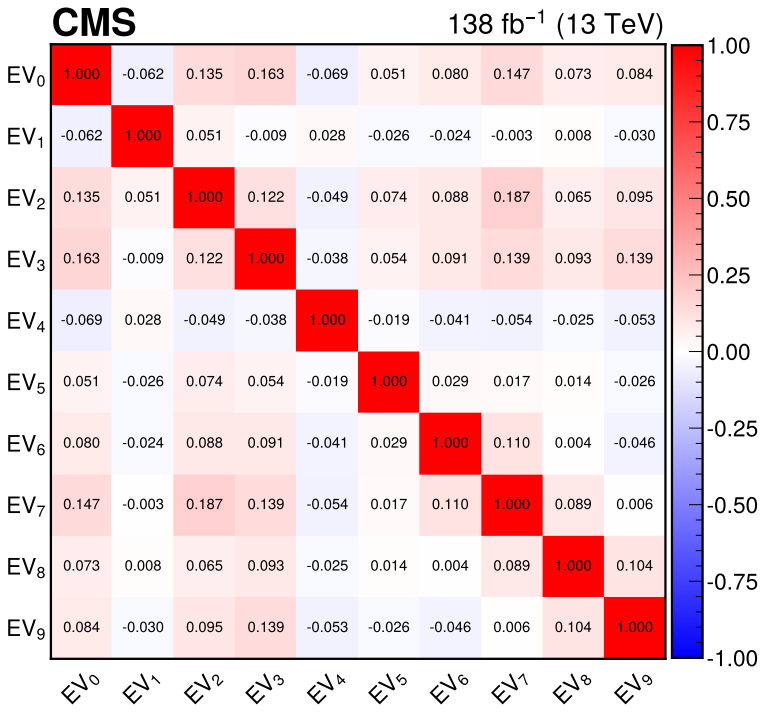

Figure 15. Correlation matrix of the linear combinations of Wilson coefficients obtained from the PCA, obtained by fitting the observed data to the $p_{\mathrm{T}}^{\mathrm{H}}$ spectra of all decay channels.

JHEP04(2026)093

9 Summary

Combined measurements of differential Higgs boson production cross sections for the observables $p_{\mathrm{T}}^{\mathrm{H}}$, N_{jets}, $|y_{\mathrm{H}}|$, $p_{\mathrm{T}}^{\mathrm{j}_1}$, m_{jj}, $|\Delta\eta_{\mathrm{jj}}|$, and $\tau_{\mathrm{C}}^{\mathrm{j}}$ are presented, using proton-proton collision data collected at $\sqrt{s} = 13\,\mathrm{TeV}$ and corresponding to an integrated luminosity of $138\,\mathrm{fb}^{-1}$. The spectra are obtained with data from the $\mathrm{H} \to \gamma\gamma$, $\mathrm{H} \to \mathrm{ZZ}^{(*)} \to 4\ell$, $\mathrm{H} \to \mathrm{WW}^{(*)} \to \mathrm{e}^{\pm}\mu^{\mp}\nu_{\ell}\overline{\nu}_{\ell}$, and $\mathrm{H} \to \tau^{+}\tau^{-}$ (both in the small and large Lorentz-boost regimes) decay channels. The precision of the combined measurement of the $p_{\mathrm{T}}^{\mathrm{H}}$ differential cross section is improved by about 23% with respect to the $\mathrm{H} \to \gamma\gamma$ channel alone. The improvement is particularly significant in the low- and high-$p_{\mathrm{T}}^{\mathrm{H}}$ regions. No significant deviations from the SM predictions are observed in the differential distributions. Additionally, the total cross section for Higgs boson production based on a combination of the $\mathrm{H} \to \gamma\gamma$ and $\mathrm{H} \to \mathrm{ZZ}^{(*)} \to 4\ell$ channels is measured to be $53.4^{+2.9}_{-2.9}\,(\mathrm{stat})^{+1.9}_{-1.8}\,(\mathrm{syst})\,\mathrm{pb}$, consistent with the SM prediction.

The obtained $p_{\mathrm{T}}^{\mathrm{H}}$ spectra are interpreted using the κ and SM effective field theory frameworks. In the former, multiple couplings are varied using the models provided in refs. [28–30]. In the latter, two-dimensional constraints are obtained for pairs of Wilson coefficients. A principal component analysis is then performed to identify nonflat directions of the likelihood. The studies performed in this context highlight that the differential fiducial cross section measurements are sensitive to a limited set of operators and related Wilson coefficients, with the most constrained ones being c_{HG}, c_{HB}, c_{HW}, and c_{HWB}. No significant deviations from the SM are observed in the results obtained with either framework.

Acknowledgments

We congratulate our colleagues in the CERN accelerator departments for the excellent performance of the LHC and thank the technical and administrative staffs at CERN and at other CMS institutes for their contributions to the success of the CMS effort. In addition, we gratefully acknowledge the computing centers and personnel of the Worldwide LHC Computing Grid and other centers for delivering so effectively the computing infrastructure essential to our analyses. Finally, we acknowledge the enduring support for the construction and operation of the LHC, the CMS detector, and the supporting computing infrastructure provided by the following funding agencies: SC (Armenia), BMBWF and FWF (Austria); FNRS and FWO (Belgium); CNPq, CAPES, FAPERJ, FAPERGS, and FAPESP (Brazil); MES and BNSF (Bulgaria); CERN; CAS, MoST, and NSFC (China); MINCIENCIAS (Colombia); MSES and CSF (Croatia); RIF (Cyprus); SENESCYT (Ecuador); ERC PRG, RVTT3 and MoER TK202 (Estonia); Academy of Finland, MEC, and HIP (Finland); CEA and CNRS/IN2P3 (France); SRNSF (Georgia); BMBF, DFG, and HGF (Germany); GSRI (Greece); NKFIH (Hungary); DAE and DST (India); IPM (Iran); SFI (Ireland); INFN (Italy); MSIP and NRF (Republic of Korea); MES (Latvia); LMTLT (Lithuania); MOE and UM (Malaysia); BUAP, CINVESTAV, CONACYT, LNS, SEP, and UASLP-FAI (Mexico); MOS (Montenegro); MBIE (New Zealand); PAEC (Pakistan); MES and NSC (Poland); FCT (Portugal); MESTD (Serbia); MICIU/AEI and PCTI (Spain); MOSTR (Sri Lanka); Swiss Funding Agencies (Switzerland); MST (Taipei); MHESI and NSTDA (Thailand); TUBITAK and TENMAK (Turkey); NASU (Ukraine); STFC (United Kingdom); DOE and NSF (U.S.A.).

JHEP04(2026)093

Individuals have received support from the Marie-Curie program and the European Research Council and Horizon 2020 Grant, contract Nos. 675440, 724704, 752730, 758316, 765710, 824093, 101115353, 101002207, and COST Action CA16108 (European Union); the Leventis Foundation; the Alfred P. Sloan Foundation; the Alexander von Humboldt Foundation; the Science Committee, project no. 22rl-037 (Armenia); the Fonds pour la Formation à la Recherche dans l'Industrie et dans l'Agriculture (FRIA-Belgium); the Beijing Municipal Science & Technology Commission, No. Z191100007219010 and Fundamental Research Funds for the Central Universities (China); the Ministry of Education, Youth and Sports (MEYS) of the Czech Republic; the Shota Rustaveli National Science Foundation, grant FR-22-985 (Georgia); the Deutsche Forschungsgemeinschaft (DFG), among others, under Germany's Excellence Strategy – EXC 2121 "Quantum Universe" – 390833306, and under project number 400140256 – GRK2497; the Hellenic Foundation for Research and Innovation (HFRI), Project Number 2288 (Greece); the Hungarian Academy of Sciences, the New National Excellence Program – ÚNKP, the NKFIH research grants K 131991, K 133046, K 138136, K 143460, K 143477, K 146913, K 146914, K 147048, 2020-2.2.1-ED-2021-00181, TKP2021-NKTA-64, and 2021-4.1.2-NEMZ_KI-2024-00036 (Hungary); the Council of Science and Industrial Research, India; ICSC – National Research Center for High Performance Computing, Big Data and Quantum Computing and FAIR – Future Artificial Intelligence Research, funded by the NextGenerationEU program (Italy); the Latvian Council of Science; the Ministry of Education and Science, project no. 2022/WK/14, and the National Science Center, contracts Opus 2021/41/B/ST2/01369 and 2021/43/B/ST2/01552 (Poland); the Fundação para a Ciência e a Tecnologia, grant CEECIND/01334/2018 (Portugal); the National Priorities Research Program by Qatar National Research Fund; MICIU/AEI/10.13039/501100011033, ERDF/EU, "European Union NextGenerationEU/PRTR", and Programa Severo Ochoa del Principado de Asturias (Spain); the Chulalongkorn Academic into Its 2nd Century Project Advancement Project, and the National Science, Research and Innovation Fund via the Program Management Unit for Human Resources & Institutional Development, Research and Innovation, grant B39G670016 (Thailand); the Kavli Foundation; the Nvidia Corporation; the SuperMicro Corporation; the Welch Foundation, contract C-1845; and the Weston Havens Foundation (U.S.A.).

A Tables for the differential cross section measurements

Tables 11–17 show the measured combined differential cross sections for the considered observables.

$p_{\mathrm{T}}^{\mathrm{H}}$ (GeV)	Best fit (fb/GeV)
σ_{0-5}	$2.86^{+0.49}_{-0.58}\,(\mathrm{syst})^{+1.75}_{-1.95}\,(\mathrm{stat}) \times 10^{2}$
σ_{5-10}	$8.73^{+0.89}_{-0.54}\,(\mathrm{syst})^{+2.90}_{-3.13}\,(\mathrm{stat}) \times 10^{2}$
σ_{10-15}	$1.28^{+0.08}_{-0.08}\,(\mathrm{syst})^{+0.26}_{-0.25}\,(\mathrm{stat}) \times 10^{3}$
σ_{15-20}	$1.12^{+0.06}_{-0.08}\,(\mathrm{syst})^{+0.26}_{-0.24}\,(\mathrm{stat}) \times 10^{3}$
σ_{20-25}	$4.16^{+0.56}_{-0.00}\,(\mathrm{syst})^{+2.14}_{-2.19}\,(\mathrm{stat}) \times 10^{2}$
σ_{25-30}	$8.13^{+0.25}_{-0.43}\,(\mathrm{syst})^{+2.14}_{-2.11}\,(\mathrm{stat}) \times 10^{2}$
σ_{30-35}	$5.14^{+0.52}_{-0.32}\,(\mathrm{syst})^{+1.74}_{-1.68}\,(\mathrm{stat}) \times 10^{2}$
σ_{35-45}	$5.85^{+0.23}_{-0.24}\,(\mathrm{syst})^{+1.28}_{-1.29}\,(\mathrm{stat}) \times 10^{2}$
σ_{45-60}	$2.71^{+0.26}_{-0.16}\,(\mathrm{syst})^{+0.62}_{-0.59}\,(\mathrm{stat}) \times 10^{2}$
σ_{60-80}	$2.88^{+0.17}_{-0.13}\,(\mathrm{syst})^{+0.46}_{-0.45}\,(\mathrm{stat}) \times 10^{2}$
σ_{80-100}	$2.37^{+0.18}_{-0.14}\,(\mathrm{syst})^{+0.36}_{-0.35}\,(\mathrm{stat}) \times 10^{2}$
$\sigma_{100-120}$	$6.16^{+0.00}_{-0.83}\,(\mathrm{syst})^{+2.97}_{-2.65}\,(\mathrm{stat}) \times 10^{1}$
$\sigma_{120-140}$	$9.07^{+0.86}_{-0.66}\,(\mathrm{syst})^{+1.73}_{-1.70}\,(\mathrm{stat}) \times 10^{1}$
$\sigma_{140-170}$	$5.31^{+0.50}_{-0.37}\,(\mathrm{syst})^{+1.08}_{-1.06}\,(\mathrm{stat}) \times 10^{1}$
$\sigma_{170-200}$	$1.39^{+0.22}_{-0.15}\,(\mathrm{syst})^{+0.65}_{-0.63}\,(\mathrm{stat}) \times 10^{1}$
$\sigma_{200-250}$	$1.47^{+0.22}_{-0.18}\,(\mathrm{syst})^{+0.25}_{-0.24}\,(\mathrm{stat}) \times 10^{1}$
$\sigma_{250-350}$	$4.28^{+0.59}_{-0.43}\,(\mathrm{syst})^{+1.00}_{-0.97}\,(\mathrm{stat}) \times 10^{0}$
$\sigma_{350-450}$	$9.67^{+2.09}_{-1.49}\,(\mathrm{syst})^{+3.27}_{-3.08}\,(\mathrm{stat}) \times 10^{-1}$
$\sigma_{>450}$	$4.37^{+1.19}_{-0.80}\,(\mathrm{syst})^{+1.77}_{-1.66}\,(\mathrm{stat}) \times 10^{-1}$

Table 11. Observed best fit differential cross section for the $p_{\mathrm{T}}^{\mathrm{H}}$ (GeV) observable. For its calculation, the last bin is assumed to have a bin width equal to that of the last but one bin.

JHEP04(2026)093

N_{jets}	Best fit (fb)
σ_0	$3.13^{+0.17}_{-0.16}\,(\text{syst})^{+0.17}_{-0.17}\,(\text{stat}) \times 10^4$
σ_1	$1.43^{+0.10}_{-0.09}\,(\text{syst})^{+0.13}_{-0.13}\,(\text{stat}) \times 10^4$
σ_2	$5.09^{+0.47}_{-0.44}\,(\text{syst})^{+0.56}_{-0.56}\,(\text{stat}) \times 10^3$
σ_3	$2.77^{+1.86}_{-1.56}\,(\text{syst})^{+2.91}_{-2.83}\,(\text{stat}) \times 10^2$
$\sigma_{>=4}$	$6.10^{+1.24}_{-1.00}\,(\text{syst})^{+1.82}_{-1.82}\,(\text{stat}) \times 10^2$

Table 12. Observed best fit differential cross section for the N_{jets} observable.

$p_{\text{T}}^{\text{j}_1}$ (GeV)	Best fit (fb/GeV)
σ_{0-30}	$1.09^{+0.09}_{-0.07}\,(\text{syst})^{+0.09}_{-0.09}\,(\text{stat}) \times 10^3$
σ_{30-40}	$4.81^{+8.97}_{-8.46}\,(\text{syst})^{+28.07}_{-25.92}\,(\text{stat}) \times 10^1$
σ_{40-55}	$7.37^{+0.69}_{-0.74}\,(\text{syst})^{+2.13}_{-2.52}\,(\text{stat}) \times 10^2$
σ_{55-75}	$1.33^{+0.34}_{-0.32}\,(\text{syst})^{+1.06}_{-1.01}\,(\text{stat}) \times 10^2$
σ_{75-95}	$9.60^{+3.00}_{-2.91}\,(\text{syst})^{+8.96}_{-9.60}\,(\text{stat}) \times 10^1$
σ_{95-120}	$6.13^{+1.25}_{-1.03}\,(\text{syst})^{+4.63}_{-4.47}\,(\text{stat}) \times 10^1$
$\sigma_{120-150}$	$8.20^{+1.23}_{-0.83}\,(\text{syst})^{+3.58}_{-3.50}\,(\text{stat}) \times 10^1$
$\sigma_{150-200}$	$7.25^{+0.00}_{-37.54}\,(\text{syst})^{+118.71}_{-117.44}\,(\text{stat}) \times 10^{-1}$
$\sigma_{>200}$	$2.41^{+0.23}_{-0.17}\,(\text{syst})^{+0.55}_{-0.53}\,(\text{stat}) \times 10^1$

Table 13. Observed best fit differential cross section for the $p_{\text{T}}^{\text{j}_1}$ (GeV) observable. For its calculation, the last bin is assumed to have a bin width equal to that of the last but one bin.

JHEP04(2026)093

$\lvert y_{\mathrm{H}}\rvert$	Best fit (fb)
$\sigma_{0-0.15}$	$2.82^{+0.09}_{-0.07}\,(\mathrm{syst})^{+0.38}_{-0.37}\,(\mathrm{stat}) \times 10^{4}$
$\sigma_{0.15-0.3}$	$2.81^{+0.09}_{-0.08}\,(\mathrm{syst})^{+0.39}_{-0.38}\,(\mathrm{stat}) \times 10^{4}$
$\sigma_{0.3-0.45}$	$2.84^{+0.08}_{-0.07}\,(\mathrm{syst})^{+0.41}_{-0.40}\,(\mathrm{stat}) \times 10^{4}$
$\sigma_{0.45-0.6}$	$2.57^{+0.10}_{-0.05}\,(\mathrm{syst})^{+0.42}_{-0.40}\,(\mathrm{stat}) \times 10^{4}$
$\sigma_{0.6-0.75}$	$1.95^{+0.06}_{-0.07}\,(\mathrm{syst})^{+0.43}_{-0.39}\,(\mathrm{stat}) \times 10^{4}$
$\sigma_{0.75-0.9}$	$2.53^{+0.09}_{-0.05}\,(\mathrm{syst})^{+0.45}_{-0.43}\,(\mathrm{stat}) \times 10^{4}$
$\sigma_{0.9-1.2}$	$1.84^{+0.09}_{-0.04}\,(\mathrm{syst})^{+0.33}_{-0.32}\,(\mathrm{stat}) \times 10^{4}$
$\sigma_{1.2-1.6}$	$1.61^{+0.07}_{-0.05}\,(\mathrm{syst})^{+0.32}_{-0.35}\,(\mathrm{stat}) \times 10^{4}$
$\sigma_{1.6-2.0}$	$1.51^{+0.09}_{-0.03}\,(\mathrm{syst})^{+0.76}_{-0.50}\,(\mathrm{stat}) \times 10^{4}$
$\sigma_{2.0-2.5}$	$2.89^{+0.93}_{-0.50}\,(\mathrm{syst})^{+5.53}_{-5.46}\,(\mathrm{stat}) \times 10^{3}$

Table 14. Observed best fit differential cross section for the $|y_{\mathrm{H}}|$ observable.

$\lvert\Delta\eta_{\mathrm{jj}}\rvert$	Best fit (fb)
$\sigma_{0-0.7}$	$4.52^{+0.22}_{-0.16}\,(\mathrm{syst})^{+1.23}_{-1.20}\,(\mathrm{stat}) \times 10^{3}$
$\sigma_{0.7-1.6}$	$2.87^{+1.59}_{-0.89}\,(\mathrm{syst})^{+9.95}_{-9.96}\,(\mathrm{stat}) \times 10^{2}$
$\sigma_{1.6-3.0}$	$2.42^{+0.17}_{-0.09}\,(\mathrm{syst})^{+0.61}_{-0.64}\,(\mathrm{stat}) \times 10^{3}$
$\sigma_{3.0-5.0}$	$1.03^{+0.09}_{-0.08}\,(\mathrm{syst})^{+0.32}_{-0.27}\,(\mathrm{stat}) \times 10^{3}$
$\sigma_{>5.0}$	$-1.61^{+0.43}_{-0.48}\,(\mathrm{syst})^{+1.74}_{-1.62}\,(\mathrm{stat}) \times 10^{2}$

Table 15. Observed best fit differential cross section for the $|\Delta\eta_{\mathrm{jj}}|$ observable. For its calculation, the last bin is assumed to have a bin width equal to that of the last but one bin.

m_{jj} (GeV)	Best fit (fb/GeV)
σ_{0-75}	$4.92^{+1.52}_{-1.40}\,(\mathrm{syst})^{+12.36}_{-12.41}\,(\mathrm{stat}) \times 10^{0}$
σ_{75-120}	$5.65^{+0.63}_{-0.31}\,(\mathrm{syst})^{+2.24}_{-2.18}\,(\mathrm{stat}) \times 10^{1}$
$\sigma_{120-180}$	$2.33^{+0.71}_{-0.30}\,(\mathrm{syst})^{+1.45}_{-1.39}\,(\mathrm{stat}) \times 10^{1}$
$\sigma_{180-300}$	$1.36^{+0.40}_{-0.16}\,(\mathrm{syst})^{+0.87}_{-0.85}\,(\mathrm{stat}) \times 10^{1}$
$\sigma_{300-500}$	$6.56^{+0.60}_{-0.28}\,(\mathrm{syst})^{+2.79}_{-2.59}\,(\mathrm{stat}) \times 10^{0}$
$\sigma_{500-1000}$	$1.75^{+0.24}_{-0.23}\,(\mathrm{syst})^{+1.09}_{-1.18}\,(\mathrm{stat}) \times 10^{0}$
$\sigma_{>1000}$	$9.04^{+1.25}_{-1.03}\,(\mathrm{syst})^{+5.22}_{-4.86}\,(\mathrm{stat}) \times 10^{-1}$

Table 16. Observed best fit differential cross section for the m_{jj} (GeV) observable. For its calculation, the last bin is assumed to have a bin width equal to that of the last but one bin.

JHEP04(2026)093

τ_C^j (GeV)	Best fit (fb/GeV)
σ_{15-20}	$5.95^{+0.34}_{-0.27}\,(\text{syst})^{+3.51}_{-3.30}\,(\text{stat}) \times 10^2$
σ_{20-30}	$4.02^{+0.26}_{-0.15}\,(\text{syst})^{+1.57}_{-1.51}\,(\text{stat}) \times 10^2$
σ_{30-50}	$1.91^{+0.09}_{-0.05}\,(\text{syst})^{+0.54}_{-0.47}\,(\text{stat}) \times 10^2$
σ_{50-80}	$6.07^{+0.29}_{-0.20}\,(\text{syst})^{+1.76}_{-1.67}\,(\text{stat}) \times 10^1$
$\sigma_{>80}$	$2.22^{+0.21}_{-0.12}\,(\text{syst})^{+0.90}_{-0.85}\,(\text{stat}) \times 10^1$

Table 17. Observed best fit differential cross section for the τ_C^j (GeV) observable. For its calculation, the last bin is assumed to have a bin width equal to that of the last but one bin.

JHEP04(2026)093

B Correlation matrices for the combinations of differential observables

Figures 16 and 17 show the bin-to-bin correlation matrices for considered observables.

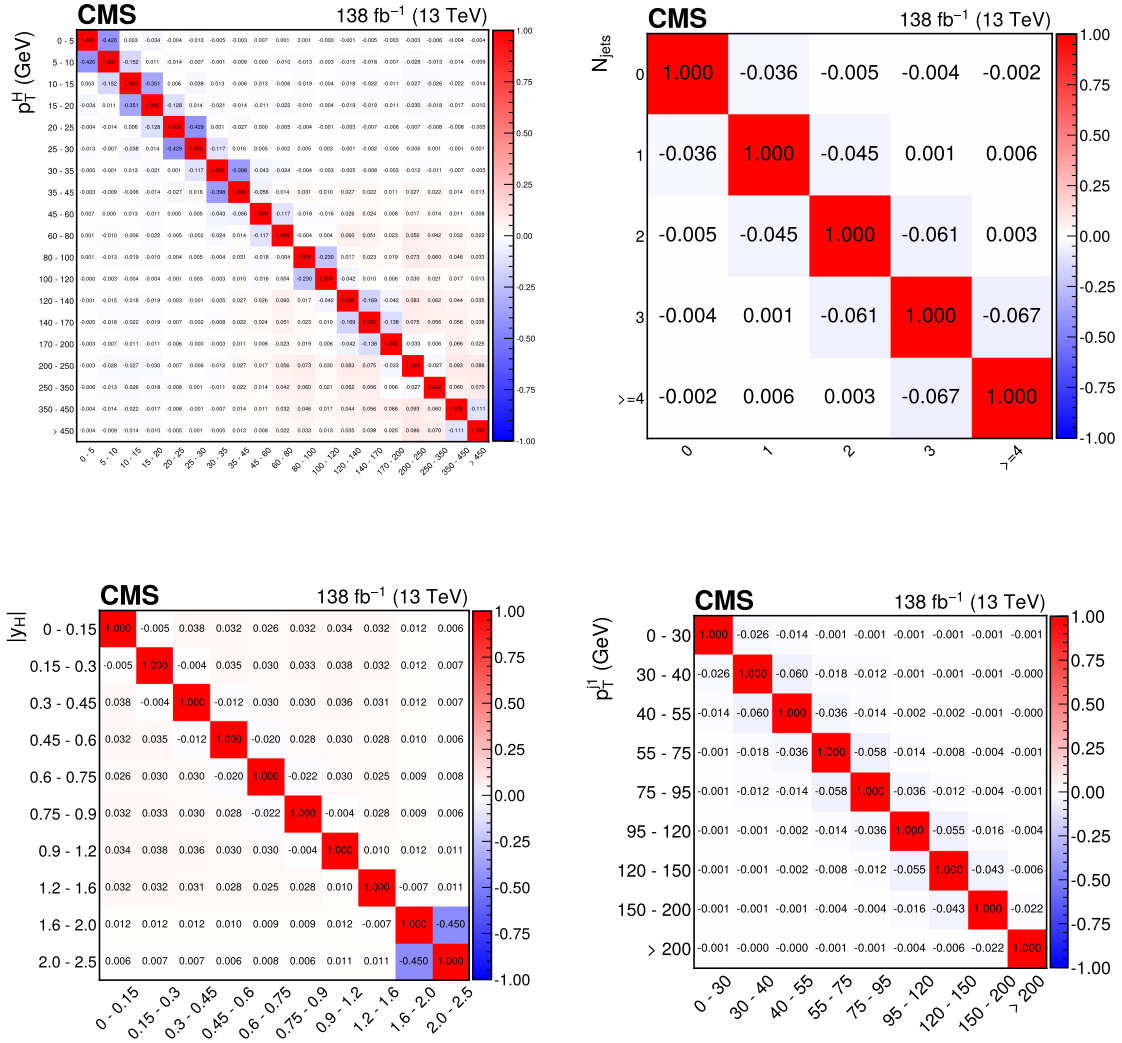

Figure 16. Bin-to-bin correlation matrices for the $p_{\mathrm{T}}^{\mathrm{H}}$ (upper left), N_{jets} (upper right), $|y_{\mathrm{H}}|$ (lower left), and $p_{\mathrm{T}}^{\mathrm{j_1}}$ (lower right) spectra.

JHEP04(2026)093

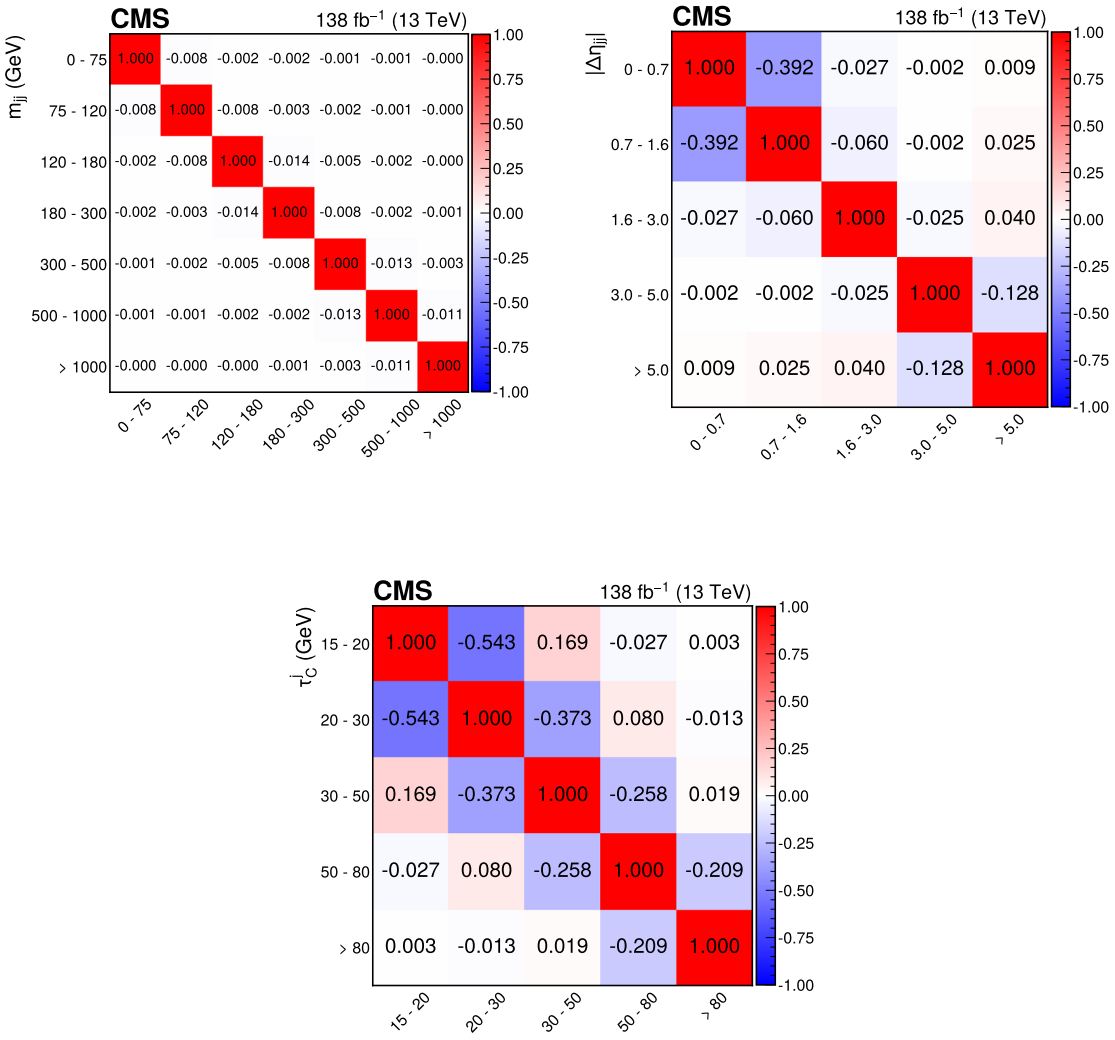

Figure 17. Bin-to-bin correlation matrices for the m_{jj} (upper left), $|\Delta\eta_{jj}|$ (upper right) and τ_C^j (lower) spectra.

JHEP04(2026)093

C $\Delta\phi_{jj}$ SMEFT scans

Figure 18 shows the two-dimensional scans for the c_{HG}-$\tilde{c}_{HG}$, c_{HB}-$\tilde{c}_{HB}$, c_{HW}-$\tilde{c}_{HW}$, and c_{HWB}-$\tilde{c}_{HWB}$ pairs with $\Delta\phi_{jj}$ spectra in $H \to \gamma\gamma$ and $H \to ZZ^{(*)} \to 4\ell$.

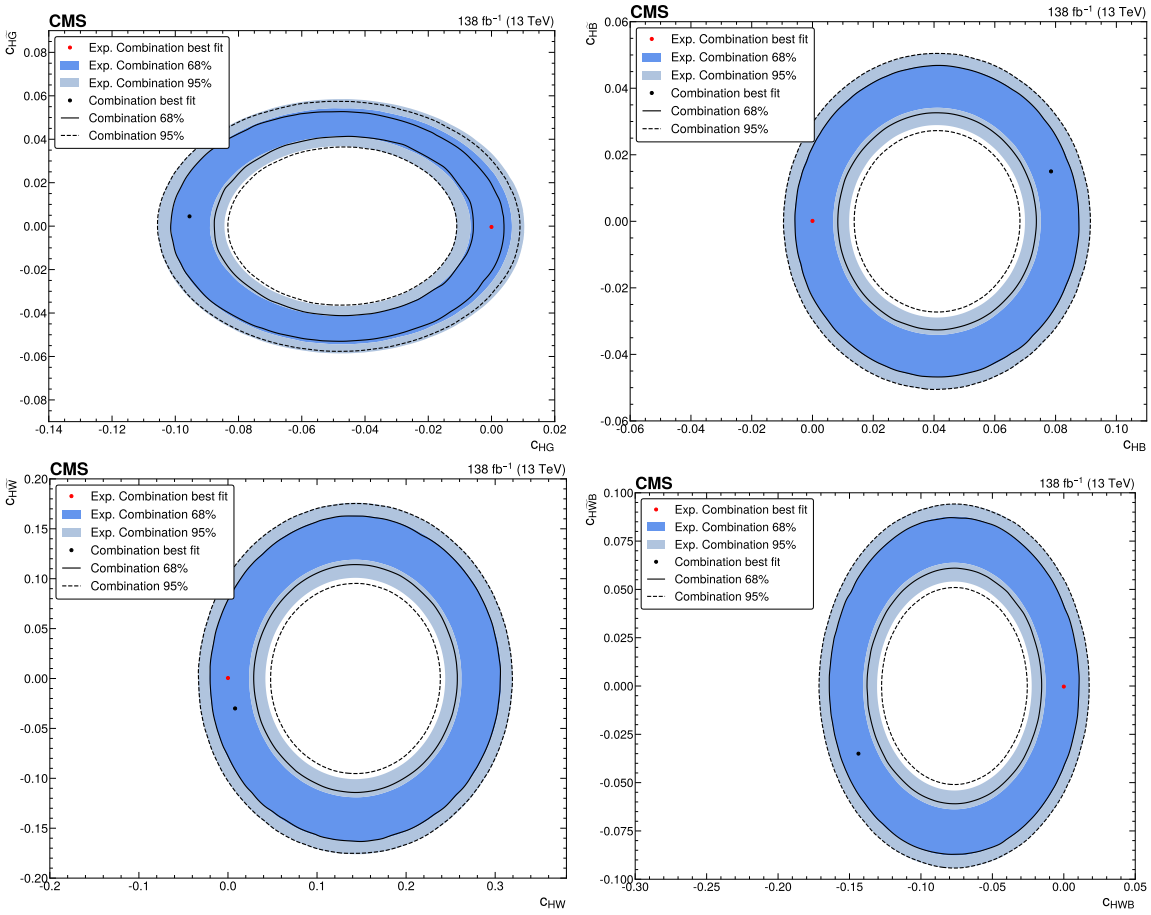

Figure 18. Two-dimensional scans for the c_{HG}-$\tilde{c}_{HG}$ (upper left), c_{HB}-$\tilde{c}_{HB}$ (upper right), c_{HW}-$\tilde{c}_{HW}$ (lower left), and c_{HWB}-$\tilde{c}_{HWB}$ (lower right) pairs with $\Delta\phi_{jj}$ spectra in $H \to \gamma\gamma$ and $H \to ZZ^{(*)} \to 4\ell$.

JHEP04(2026)093

D SMEFT scans to eigenvectors

Figures 19–21 show the observed and expected profile likelihood scans for the first ten eigenvectors obtained from the PCA.

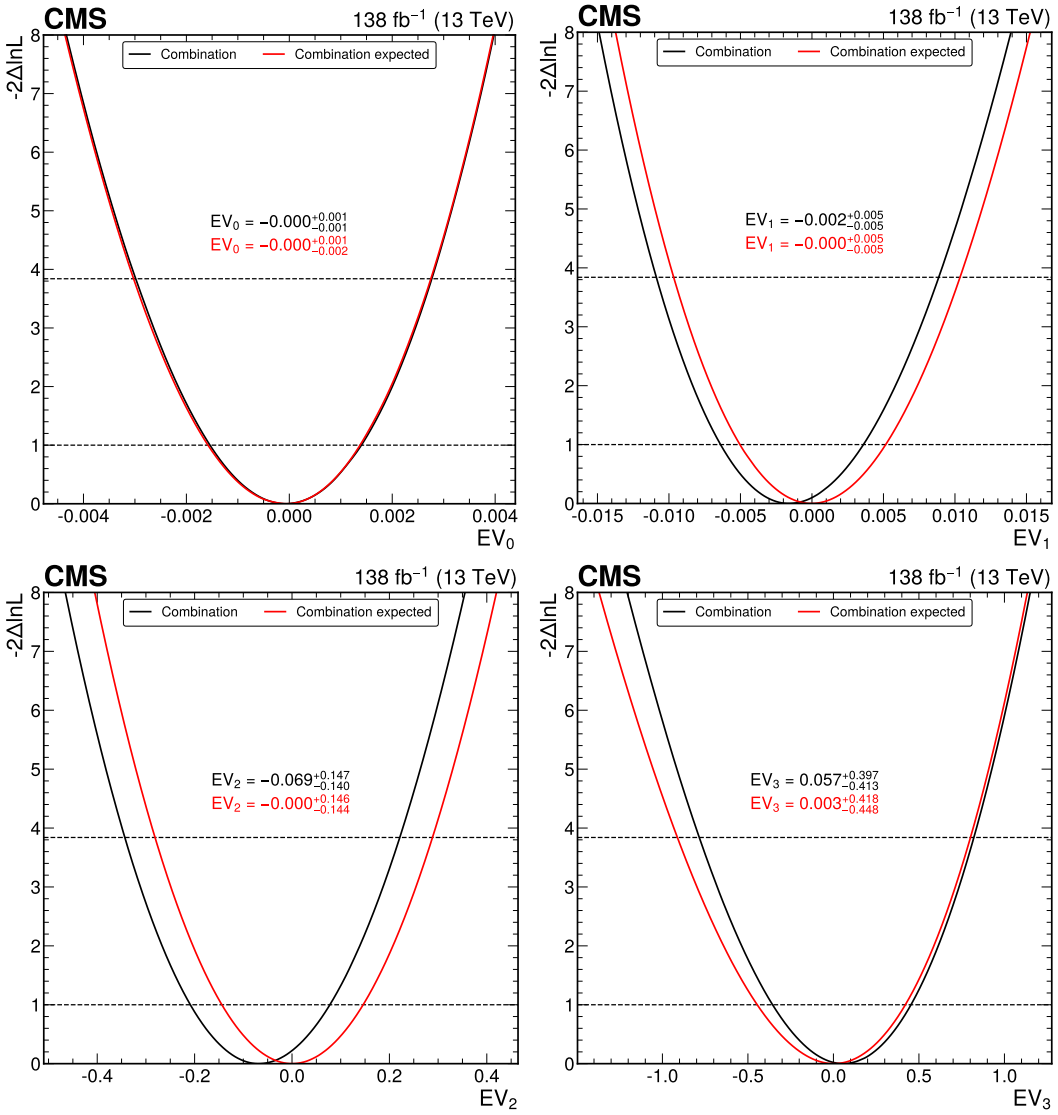

Figure 19. Observed and expected profile likelihood scans for eigenvectors 0 to 3.

JHEP04(2026)093

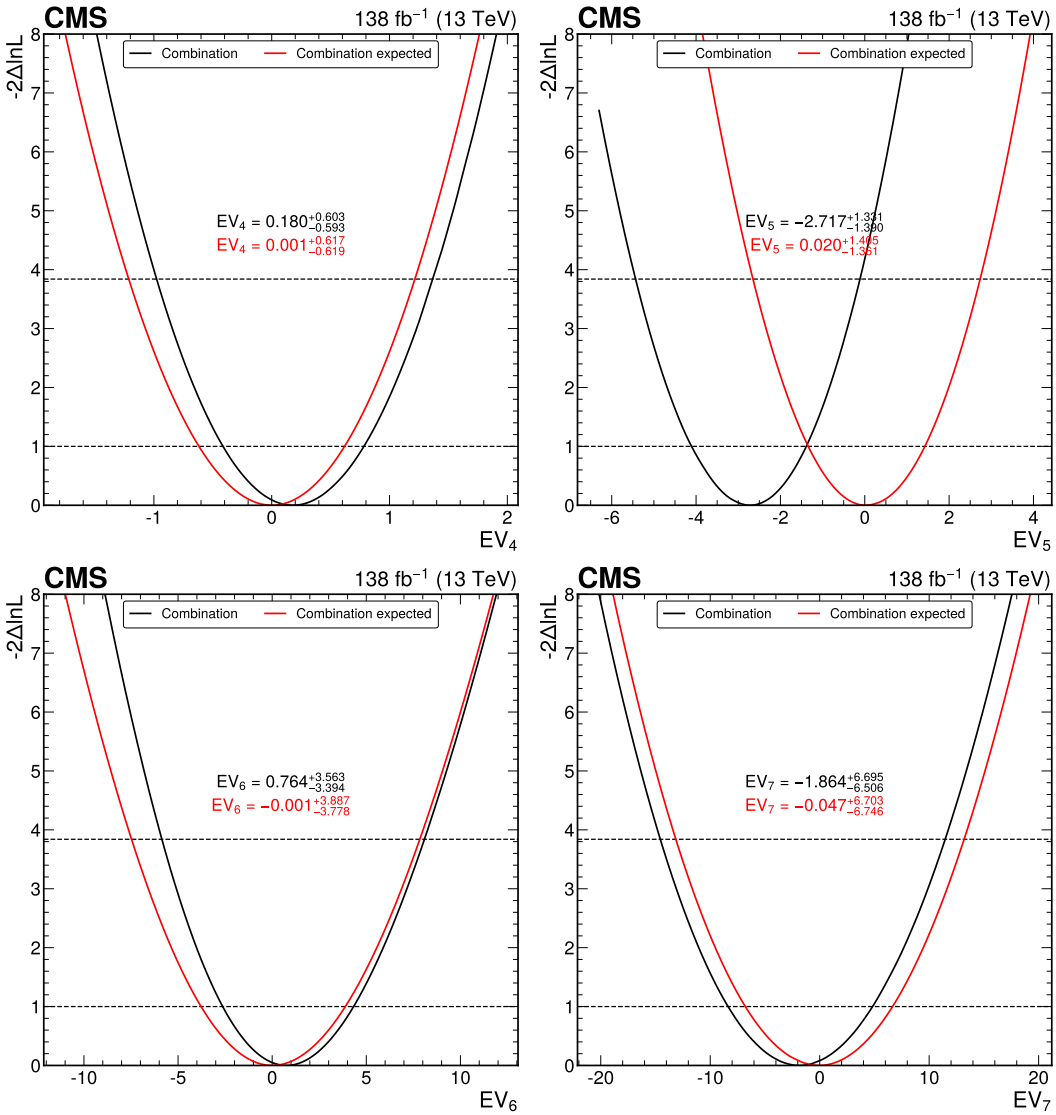

Figure 20. Observed and expected profile likelihood scans for eigenvectors 4 to 7.

JHEP04(2026)093

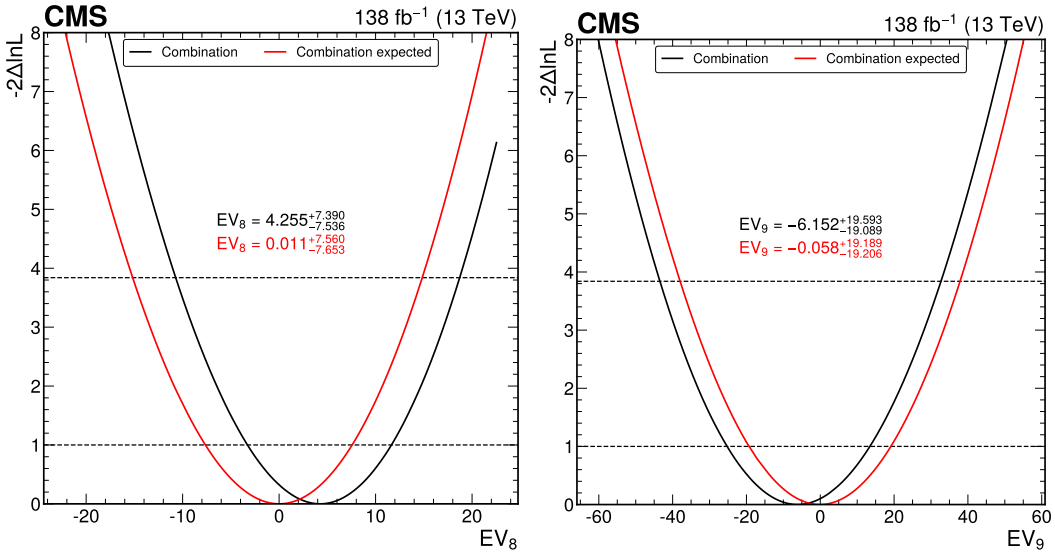

Figure 21. Observed and expected profile likelihood scans for eigenvectors 8 and 9.

Data Availability Statement. Release and preservation of data used by the CMS Collaboration as the basis for publications is guided by the CMS data preservation, re-use and open access policy.

Code Availability Statement. The CMS core software is publicly available on GitHub.

References

[1] CMS collaboration, *Observation of a New Boson at a Mass of 125 GeV with the CMS Experiment at the LHC*, *Phys. Lett. B* **716** (2012) 30 [arXiv:1207.7235] [INSPIRE].

[2] CMS collaboration, *Observation of a New Boson with Mass Near 125 GeV in pp Collisions at $\sqrt{s} = 7$ and 8 TeV*, *JHEP* **06** (2013) 081 [arXiv:1303.4571] [INSPIRE].

[3] ATLAS collaboration, *Observation of a new particle in the search for the Standard Model Higgs boson with the ATLAS detector at the LHC*, *Phys. Lett. B* **716** (2012) 1 [arXiv:1207.7214] [INSPIRE].

[4] CMS collaboration, *Precision luminosity measurement in proton-proton collisions at $\sqrt{s} = 13$ TeV in 2015 and 2016 at CMS*, *Eur. Phys. J. C* **81** (2021) 800 [arXiv:2104.01927] [INSPIRE].

[5] CMS collaboration, *Measurement of the Higgs boson inclusive and differential fiducial production cross sections in the diphoton decay channel with pp collisions at $\sqrt{s} = 13$ TeV*, *JHEP* **07** (2023) 091 [arXiv:2208.12279] [INSPIRE].

[6] CMS collaboration, *Measurements of inclusive and differential cross sections for the Higgs boson production and decay to four-leptons in proton-proton collisions at $\sqrt{s} = 13$ TeV*, *JHEP* **08** (2023) 040 [arXiv:2305.07532] [INSPIRE].

JHEP04(2026)093

[7] CMS collaboration, *Measurement of the inclusive and differential Higgs boson production cross sections in the leptonic WW decay mode at $\sqrt{s} = 13$ TeV*, *JHEP* **03** (2021) 003 [arXiv:2007.01984] [INSPIRE].

[8] CMS collaboration, *Measurement of the inclusive and differential Higgs boson production cross sections in the decay mode to a pair of τ leptons in pp collisions at $\sqrt{s} = 13$ TeV*, *Phys. Rev. Lett.* **128** (2022) 081805 [arXiv:2107.11486] [INSPIRE].

[9] CMS collaboration, *Measurement of the production cross section of a Higgs boson with large transverse momentum in its decays to a pair of τ leptons in proton-proton collisions at $\sqrt{s} = 13$ TeV*, *Phys. Lett. B* **857** (2024) 138964 [arXiv:2403.20201] [INSPIRE].

[10] S. Gangal, M. Stahlhofen and F.J. Tackmann, *Rapidity-Dependent Jet Vetoes*, *Phys. Rev. D* **91** (2015) 054023 [arXiv:1412.4792] [INSPIRE].

[11] LHC Higgs Cross Section Working Group collaboration, *Handbook of LHC Higgs Cross Sections: 3. Higgs Properties*, arXiv:1307.1347 [DOI:10.5170/CERN-2013-004] [INSPIRE].

[12] LHC Higgs Cross Section Working Group collaboration, *LHC HXSWG interim recommendations to explore the coupling structure of a Higgs-like particle*, arXiv:1209.0040 [INSPIRE].

[13] B. Grzadkowski, M. Iskrzynski, M. Misiak and J. Rosiek, *Dimension-Six Terms in the Standard Model Lagrangian*, *JHEP* **10** (2010) 085 [arXiv:1008.4884] [INSPIRE].

[14] CMS collaboration, *Measurement and interpretation of differential cross sections for Higgs boson production at $\sqrt{s} = 13$ TeV*, *Phys. Lett. B* **792** (2019) 369 [arXiv:1812.06504] [INSPIRE].

[15] HEPData record for this analysis, (2025) DOI:10.17182/hepdata.156816.

[16] ATLAS collaboration, *Measurements of the Higgs boson inclusive and differential fiducial cross-sections in the diphoton decay channel with pp collisions at $\sqrt{s} = 13$ TeV with the ATLAS detector*, *JHEP* **08** (2022) 027 [arXiv:2202.00487] [INSPIRE].

[17] ATLAS collaboration, *Interpretations of the ATLAS measurements of Higgs boson production and decay rates and differential cross-sections in pp collisions at $\sqrt{s} = 13$ TeV*, *JHEP* **11** (2024) 097 [arXiv:2402.05742] [INSPIRE].

[18] CMS collaboration, *Development of the CMS detector for the CERN LHC Run 3*, 2024 *JINST* **19** P05064 [arXiv:2309.05466] [INSPIRE].

[19] LHC Higgs Cross Section Working Group collaboration, *Handbook of LHC Higgs Cross Sections: 4. Deciphering the Nature of the Higgs Sector*, *CERN Yellow Rep. Monogr.* **2** (2017) 1 [arXiv:1610.07922] [INSPIRE].

[20] CMS collaboration, *The CMS statistical analysis and combination tool: COMBINE*, *Comput. Softw. Big Sci.* **8** (2024) 19 [arXiv:2404.06614] [INSPIRE].

[21] P. Nason, *A new method for combining NLO QCD with shower Monte Carlo algorithms*, *JHEP* **11** (2004) 040 [hep-ph/0409146] [INSPIRE].

[22] S. Frixione, P. Nason and C. Oleari, *Matching NLO QCD computations with Parton Shower simulations: the POWHEG method*, *JHEP* **11** (2007) 070 [arXiv:0709.2092] [INSPIRE].

[23] S. Alioli, P. Nason, C. Oleari and E. Re, *A general framework for implementing NLO calculations in shower Monte Carlo programs: the POWHEG BOX*, *JHEP* **06** (2010) 043 [arXiv:1002.2581] [INSPIRE].

JHEP04(2026)093

[24] E. Bagnaschi, G. Degrassi, P. Slavich and A. Vicini, *Higgs production via gluon fusion in the POWHEG approach in the SM and in the MSSM*, *JHEP* **02** (2012) 088 [arXiv:1111.2854] [INSPIRE].

[25] K. Hamilton, P. Nason, E. Re and G. Zanderighi, *NNLOPS simulation of Higgs boson production*, *JHEP* **10** (2013) 222 [arXiv:1309.0017] [INSPIRE].

[26] K. Hamilton, P. Nason and G. Zanderighi, *MINLO: Multi-Scale Improved NLO*, *JHEP* **10** (2012) 155 [arXiv:1206.3572] [INSPIRE].

[27] A. Kardos, P. Nason and C. Oleari, *Three-jet production in POWHEG*, *JHEP* **04** (2014) 043 [arXiv:1402.4001] [INSPIRE].

[28] F. Bishara, U. Haisch, P.F. Monni and E. Re, *Constraining Light-Quark Yukawa Couplings from Higgs Distributions*, *Phys. Rev. Lett.* **118** (2017) 121801 [arXiv:1606.09253] [INSPIRE].

[29] M. Grazzini, A. Ilnicka, M. Spira and M. Wiesemann, *Effective Field Theory for Higgs properties parametrisation: the transverse momentum spectrum case*, in the proceedings of the *52nd Rencontres de Moriond on QCD and High Energy Interactions*, La Thuile, Italy, March 25 – April 01 (2017) [arXiv:1705.05143] [INSPIRE].

[30] M. Grazzini, A. Ilnicka, M. Spira and M. Wiesemann, *Modeling BSM effects on the Higgs transverse-momentum spectrum in an EFT approach*, *JHEP* **03** (2017) 115 [arXiv:1612.00283] [INSPIRE].

[31] I. Brivio, *SMEFTsim 3.0 — a practical guide*, *JHEP* **04** (2021) 073 [arXiv:2012.11343] [INSPIRE].

[32] C. Degrande et al., *Automated one-loop computations in the standard model effective field theory*, *Phys. Rev. D* **103** (2021) 096024 [arXiv:2008.11743] [INSPIRE].

[33] S. Dawson and P.P. Giardino, *Electroweak corrections to Higgs boson decays to $\gamma\gamma$ and W^+W^- in standard model EFT*, *Phys. Rev. D* **98** (2018) 095005 [arXiv:1807.11504] [INSPIRE].

[34] G. Brooijmans et al., *Les Houches 2019 Physics at TeV Colliders: New Physics Working Group Report*, in the proceedings of the *11th Les Houches Workshop on Physics at TeV Colliders: PhysTeV Les Houches*, Les Houches, France, June 10–28 (2019) [arXiv:2002.12220] [INSPIRE].

[35] J. Alwall et al., *The automated computation of tree-level and next-to-leading order differential cross sections, and their matching to parton shower simulations*, *JHEP* **07** (2014) 079 [arXiv:1405.0301] [INSPIRE].

[36] T. Sjöstrand et al., *An introduction to PYTHIA 8.2*, *Comput. Phys. Commun.* **191** (2015) 159 [arXiv:1410.3012] [INSPIRE].

[37] C. Bierlich et al., *Robust Independent Validation of Experiment and Theory: Rivet version 3*, *SciPost Phys.* **8** (2020) 026 [arXiv:1912.05451] [INSPIRE].

[38] G. Cowan, K. Cranmer, E. Gross and O. Vitells, *Asymptotic formulae for likelihood-based tests of new physics*, *Eur. Phys. J. C* **71** (2011) 1554 [*Erratum ibid.* **73** (2013) 2501] [arXiv:1007.1727] [INSPIRE].

JHEP04(2026)093

The CMS collaboration

V. Chekhovsky[1], A. Hayrapetyan[1], V. Makarenko[1], A. Tumasyan[1,a], W. Adam[2], J.W. Andrejkovic[2], L. Benato[2], T. Bergauer[2], S. Chatterjee[2], K. Damanakis[2], M. Dragicevic[2], P.S. Hussain[2], M. Jeitler[2,b], N. Krammer[2], A. Li[2], D. Liko[2], I. Mikulec[2], J. Schieck[2,b], D. Schwarz[2], R. Schöfbeck[2,b], M. Sonawane[2], W. Waltenberger[2], C.-E. Wulz[2,b], T. Janssen[3], H. Kwon[3], T. Van Laer[3], P. Van Mechelen[3], N. Breugelmans[4], J. D'Hondt[4], S. Dansana[4], A. De Moor[4], M. Delcourt[4], F. Heyen[4], Y. Hong[4], S. Lowette[4], I. Makarenko[4], D. Müller[4], S. Tavernier[4], M. Tytgat[4,c], G.P. Van Onsem[4], S. Van Putte[4], D. Vannerom[4], B. Bilin[5], B. Clerbaux[5], A.K. Das[5], I. De Bruyn[5], G. De Lentdecker[5], H. Evard[5], L. Favart[5], P. Gianneios[5], A. Khalilzadeh[5], F.A. Khan[5], A. Malara[5], M.A. Shahzad[5], L. Thomas[5], M. Vanden Bemden[5], C. Vander Velde[5], P. Vanlaer[5], M. De Coen[6], D. Dobur[6], G. Gokbulut[6], J. Knolle[6], L. Lambrecht[6], D. Marckx[6], K. Skovpen[6], N. Van Den Bossche[6], J. van der Linden[6], J. Vandenbroeck[6], L. Wezenbeek[6], S. Bein[7], A. Benecke[7], A. Bethani[7], G. Bruno[7], C. Caputo[7], J. De Favereau De Jeneret[7], C. Delaere[7], I.S. Donertas[7], A. Giammanco[7], A.O. Guzel[7], Sa. Jain[7], V. Lemaitre[7], J. Lidrych[7], P. Mastrapasqua[7], T.T. Tran[7], S. Turkcapar[7], G.A. Alves[8], E. Coelho[8], G. Correia Silva[8], C. Hensel[8], T. Menezes De Oliveira[8], C. Mora Herrera[8,d], P. Rebello Teles[8], M. Soeiro[8], E.J. Tonelli Manganote[8,e], A. Vilela Pereira[8,d], W.L. Aldá Júnior[9], M. Barroso Ferreira Filho[9], H. Brandao Malbouisson[9], W. Carvalho[9], J. Chinellato[9,f], E.M. Da Costa[9], G.G. Da Silveira[9,g], D. De Jesus Damiao[9], S. Fonseca De Souza[9], R. Gomes De Souza[9], T. Laux Kuhn[9,g], M. Macedo[9], J. Martins[9], K. Mota Amarilo[9], L. Mundim[9], H. Nogima[9], J.P. Pinheiro[9], A. Santoro[9], A. Sznajder[9], M. Thiel[9], C.A. Bernardes[10,g], L. Calligaris[10], E.M. Gregores[10], I. Maietto Silverio[10], P.G. Mercadante[10], S.F. Novaes[10], B. Orzari[10], Sandra S. Padula[10], V. Scheurer[10], T.R. Fernandez Perez Tomei[10], A. Aleksandrov[11], G. Antchev[11], R. Hadjiiska[11], P. Iaydjiev[11], M. Misheva[11], M. Shopova[11], G. Sultanov[11], A. Dimitrov[12], L. Litov[12], B. Pavlov[12], P. Petkov[12], A. Petrov[12], E. Shumka[12], S. Keshri[13], D. Laroze[13], S. Thakur[13], T. Cheng[14], T. Javaid[14], L. Yuan[14], Z. Hu[15], Z. Liang[15], J. Liu[15], G.M. Chen[16,h], H.S. Chen[16,h], M. Chen[16,h], F. Iemmi[16], C.H. Jiang[16], A. Kapoor[16,i], H. Liao[16], Z.-A. Liu[16,j], R. Sharma[16,k], J.N. Song[16,j], J. Tao[16], C. Wang[16,h], J. Wang[16], Z. Wang[16,h], H. Zhang[16], J. Zhao[16], A. Agapitos[17], Y. Ban[17], A. Carvalho Antunes De Oliveira[17], S. Deng[17], B. Guo[17], C. Jiang[17], A. Levin[17], C. Li[17], Q. Li[17], Y. Mao[17], S. Qian[17], S.J. Qian[17], X. Qin[17], X. Sun[17], D. Wang[17], H. Yang[17], Y. Zhao[17], C. Zhou[17], S. Yang[18], Z. You[19], K. Jaffel[20], N. Lu[20], G. Bauer[21,l], B. Li[21,m], H. Wang[21], K. Yi[21,n], J. Zhang[21], Y. Li[22], Z. Lin[23], C. Lu[23], M. Xiao[23], C. Avila[24], D.A. Barbosa Trujillo[24], A. Cabrera[24], C. Florez[24], J. Fraga[24], J.A. Reyes Vega[24], J. Jaramillo[25], C. Rendón[25], M. Rodriguez[25], A.A. Ruales Barbosa[25], J.D. Ruiz Alvarez[25], D. Giljanovic[26], N. Godinovic[26], D. Lelas[26], A. Sculac[26], M. Kovac[27], A. Petkovic[27], T. Sculac[27], P. Bargassa[28], V. Brigljevic[28], B.K. Chitroda[28], D. Ferencek[28], K. Jakovcic[28], A. Starodumov[28,o], T. Susa[28], A. Attikis[29], K. Christoforou[29], A. Hadjiagapiou[29], C. Leonidou[29], J. Mousa[29], C. Nicolaou[29], L. Paizanos[29], F. Ptochos[29], P.A. Razis[29], H. Rykaczewski[29], H. Saka[29], A. Stepennov[29], M. Finger[30], M. Finger Jr.[30], A. Kveton[30],

JHEP04(2026)093

E. Ayala[31], E. Carrera Jarrin[32], B. El-mahdy[33], S. Khalil[33,p], E. Salama[33,q,r], M.A. Mahmoud[34], M. Abdullah Al-Mashad[34], K. Ehataht[35], M. Kadastik[35], T. Lange[35], C. Nielsen[35], J. Pata[35], M. Raidal[35], L. Tani[35], C. Veelken[35], K. Osterberg[36], M. Voutilainen[36], N. Bin Norjoharuddeen[37], E. Brücken[37], F. Garcia[37], P. Inkaew[37], K.T.S. Kallonen[37], T. Lampén[37], K. Lassila-Perini[37], S. Lehti[37], T. Lindén[37], M. Myllymäki[37], M.m. Rantanen[37], J. Tuominiemi[37], H. Kirschenmann[38], P. Luukka[38], H. Petrow[38], M. Besancon[39], F. Couderc[39], M. Dejardin[39], D. Denegri[39], J.L. Faure[39], F. Ferri[39], S. Ganjour[39], P. Gras[39], G. Hamel de Monchenault[39], M. Kumar[39], V. Lohezic[39], J. Malcles[39], F. Orlandi[39], L. Portales[39], A. Rosowsky[39], M.Ö. Sahin[39], A. Savoy-Navarro[39,s], P. Simkina[39], M. Titov[39], M. Tornago[39], F. Beaudette[40], G. Boldrini[40], P. Busson[40], A. Cappati[40], C. Charlot[40], M. Chiusi[40], T.D. Cuisset[40], F. Damas[40], O. Davignon[40], A. De Wit[40], I.T. Ehle[40], B.A. Fontana Santos Alves[40], S. Ghosh[40], A. Gilbert[40], R. Granier de Cassagnac[40], B. Harikrishnan[40], L. Kalipoliti[40], G. Liu[40], M. Manoni[40], M. Nguyen[40], S. Obraztsov[40], C. Ochando[40], R. Salerno[40], J.B. Sauvan[40], Y. Sirois[40], G. Sokmen[40], L. Urda Gómez[40], E. Vernazza[40], A. Zabi[40], A. Zghiche[40], J.-L. Agram[41,t], J. Andrea[41], D. Bloch[41], J.-M. Brom[41], E.C. Chabert[41], C. Collard[41], S. Falke[41], U. Goerlach[41], R. Haeberle[41], A.-C. Le Bihan[41], M. Meena[41], O. Poncet[41], G. Saha[41], M.A. Sessini[41], P. Van Hove[41], P. Vaucelle[41], A. Di Florio[42], D. Amram[43], S. Beauceron[43], B. Blancon[43], G. Boudoul[43], N. Chanon[43], D. Contardo[43], P. Depasse[43], C. Dozen[43,u], H. El Mamouni[43], J. Fay[43], S. Gascon[43], M. Gouzevitch[43], C. Greenberg[43], G. Grenier[43], B. Ille[43], E. Jourd'huy[43], I.B. Laktineh[43], M. Lethuillier[43], L. Mirabito[43], S. Perries[43], A. Purohit[43], M. Vander Donckt[43], P. Verdier[43], J. Xiao[43], A. Khvedelidze[44,v], I. Lomidze[44], Z. Tsamalaidze[44,v], V. Botta[45], S. Consuegra Rodríguez[45], L. Feld[45], K. Klein[45], M. Lipinski[45], D. Meuser[45], A. Pauls[45], D. Pérez Adán[45], N. Röwert[45], M. Teroerde[45], S. Diekmann[46], A. Dodonova[46], N. Eich[46], D. Eliseev[46], F. Engelke[46], J. Erdmann[46], M. Erdmann[46], B. Fischer[46], T. Hebbeker[46], K. Hoepfner[46], F. Ivone[46], A. Jung[46], N. Kumar[46], M.y. Lee[46], F. Mausolf[46], M. Merschmeyer[46], A. Meyer[46], F. Nowotny[46], A. Pozdnyakov[46], Y. Rath[46], W. Redjeb[46], F. Rehm[46], H. Reithler[46], V. Sarkisovi[46], A. Schmidt[46], C. Seth[46], A. Sharma[46], J.L. Spah[46], F. Torres Da Silva De Araujo[46,w], S. Wiedenbeck[46], S. Zaleski[46], C. Dziwok[47], G. Flügge[47], T. Kress[47], A. Nowack[47], O. Pooth[47], A. Stahl[47], T. Ziemons[47], A. Zotz[47], H. Aarup Petersen[48], M. Aldaya Martin[48], J. Alimena[48], S. Amoroso[48], Y. An[48], J. Bach[48], S. Baxter[48], M. Bayatmakou[48], H. Becerril Gonzalez[48], O. Behnke[48], A. Belvedere[48], F. Blekman[48,x], K. Borras[48,y], A. Campbell[48], A. Cardini[48], F. Colombina[48], M. De Silva[48], G. Eckerlin[48], D. Eckstein[48], L.I. Estevez Banos[48], E. Gallo[48,x], A. Geiser[48], V. Guglielmi[48], M. Guthoff[48], A. Hinzmann[48], L. Jeppe[48], B. Kaech[48], M. Kasemann[48], C. Kleinwort[48], R. Kogler[48], M. Komm[48], D. Krücker[48], W. Lange[48], D. Leyva Pernia[48], K. Lipka[48,z], W. Lohmann[48,aa], F. Lorkowski[48], R. Mankel[48], I.-A. Melzer-Pellmann[48], M. Mendizabal Morentin[48], A.B. Meyer[48], G. Milella[48], K. Moral Figueroa[48], A. Mussgiller[48], L.P. Nair[48], J. Niedziela[48], A. Nürnberg[48], J. Park[48], E. Ranken[48], A. Raspereza[48], D. Rastorguev[48], L. Rygaard[48], J. Rübenach[48], M. Scham[48,ab,ac], S. Schnake[48,y], C. Schwanenberger[48,x], P. Schütze[48], D. Selivanova[48], K. Sharko[48],

JHEP04(2026)093

M. Shchedrolosiev[48], D. Stafford[48], F. Vazzoler[48], A. Ventura Barroso[48], R. Walsh[48], D. Wang[48], Q. Wang[48], K. Wichmann[48], L. Wiens[48,y], C. Wissing[48], Y. Yang[48], S. Zakharov[48], A. Zimermmane Castro Santos[48], A. Albrecht[49], S. Albrecht[49], M. Antonello[49], S. Bollweg[49], M. Bonanomi[49], P. Connor[49], K. El Morabit[49], Y. Fischer[49], E. Garutti[49], A. Grohsjean[49], J. Haller[49], D. Hundhausen[49], H.R. Jabusch[49], G. Kasieczka[49], P. Keicher[49], R. Klanner[49], W. Korcari[49], T. Kramer[49], C.c. Kuo[49], V. Kutzner[49], F. Labe[49], J. Lange[49], A. Lobanov[49], C. Matthies[49], L. Moureaux[49], M. Mrowietz[49], A. Nigamova[49], Y. Nissan[49], A. Paasch[49], K.J. Pena Rodriguez[49], T. Quadfasel[49], B. Raciti[49], M. Rieger[49], D. Savoiu[49], J. Schindler[49], P. Schleper[49], M. Schröder[49], J. Schwandt[49], M. Sommerhalder[49], H. Stadie[49], G. Steinbrück[49], A. Tews[49], B. Wiederspan[49], M. Wolf[49], S. Brommer[50], E. Butz[50], Y.M. Chen[50], T. Chwalek[50], A. Dierlamm[50], G.G. Dincer[50], U. Elicabuk[50], N. Faltermann[50], M. Giffels[50], A. Gottmann[50], F. Hartmann[50,ad], R. Hofsaess[50], M. Horzela[50], U. Husemann[50], J. Kieseler[50], M. Klute[50], O. Lavoryk[50], J.M. Lawhorn[50], M. Link[50], A. Lintuluoto[50], S. Maier[50], M. Mormile[50], Th. Müller[50], M. Neukum[50], M. Oh[50], E. Pfeffer[50], M. Presilla[50], G. Quast[50], K. Rabbertz[50], B. Regnery[50], R. Schmieder[50], N. Shadskiy[50], I. Shvetsov[50], H.J. Simonis[50], L. Sowa[50], L. Stockmeier[50], K. Tauqeer[50], M. Toms[50], B. Topko[50], N. Trevisani[50], T. Voigtländer[50], R.F. Von Cube[50], J. Von Den Driesch[50], M. Wassmer[50], S. Wieland[50], F. Wittig[50], R. Wolf[50], X. Zuo[50], G. Anagnostou[51], G. Daskalakis[51], A. Kyriakis[51], A. Papadopoulos[51,ad], A. Stakia[51], G. Melachroinos[52], Z. Painesis[52], I. Paraskevas[52], N. Saoulidou[52], K. Theofilatos[52], E. Tziaferi[52], K. Vellidis[52], I. Zisopoulos[52], G. Bakas[53], T. Chatzistavrou[53], G. Karapostoli[53], K. Kousouris[53], I. Papakrivopoulos[53], E. Siamarkou[53], G. Tsipolitis[53], I. Bestintzanos[54], I. Evangelou[54], C. Foudas[54], C. Kamtsikis[54], P. Katsoulis[54], P. Kokkas[54], P.G. Kosmoglou Kioseoglou[54], N. Manthos[54], I. Papadopoulos[54], J. Strologas[54], C. Hajdu[55], D. Horvath[55,ae,af], K. Márton[55], A.J. Rádl[55,ag], F. Sikler[55], V. Veszpremi[55], M. Csanád[56], K. Farkas[56], A. Fehérkuti[56,ah], M.M.A. Gadallah[56,ai], Á. Kadlecsik[56], P. Major[56], G. Pásztor[56], G.I. Veres[56], B. Ujvari[57], G. Zilizi[57], G. Bencze[58], S. Czellar[58], J. Molnar[58], Z. Szillasi[58], T. Csorgo[59,ah], F. Nemes[59,ah], T. Novak[59], S. Bansal[60], S.B. Beri[60], V. Bhatnagar[60], G. Chaudhary[60], S. Chauhan[60], N. Dhingra[60,aj], A. Kaur[60], A. Kaur[60], H. Kaur[60], M. Kaur[60], S. Kumar[60], T. Sheokand[60], J.B. Singh[60], A. Singla[60], A. Bhardwaj[61], A. Chhetri[61], B.C. Choudhary[61], A. Kumar[61], A. Kumar[61], M. Naimuddin[61], S. Saumya[61], K. Ranjan[61], M.K. Saini[61], S. Mukherjee[62], S. Baradia[63], S. Barman[63,ak], S. Bhattacharya[63], S. Das Gupta[63], S. Dutta[63], S. Dutta[63], S. Sarkar[63], M.M. Ameen[64], P.K. Behera[64], S.C. Behera[64], S. Chatterjee[64], G. Dash[64], P. Jana[64], P. Kalbhor[64], S. Kamble[64], J.R. Komaragiri[64,al], D. Kumar[64,al], T. Mishra[64], B. Parida[64,am], P.R. Pujahari[64], N.R. Saha[64], A.K. Sikdar[64], R.K. Singh[64], P. Verma[64], S. Verma[64], A. Vijay[64], S. Dugad[65], G.B. Mohanty[65], M. Shelake[65], P. Suryadevara[65], A. Bala[66], S. Banerjee[66], S. Bhowmik[66,an], R.M. Chatterjee[66], M. Guchait[66], Sh. Jain[66], A. Jaiswal[66], B.M. Joshi[66], S. Kumar[66], G. Majumder[66], K. Mazumdar[66], S. Parolia[66], A. Thachayath[66], S. Bahinipati[67,ao], C. Kar[67], D. Maity[67,ap], P. Mal[67], K. Naskar[67,ap], A. Nayak[67,ap], S. Nayak[67], K. Pal[67], R. Raturi[67], P. Sadangi[67], S.K. Swain[67], S. Varghese[67,ap], D. Vats[67,ap], S. Acharya[68,aq], A. Alpana[68], S. Dube[68], B. Gomber[68,aq],

JHEP04(2026)093

P. Hazarika[68], B. Kansal[68], A. Laha[68], B. Sahu[68,aq], S. Sharma[68], K.Y. Vaish[68], H. Bakhshiansohi[69,ar], A. Jafari[69,as], M. Zeinali[69,at], S. Bashiri[70], S. Chenarani[70,au], S.M. Etesami[70], Y. Hosseini[70], M. Khakzad[70], E. Khazaie[70], M. Mohammadi Najafabadi[70], S. Tizchang[70,av], M. Felcini[71], M. Grunewald[71], M. Abbrescia[72a,72b], A. Colaleo[72a,72b], D. Creanza[72a,72c], B. D'Anzi[72a,72b], N. De Filippis[72a,72c], M. De Palma[72a,72b], W. Elmetenawee[72a,72b,aw], N. Ferrara[72a,72b], L. Fiore[72a], G. Iaselli[72a,72c], L. Longo[72a], M. Louka[72a,72b], G. Maggi[72a,72c], M. Maggi[72a], I. Margjeka[72a], V. Mastrapasqua[72a,72b], S. My[72a,72b], S. Nuzzo[72a,72b], A. Pellecchia[72a,72b], A. Pompili[72a,72b], G. Pugliese[72a,72c], R. Radogna[72a,72b], D. Ramos[72a], A. Ranieri[72a], L. Silvestris[72a], F.M. Simone[72a,72c], A. Stamerra[72a,72b], Ü. Sözbilir[72a], D. Troiano[72a,72b], R. Venditti[72a,72b], P. Verwilligen[72a], A. Zaza[72a,72b], G. Abbiendi[73a], C. Battilana[73a,73b], D. Bonacorsi[73a,73b], P. Capiluppi[73a,73b], A. Castro[73a,73b,†], F.R. Cavallo[73a], M. Cuffiani[73a,73b], G.M. Dallavalle[73a], T. Diotalevi[73a,73b], F. Fabbri[73a], A. Fanfani[73a,73b], D. Fasanella[73a], P. Giacomelli[73a], L. Giommi[73a,73b], C. Grandi[73a], L. Guiducci[73a,73b], S. Lo Meo[73a,ax], M. Lorusso[73a,73b], L. Lunerti[73a], S. Marcellini[73a], G. Masetti[73a], F.L. Navarria[73a,73b], G. Paggi[73a,73b], A. Perrotta[73a], F. Primavera[73a,73b], A.M. Rossi[73a,73b], S. Rossi Tisbeni[73a,73b], T. Rovelli[73a,73b], G.P. Siroli[73a,73b], S. Costa[74a,74b,ay], A. Di Mattia[74a], A. Lapertosa[74a], R. Potenza[74a,74b], A. Tricomi[74a,74b,ay], P. Assiouras[75a], G. Barbagli[75a], G. Bardelli[75a,75b], M. Bartolini[75a,75b], B. Camaiani[75a,75b], A. Cassese[75a], R. Ceccarelli[75a], V. Ciulli[75a,75b], C. Civinini[75a], R. D'Alessandro[75a,75b], E. Focardi[75a,75b], T. Kello[75a], G. Latino[75a,75b], P. Lenzi[75a,75b], M. Lizzo[75a], M. Meschini[75a], S. Paoletti[75a], A. Papanastassiou[75a,75b], G. Sguazzoni[75a], L. Viliani[75a], L. Benussi[76], S. Colafranceschi[76], S. Meola[76,az], D. Piccolo[76], M. Alves Gallo Pereira[77a], F. Ferro[77a], E. Robutti[77a], S. Tosi[77a,77b], A. Benaglia[78a], F. Brivio[78a], F. Cetorelli[78a,78b], F. De Guio[78a,78b], M.E. Dinardo[78a,78b], P. Dini[78a], S. Gennai[78a], R. Gerosa[78a,78b], A. Ghezzi[78a,78b], P. Govoni[78a,78b], L. Guzzi[78a], G. Lavizzari[78a,78b], M.T. Lucchini[78a,78b], M. Malberti[78a], S. Malvezzi[78a], A. Massironi[78a], D. Menasce[78a], L. Moroni[78a], M. Paganoni[78a,78b], S. Palluotto[78a,78b], D. Pedrini[78a], A. Perego[78a,78b], B.S. Pinolini[78a], G. Pizzati[78a,78b], S. Ragazzi[78a,78b], T. Tabarelli de Fatis[78a,78b], S. Buontempo[79a], A. Cagnotta[79a,79b], F. Carnevali[79a,79b], N. Cavallo[79a,79c], F. Fabozzi[79a,79c], A.O.M. Iorio[79a,79b], L. Lista[79a,79b,ba], P. Paolucci[79a,ad], B. Rossi[79a], R. Ardino[80a], P. Azzi[80a], N. Bacchetta[80a,bb], M. Bellato[80a], M. Benettoni[80a], D. Bisello[80a,80b], P. Bortignon[80a], G. Bortolato[80a,80b], A.C.M. Bulla[80a], R. Carlin[80a,80b], P. Checchia[80a], T. Dorigo[80a,bc], F. Gasparini[80a,80b], U. Gasparini[80a,80b], S. Giorgetti[80a], E. Lusiani[80a], M. Margoni[80a,80b], J. Pazzini[80a,80b], P. Ronchese[80a,80b], R. Rossin[80a,80b], F. Simonetto[80a,80b], M. Tosi[80a,80b], A. Triossi[80a,80b], S. Ventura[80a], M. Zanetti[80a,80b], P. Zotto[80a,80b], A. Zucchetta[80a,80b], A. Braghieri[81a], S. Calzaferri[81a], D. Fiorina[81a], P. Montagna[81a,81b], M. Pelliccioni[81a], V. Re[81a], C. Riccardi[81a,81b], P. Salvini[81a], I. Vai[81a,81b], P. Vitulo[81a,81b], S. Ajmal[82a,82b], M.E. Ascioti[82a,82b], G.M. Bilei[82a], C. Carrivale[82a,82b], D. Ciangottini[82a,82b], L. Fanò[82a,82b], V. Mariani[82a,82b], M. Menichelli[82a], F. Moscatelli[82a,bd], A. Rossi[82a,82b], A. Santocchia[82a,82b], D. Spiga[82a], T. Tedeschi[82a,82b], C. Aimè[83a], C.A. Alexe[83a,83c], P. Asenov[83a,83b], P. Azzurri[83a], G. Bagliesi[83a], R. Bhattacharya[83a], L. Bianchini[83a,83b], T. Boccali[83a], E. Bossini[83a], D. Bruschini[83a,83c], R. Castaldi[83a], M.A. Ciocci[83a,83b],

JHEP04(2026)093

M. Cipriani[83a,83b], V. D'Amante[83a,83d], R. Dell'Orso[83a], S. Donato[83a,83b], A. Giassi[83a], F. Ligabue[83a,83c], A.C. Marini[83a,83b], D. Matos Figueiredo[83a], A. Messineo[83a,83b], S. Mishra[83a], V.K. Muraleedharan Nair Bindhu[83a,83b,ap], M. Musich[83a,83b], S. Nandan[83a], F. Palla[83a], A. Rizzi[83a,83b], G. Rolandi[83a,83c], S. Roy Chowdhury[83a], T. Sarkar[83a], A. Scribano[83a], P. Spagnolo[83a], F. Tenchini[83a,83b], R. Tenchini[83a], G. Tonelli[83a,83b], N. Turini[83a,83d], F. Vaselli[83a,83c], A. Venturi[83a], P.G. Verdini[83a], P. Barria[84a], C. Basile[84a,84b], F. Cavallari[84a], L. Cunqueiro Mendez[84a,84b], D. Del Re[84a,84b], E. Di Marco[84a,84b], M. Diemoz[84a], F. Errico[84a,84b], R. Gargiulo[84a,84b], E. Longo[84a,84b], L. Martikainen[84a,84b], J. Mijuskovic[84a,84b], G. Organtini[84a,84b], F. Pandolfi[84a], R. Paramatti[84a,84b], C. Quaranta[84a,84b], S. Rahatlou[84a,84b], C. Rovelli[84a], F. Santanastasio[84a,84b], L. Soffi[84a], V. Vladimirov[84a,84b], N. Amapane[85a,85b], R. Arcidiacono[85a,85c], S. Argiro[85a,85b], M. Arneodo[85a,85c], N. Bartosik[85a], R. Bellan[85a,85b], C. Biino[85a], C. Borca[85a,85b], N. Cartiglia[85a], M. Costa[85a,85b], R. Covarelli[85a,85b], N. Demaria[85a], L. Finco[85a], M. Grippo[85a,85b], B. Kiani[85a,85b], F. Legger[85a], F. Luongo[85a,85b], C. Mariotti[85a], L. Markovic[85a,85b], S. Maselli[85a], A. Mecca[85a,85b], L. Menzio[85a,85b], P. Meridiani[85a], E. Migliore[85a,85b], M. Monteno[85a], R. Mulargia[85a], M.M. Obertino[85a,85b], G. Ortona[85a], L. Pacher[85a,85b], N. Pastrone[85a], M. Ruspa[85a,85c], F. Siviero[85a,85b], V. Sola[85a,85b], A. Solano[85a,85b], A. Staiano[85a], C. Tarricone[85a,85b], D. Trocino[85a], G. Umoret[85a,85b], R. White[85a,85b], J. Babbar[86a,86b], S. Belforte[86a], V. Candelise[86a,86b], M. Casarsa[86a], F. Cossutti[86a], K. De Leo[86a], G. Della Ricca[86a,86b], S. Dogra[87], J. Hong[87], J. Kim[87], D. Lee[87], H. Lee[87], S.W. Lee[87], C.S. Moon[87], Y.D. Oh[87], M.S. Ryu[87], S. Sekmen[87], B. Tae[87], Y.C. Yang[87], M.S. Kim[88], G. Bak[89], P. Gwak[89], H. Kim[89], D.H. Moon[89], E. Asilar[90], J. Choi[90,be], D. Kim[90], T.J. Kim[90], J.A. Merlin[90], Y. Ryou[90], S. Choi[91], S. Han[91], B. Hong[91], K. Lee[91], K.S. Lee[91], S. Lee[91], J. Yoo[91], J. Goh[92], S. Yang[92], Y. Kang[93], H. S. Kim[93], Y. Kim[93], S. Lee[93], J. Almond[94], J.H. Bhyun[94], J. Choi[94], J. Choi[94], W. Jun[94], J. Kim[94], Y.W. Kim[94], S. Ko[94], H. Lee[94], J. Lee[94], J. Lee[94], B.H. Oh[94], S.B. Oh[94], H. Seo[94], U.K. Yang[94], I. Yoon[94], W. Jang[95], D.Y. Kang[95], S. Kim[95], B. Ko[95], J.S.H. Lee[95], Y. Lee[95], I.C. Park[95], Y. Roh[95], I.J. Watson[95], S. Ha[96], K. Hwang[96], B. Kim[96], K. Lee[96], H.D. Yoo[96], M. Choi[97], M.R. Kim[97], H. Lee[97], Y. Lee[97], I. Yu[97], T. Beyrouthy[98], Y. Gharbia[98], F. Alazemi[99], K. Dreimanis[100], A. Gaile[100], C. Munoz Diaz[100], D. Osite[100], G. Pikurs[100], A. Potrebko[100], M. Seidel[100], D. Sidiropoulos Kontos[100], N.R. Strautnieks[101], M. Ambrozas[102], A. Juodagalvis[102], A. Rinkevicius[102], G. Tamulaitis[102], I. Yusuff[103,bf], Z. Zolkapli[103], J.F. Benitez[104], A. Castaneda Hernandez[104], H.A. Encinas Acosta[104], L.G. Gallegos Maríñez[104], M. León Coello[104], J.A. Murillo Quijada[104], A. Sehrawat[104], L. Valencia Palomo[104], G. Ayala[105], H. Castilla-Valdez[105], H. Crotte Ledesma[105], E. De La Cruz-Burelo[105], I. Heredia-De La Cruz[105,bg], R. Lopez-Fernandez[105], J. Mejia Guisao[105], A. Sánchez Hernández[105], C. Oropeza Barrera[106], D.L. Ramirez Guadarrama[106], M. Ramírez García[106], I. Bautista[107], F.E. Neri Huerta[107], I. Pedraza[107], H.A. Salazar Ibarguen[107], C. Uribe Estrada[107], I. Bubanja[108], N. Raicevic[108], P.H. Butler[109], A. Ahmad[110], M.I. Asghar[110], A. Awais[110], M.I.M. Awan[110], H.R. Hoorani[110], W.A. Khan[110], V. Avati[111], A. Bellora[111], L. Forthomme[111], L. Grzanka[111], M. Malawski[111], K. Piotrzkowski[111], H. Bialkowska[112], M. Bluj[112],

JHEP04(2026)093

M. Górski[112], M. Kazana[112], M. Szleper[112], P. Zalewski[112], K. Bunkowski[113], K. Doroba[113], A. Kalinowski[113], M. Konecki[113], J. Krolikowski[113], A. Muhammad[113], P. Fokow[114], K. Pozniak[114], W. Zabolotny[114], M. Araujo[115], D. Bastos[115], C. Beirão Da Cruz E Silva[115], A. Boletti[115], M. Bozzo[115], T. Camporesi[115], G. Da Molin[115], P. Faccioli[115], M. Gallinaro[115], J. Hollar[115], N. Leonardo[115], G.B. Marozzo[115], A. Petrilli[115], M. Pisano[115], J. Seixas[115], J. Varela[115], J.W. Wulff[115], P. Adzic[116], P. Milenovic[116], D. Devetak[117], M. Dordevic[117], J. Milosevic[117], L. Nadderd[117], V. Rekovic[117], M. Stojanovic[117], J. Alcaraz Maestre[118], J.A. Brochero Cifuentes[118], M. Cepeda[118], M. Cerrada[118], N. Colino[118], B. De La Cruz[118], A. Delgado Peris[118], A. Escalante Del Valle[118], Cristina F. Bedoya[118], D. Fernández Del Val[118], J.P. Fernández Ramos[118], J. Flix[118], M.C. Fouz[118], O. Gonzalez Lopez[118], S. Goy Lopez[118], J.M. Hernandez[118], M.I. Josa[118], J. Llorente Merino[118], Oliver M. Carretero[118], C. Martin Perez[118], E. Martin Viscasillas[118], D. Moran[118], C. M. Morcillo Perez[118], Á. Navarro Tobar[118], C. Perez Dengra[118], J. Puerta Pelayo[118], A. Pérez-Calero Yzquierdo[118], I. Redondo[118], J. Sastre[118], J. Vazquez Escobar[118], J.F. de Trocóniz[119], B. Alvarez Gonzalez[120], J. Cuevas[120], J. Fernandez Menendez[120], S. Folgueras[120], I. Gonzalez Caballero[120], P. Leguina[120], E. Palencia Cortezon[120], J. Prado Pico[120], V. Rodríguez Bouza[120], A. Soto Rodríguez[120], A. Trapote[120], C. Vico Villalba[120], P. Vischia[120], S. Blanco Fernández[121], I.J. Cabrillo[121], A. Calderon[121], J. Duarte Campderros[121], M. Fernandez[121], G. Gomez[121], C. Lasaosa García[121], R. Lopez Ruiz[121], C. Martinez Rivero[121], P. Martinez Ruiz del Arbol[121], F. Matorras[121], P. Matorras Cuevas[121], E. Navarrete Ramos[121], J. Piedra Gomez[121], L. Scodellaro[121], I. Vila[121], J.M. Vizan Garcia[121], D.D.C. Wickramarathna[122], B. Kailasapathy[122,bh], W.G.D. Dharmaratna[123,bi], K. Liyanage[123], N. Perera[123], D. Abbaneo[124], C. Amendola[124], E. Auffray[124], J. Baechler[124], D. Barney[124], A. Bermúdez Martínez[124], M. Bianco[124], A.A. Bin Anuar[124], A. Bocci[124], L. Borgonovi[124], C. Botta[124], A. Bragagnolo[124], E. Brondolin[124], C.E. Brown[124], C. Caillol[124], G. Cerminara[124], N. Chernyavskaya[124], D. d'Enterria[124], A. Dabrowski[124], A. David[124], A. De Roeck[124], M.M. Defranchis[124], M. Deile[124], M. Dobson[124], G. Franzoni[124], W. Funk[124], S. Giani[124], D. Gigi[124], K. Gill[124], F. Glege[124], M. Glowacki[124], J. Hegeman[124], J.K. Heikkilä[124], B. Huber[124], V. Innocente[124], T. James[124], P. Janot[124], O. Kaluzinska[124], O. Karacheban[124,aa], G. Karathanasis[124], S. Laurila[124], P. Lecoq[124], E. Leutgeb[124], C. Lourenço[124], M. Magherini[124], L. Malgeri[124], M. Mannelli[124], M. Matthewman[124], A. Mehta[124], F. Meijers[124], S. Mersi[124], E. Meschi[124], M. Migliorini[124], V. Milosevic[124], F. Monti[124], F. Moortgat[124], M. Mulders[124], I. Neutelings[124], S. Orfanelli[124], F. Pantaleo[124], G. Petrucciani[124], A. Pfeiffer[124], M. Pierini[124], M. Pitt[124], H. Qu[124], D. Rabady[124], B. Ribeiro Lopes[124], F. Riti[124], M. Rovere[124], H. Sakulin[124], R. Salvatico[124], S. Sanchez Cruz[124], S. Scarfi[124], C. Schwick[124], M. Selvaggi[124], A. Sharma[124], K. Shchelina[124], P. Silva[124], P. Sphicas[124,bj], A.G. Stahl Leiton[124], A. Steen[124], S. Summers[124], D. Treille[124], P. Tropea[124], D. Walter[124], J. Wanczyk[124,bk], J. Wang[124], S. Wuchterl[124], P. Zehetner[124], P. Zejdl[124], W.D. Zeuner[124], T. Bevilacqua[125,bl], L. Caminada[125,bl], A. Ebrahimi[125], W. Erdmann[125], R. Horisberger[125], Q. Ingram[125],

JHEP04(2026)093

H.C. Kaestli[125], D. Kotlinski[125], C. Lange[125], M. Missiroli[125,bl], L. Noehte[125,bl], T. Rohe[125], A. Samalan[125], T.K. Aarrestad[126], M. Backhaus[126], G. Bonomelli[126], A. Calandri[126], C. Cazzaniga[126], K. Datta[126], P. De Bryas Dexmiers D'archiac[126,bk], A. De Cosa[126], G. Dissertori[126], M. Dittmar[126], M. Donegà[126], F. Eble[126], M. Galli[126], K. Gedia[126], F. Glessgen[126], C. Grab[126], T.G. Harte[126], D. Hits[126], N. Härringer[126], W. Lustermann[126], A.-M. Lyon[126], R.A. Manzoni[126], M. Marchegiani[126], L. Marchese[126], A. Mascellani[126,bk], F. Nessi-Tedaldi[126], F. Pauss[126], V. Perovic[126], S. Pigazzini[126], B. Ristic[126], R. Seidita[126], J. Steggemann[126,bk], A. Tarabini[126], D. Valsecchi[126], R. Wallny[126], C. Amsler[127,bm], P. Bärtschi[127], M.F. Canelli[127], K. Cormier[127], M. Huwiler[127], W. Jin[127], A. Jofrehei[127], B. Kilminster[127], S. Leontsinis[127], S.P. Liechti[127], A. Macchiolo[127], P. Meiring[127], F. Meng[127], J. Motta[127], A. Reimers[127], P. Robmann[127], M. Senger[127], E. Shokr[127], F. Stäger[127], R. Tramontano[127], C. Adloff[128,bn], D. Bhowmik[128], C.M. Kuo[128], W. Lin[128], P.K. Rout[128], P.C. Tiwari[128,al], L. Ceard[129], K.F. Chen[129], Z.g. Chen[129], A. De Iorio[129], W.-S. Hou[129], T.h. Hsu[129], Y.w. Kao[129], S. Karmakar[129], G. Kole[129], Y.y. Li[129], R.-S. Lu[129], E. Paganis[129], X.f. Su[129], J. Thomas-Wilsker[129], L.s. Tsai[129], D. Tsionou[129], H.y. Wu[129], E. Yazgan[129], C. Asawatangtrakuldee[130], N. Srimanobhas[130], V. Wachirapusitanand[130], Y. Maghrbi[131], D. Agyel[132], F. Boran[132], F. Dolek[132], I. Dumanoglu[132,bo], E. Eskut[132], Y. Guler[132,bp], E. Gurpinar Guler[132,bp], C. Isik[132], O. Kara[132], A. Kayis Topaksu[132], Y. Komurcu[132], G. Onengut[132], K. Ozdemir[132,bq], A. Polatoz[132], B. Tali[132,br], U.G. Tok[132], E. Uslan[132], I.S. Zorbakir[132], M. Yalvac[133,bs], B. Akgun[134], I.O. Atakisi[134], E. Gülmez[134], M. Kaya[134,bt], O. Kaya[134,bu], S. Tekten[134,bv], A. Cakir[135], K. Cankocak[135,bo,bw], S. Sen[135,bx], O. Aydilek[136,by], B. Hacisahinoglu[136], I. Hos[136,bz], B. Kaynak[136], S. Ozkorucuklu[136], O. Potok[136], H. Sert[136], C. Simsek[136], C. Zorbilmez[136], S. Cerci[137], B. Isildak[137,ca], D. Sunar Cerci[137], T. Yetkin[137], A. Boyaryntsev[138], B. Grynyov[138], L. Levchuk[139], D. Anthony[140], J.J. Brooke[140], A. Bundock[140], F. Bury[140], E. Clement[140], D. Cussans[140], H. Flacher[140], J. Goldstein[140], H.F. Heath[140], M.-L. Holmberg[140], L. Kreczko[140], S. Paramesvaran[140], L. Robertshaw[140], V.J. Smith[140], K. Walkingshaw Pass[140], A.H. Ball[141], K.W. Bell[141], A. Belyaev[141,cb], C. Brew[141], R.M. Brown[141], D.J.A. Cockerill[141], C. Cooke[141], A. Elliot[141], K.V. Ellis[141], K. Harder[141], S. Harper[141], J. Linacre[141], K. Manolopoulos[141], D.M. Newbold[141], E. Olaiya[141], D. Petyt[141], T. Reis[141], A.R. Sahasransu[141], G. Salvi[141], T. Schuh[141], C.H. Shepherd-Themistocleous[141], I.R. Tomalin[141], K.C. Whalen[141], T. Williams[141], I. Andreou[142], R. Bainbridge[142], P. Bloch[142], O. Buchmuller[142], C.A. Carrillo Montoya[142], G.S. Chahal[142,cc], D. Colling[142], J.S. Dancu[142], I. Das[142], P. Dauncey[142], G. Davies[142], M. Della Negra[142], S. Fayer[142], G. Fedi[142], G. Hall[142], A. Howard[142], G. Iles[142], C.R. Knight[142], P. Krueper[142], J. Langford[142], K.H. Law[142], J. León Holgado[142], L. Lyons[142], A.-M. Magnan[142], B. Maier[142], S. Mallios[142], M. Mieskolainen[142], J. Nash[142,cd], M. Pesaresi[142], P.B. Pradeep[142], B.C. Radburn-Smith[142], A. Richards[142], A. Rose[142], L. Russell[142], K. Savva[142], C. Seez[142], R. Shukla[142], A. Tapper[142], K. Uchida[142], G.P. Uttley[142], T. Virdee[142,ad], M. Vojinovic[142], N. Wardle[142], D. Winterbottom[142], J.E. Cole[143], A. Khan[143], P. Kyberd[143], I.D. Reid[143], S. Abdullin[144], A. Brinkerhoff[144], E. Collins[144], M.R. Darwish[144], J. Dittmann[144], K. Hatakeyama[144],

JHEP04(2026)093

V. Hegde[144], J. Hiltbrand[144], B. McMaster[144], J. Samudio[144], S. Sawant[144], C. Sutantawibul[144], J. Wilson[144], R. Bartek[145], A. Dominguez[145], A.E. Simsek[145], S.S. Yu[145], B. Bam[146], A. Buchot Perraguin[146], R. Chudasama[146], S.I. Cooper[146], C. Crovella[146], S.V. Gleyzer[146], E. Pearson[146], C.U. Perez[146], P. Rumerio[146,ce], E. Usai[146], R. Yi[146], A. Akpinar[147], C. Cosby[147], G. De Castro[147], Z. Demiragli[147], C. Erice[147], C. Fangmeier[147], C. Fernandez Madrazo[147], E. Fontanesi[147], D. Gastler[147], F. Golf[147], S. Jeon[147], J. O'cain[147], I. Reed[147], J. Rohlf[147], K. Salyer[147], D. Sperka[147], D. Spitzbart[147], I. Suarez[147], A. Tsatsos[147], A.G. Zecchinelli[147], G. Barone[148], G. Benelli[148], D. Cutts[148], S. Ellis[148], L. Gouskos[148], M. Hadley[148], U. Heintz[148], K.W. Ho[148], J.M. Hogan[148,cf], T. Kwon[148], G. Landsberg[148], K.T. Lau[148], J. Luo[148], S. Mondal[148], T. Russell[148], S. Sagir[148,cg], X. Shen[148], M. Stamenkovic[148], N. Venkatasubramanian[148], S. Abbott[149], B. Barton[149], C. Brainerd[149], R. Breedon[149], H. Cai[149], M. Calderon De La Barca Sanchez[149], M. Chertok[149], M. Citron[149], J. Conway[149], P.T. Cox[149], R. Erbacher[149], F. Jensen[149], O. Kukral[149], G. Mocellin[149], M. Mulhearn[149], S. Ostrom[149], W. Wei[149], S. Yoo[149], F. Zhang[149], K. Adamidis[150], M. Bachtis[150], D. Campos[150], R. Cousins[150], A. Datta[150], G. Flores Avila[150], J. Hauser[150], M. Ignatenko[150], M.A. Iqbal[150], T. Lam[150], Y.f. Lo[150], E. Manca[150], A. Nunez Del Prado[150], D. Saltzberg[150], V. Valuev[150], R. Clare[151], J.W. Gary[151], G. Hanson[151], A. Aportela[152], A. Arora[152], J.G. Branson[152], S. Cittolin[152], S. Cooperstein[152], D. Diaz[152], J. Duarte[152], L. Giannini[152], Y. Gu[152], J. Guiang[152], R. Kansal[152], V. Krutelyov[152], R. Lee[152], J. Letts[152], M. Masciovecchio[152], F. Mokhtar[152], S. Mukherjee[152], M. Pieri[152], D. Primosch[152], M. Quinnan[152], V. Sharma[152], M. Tadel[152], E. Vourliotis[152], F. Würthwein[152], Y. Xiang[152], A. Yagil[152], A. Barzdukas[153], L. Brennan[153], C. Campagnari[153], K. Downham[153], C. Grieco[153], M.M. Hussain[153], J. Incandela[153], J. Kim[153], A.J. Li[153], P. Masterson[153], H. Mei[153], J. Richman[153], S.N. Santpur[153], U. Sarica[153], R. Schmitz[153], F. Setti[153], J. Sheplock[153], D. Stuart[153], T.Á. Vámi[153], X. Yan[153], D. Zhang[153], S. Bhattacharya[154], A. Bornheim[154], O. Cerri[154], J. Mao[154], H.B. Newman[154], G. Reales Gutiérrez[154], M. Spiropulu[154], J.R. Vlimant[154], C. Wang[154], S. Xie[154], R.Y. Zhu[154], J. Alison[155], S. An[155], P. Bryant[155], M. Cremonesi[155], V. Dutta[155], T. Ferguson[155], T.A. Gómez Espinosa[155], A. Harilal[155], A. Kallil Tharayil[155], M. Kanemura[155], C. Liu[155], T. Mudholkar[155], S. Murthy[155], P. Palit[155], K. Park[155], M. Paulini[155], A. Roberts[155], A. Sanchez[155], W. Terrill[155], J.P. Cumalat[156], W.T. Ford[156], A. Hart[156], A. Hassani[156], N. Manganelli[156], J. Pearkes[156], C. Savard[156], N. Schonbeck[156], K. Stenson[156], K.A. Ulmer[156], S.R. Wagner[156], N. Zipper[156], D. Zuolo[156], J. Alexander[157], X. Chen[157], D.J. Cranshaw[157], J. Dickinson[157], J. Fan[157], X. Fan[157], S. Hogan[157], P. Kotamnives[157], J. Monroy[157], M. Oshiro[157], J.R. Patterson[157], M. Reid[157], A. Ryd[157], J. Thom[157], P. Wittich[157], R. Zou[157], M. Albrow[158], M. Alyari[158], O. Amram[158], G. Apollinari[158], A. Apresyan[158], L.A.T. Bauerdick[158], D. Berry[158], J. Berryhill[158], P.C. Bhat[158], K. Burkett[158], J.N. Butler[158], A. Canepa[158], G.B. Cerati[158], H.W.K. Cheung[158], F. Chlebana[158], G. Cummings[158], I. Dutta[158], V.D. Elvira[158], J. Freeman[158], A. Gandrakota[158], Z. Gecse[158], L. Gray[158], D. Green[158], A. Grummer[158], S. Grünendahl[158], D. Guerrero[158], O. Gutsche[158], R.M. Harris[158], T.C. Herwig[158], J. Hirschauer[158], B. Jayatilaka[158], S. Jindariani[158], M. Johnson[158],

JHEP04(2026)093

U. Joshi[158], T. Klijnsma[158], B. Klima[158], K.H.M. Kwok[158], S. Lammel[158], C. Lee[158], D. Lincoln[158], R. Lipton[158], T. Liu[158], K. Maeshima[158], D. Mason[158], P. McBride[158], P. Merkel[158], S. Mrenna[158], S. Nahn[158], J. Ngadiuba[158], D. Noonan[158], S. Norberg[158], V. Papadimitriou[158], N. Pastika[158], K. Pedro[158], C. Pena[158,ch], F. Ravera[158], A. Reinsvold Hall[158,ci], L. Ristori[158], M. Safdari[158], E. Sexton-Kennedy[158], N. Smith[158], A. Soha[158], L. Spiegel[158], S. Stoynev[158], J. Strait[158], L. Taylor[158], S. Tkaczyk[158], N.V. Tran[158], L. Uplegger[158], E.W. Vaandering[158], I. Zoi[158], C. Aruta[159], P. Avery[159], D. Bourilkov[159], P. Chang[159], V. Cherepanov[159], R.D. Field[159], C. Huh[159], E. Koenig[159], M. Kolosova[159], J. Konigsberg[159], A. Korytov[159], K. Matchev[159], N. Menendez[159], G. Mitselmakher[159], K. Mohrman[159], A. Muthirakalayil Madhu[159], N. Rawal[159], S. Rosenzweig[159], Y. Takahashi[159], J. Wang[159], T. Adams[160], A. Al Kadhim[160], A. Askew[160], S. Bower[160], R. Hashmi[160], R.S. Kim[160], S. Kim[160], T. Kolberg[160], G. Martinez[160], H. Prosper[160], P.R. Prova[160], M. Wulansatiti[160], R. Yohay[160], J. Zhang[160], B. Alsufyani[161], S. Butalla[161], S. Das[161], T. Elkafrawy[161,cj], M. Hohlmann[161], E. Yanes[161], M.R. Adams[162], A. Baty[162], C. Bennett[162], R. Cavanaugh[162], D. S. Lemos[162], R. Escobar Franco[162], O. Evdokimov[162], C.E. Gerber[162], H. Gupta[162], M. Hawksworth[162], A. Hingrajiya[162], D.J. Hofman[162], J.h. Lee[162], C. Mills[162], S. Nanda[162], G. Oh[162], B. Ozek[162], D. Pilipovic[162], R. Pradhan[162], E. Prifti[162], P. Roy[162], T. Roy[162], S. Rudrabhatla[162], N. Singh[162], M.B. Tonjes[162], N. Varelas[162], M.A. Wadud[162], Z. Ye[162], J. Yoo[162], M. Alhusseini[163], D. Blend[163], K. Dilsiz[163,ck], L. Emediato[163], G. Karaman[163], O.K. Köseyan[163], J.-P. Merlo[163], A. Mestvirishvili[163,cl], O. Neogi[163], H. Ogul[163,cm], Y. Onel[163], A. Penzo[163], C. Snyder[163], E. Tiras[163,cn], B. Blumenfeld[164], L. Corcodilos[164], J. Davis[164], A.V. Gritsan[164], L. Kang[164], S. Kyriacou[164], P. Maksimovic[164], M. Roguljic[164], J. Roskes[164], S. Sekhar[164], M. Swartz[164], A. Abreu[165], L.F. Alcerro Alcerro[165], J. Anguiano[165], S. Arteaga Escatel[165], P. Baringer[165], A. Bean[165], Z. Flowers[165], D. Grove[165], J. King[165], G. Krintiras[165], M. Lazarovits[165], C. Le Mahieu[165], J. Marquez[165], M. Murray[165], M. Nickel[165], S. Popescu[165,co], C. Rogan[165], C. Royon[165], S. Sanders[165], C. Smith[165], G. Wilson[165], B. Allmond[166], R. Gujju Gurunadha[166], A. Ivanov[166], K. Kaadze[166], Y. Maravin[166], J. Natoli[166], D. Roy[166], G. Sorrentino[166], A. Baden[167], A. Belloni[167], J. Bistany-riebman[167], S.C. Eno[167], N.J. Hadley[167], S. Jabeen[167], R.G. Kellogg[167], T. Koeth[167], B. Kronheim[167], S. Lascio[167], A.C. Mignerey[167], S. Nabili[167], C. Palmer[167], C. Papageorgakis[167], M.M. Paranjpe[167], E. Popova[167,cp], A. Shevelev[167], L. Wang[167], L. Zhang[167], C. Baldenegro Barrera[168], J. Bendavid[168], S. Bright-Thonney[168], I.A. Cali[168], P.c. Chou[168], M. D'Alfonso[168], J. Eysermans[168], C. Freer[168], G. Gomez-Ceballos[168], M. Goncharov[168], G. Grosso[168], P. Harris[168], D. Hoang[168], D. Kovalskyi[168], J. Krupa[168], L. Lavezzo[168], Y.-J. Lee[168], K. Long[168], C. Mcginn[168], A. Novak[168], M.I. Park[168], C. Paus[168], C. Reissel[168], C. Roland[168], G. Roland[168], S. Rothman[168], G.S.F. Stephans[168], Z. Wang[168], B. Wyslouch[168], T. J. Yang[168], B. Crossman[169], C. Kapsiak[169], M. Krohn[169], D. Mahon[169], J. Mans[169], B. Marzocchi[169], M. Revering[169], R. Rusack[169], R. Saradhy[169], N. Strobbe[169], K. Bloom[170], D.R. Claes[170], G. Haza[170], J. Hossain[170], C. Joo[170], I. Kravchenko[170], A. Rohilla[170], J.E. Siado[170], W. Tabb[170], A. Vagnerini[170], A. Wightman[170], F. Yan[170], D. Yu[170], H. Bandyopadhyay[171],

JHEP04(2026)093

L. Hay[171], H.w. Hsia[171], I. Iashvili[171], A. Kalogeropoulos[171], A. Kharchilava[171], M. Morris[171], D. Nguyen[171], S. Rappoccio[171], H. Rejeb Sfar[171], A. Williams[171], P. Young[171], G. Alverson[172], E. Barberis[172], J. Bonilla[172], B. Bylsma[172], M. Campana[172], J. Dervan[172], Y. Haddad[172], Y. Han[172], I. Israr[172], A. Krishna[172], P. Levchenko[172], J. Li[172], M. Lu[172], R. Mccarthy[172], D.M. Morse[172], T. Orimoto[172], A. Parker[172], L. Skinnari[172], E. Tsai[172], D. Wood[172], S. Dittmer[173], K.A. Hahn[173], D. Li[173], Y. Liu[173], M. Mcginnis[173], Y. Miao[173], D.G. Monk[173], M.H. Schmitt[173], A. Taliercio[173], M. Velasco[173], G. Agarwal[174], R. Band[174], R. Bucci[174], S. Castells[174], A. Das[174], R. Goldouzian[174], M. Hildreth[174], K. Hurtado Anampa[174], T. Ivanov[174], C. Jessop[174], K. Lannon[174], J. Lawrence[174], N. Loukas[174], L. Lutton[174], J. Mariano[174], N. Marinelli[174], I. Mcalister[174], T. McCauley[174], C. Mcgrady[174], C. Moore[174], Y. Musienko[174,o], H. Nelson[174], M. Osherson[174], A. Piccinelli[174], R. Ruchti[174], A. Townsend[174], Y. Wan[174], M. Wayne[174], H. Yockey[174], M. Zarucki[174], L. Zygala[174], A. Basnet[175], M. Carrigan[175], L.S. Durkin[175], C. Hill[175], M. Joyce[175], M. Nunez Ornelas[175], K. Wei[175], D.A. Wenzl[175], B.L. Winer[175], B. R. Yates[175], H. Bouchamaoui[176], K. Coldham[176], P. Das[176], G. Dezoort[176], P. Elmer[176], P. Fackeldey[176], A. Frankenthal[176], B. Greenberg[176], N. Haubrich[176], K. Kennedy[176], G. Kopp[176], S. Kwan[176], Y. Lai[176], D. Lange[176], A. Loeliger[176], D. Marlow[176], I. Ojalvo[176], J. Olsen[176], F. Simpson[176], D. Stickland[176], C. Tully[176], L.H. Vage[176], S. Malik[177], R. Sharma[177], A.S. Bakshi[178], S. Chandra[178], R. Chawla[178], A. Gu[178], L. Gutay[178], M. Jones[178], A.W. Jung[178], A. K. Virdi[178], A.M. Koshy[178], M. Liu[178], G. Negro[178], N. Neumeister[178], G. Paspalaki[178], S. Piperov[178], J.F. Schulte[178], F. Wang[178], A. Wildridge[178], W. Xie[178], Y. Yao[178], J. Dolen[179], N. Parashar[179], A. Pathak[179], D. Acosta[180], A. Agrawal[180], T. Carnahan[180], K.M. Ecklund[180], P.J. Fernández Manteca[180], S. Freed[180], P. Gardner[180], F.J.M. Geurts[180], I. Krommydas[180], W. Li[180], J. Lin[180], O. Miguel Colin[180], B.P. Padley[180], R. Redjimi[180], J. Rotter[180], E. Yigitbasi[180], Y. Zhang[180], A. Bodek[181], P. de Barbaro[181], R. Demina[181], J.L. Dulemba[181], A. Garcia-Bellido[181], O. Hindrichs[181], A. Khukhunaishvili[181], N. Parmar[181], P. Parygin[181,cp], R. Taus[181], B. Chiarito[182], J.P. Chou[182], S.V. Clark[182], D. Gadkari[182], Y. Gershtein[182], E. Halkiadakis[182], M. Heindl[182], C. Houghton[182], D. Jaroslawski[182], S. Konstantinou[182], I. Laflotte[182], A. Lath[182], R. Montalvo[182], K. Nash[182], J. Reichert[182], P. Saha[182], S. Salur[182], S. Schnetzer[182], S. Somalwar[182], R. Stone[182], S.A. Thayil[182], S. Thomas[182], J. Vora[182], D. Ally[183], A.G. Delannoy[183], S. Fiorendi[183], S. Higginbotham[183], T. Holmes[183], A.R. Kanuganti[183], N. Karunarathna[183], L. Lee[183], E. Nibigira[183], S. Spanier[183], D. Aebi[184], M. Ahmad[184], T. Akhter[184], K. Androsov[184,bk], O. Bouhali[184,cq], R. Eusebi[184], J. Gilmore[184], T. Huang[184], T. Kamon[184,cr], H. Kim[184], S. Luo[184], R. Mueller[184], D. Overton[184], A. Safonov[184], N. Akchurin[185], J. Damgov[185], Y. Feng[185], N. Gogate[185], Y. Kazhykarim[185], K. Lamichhane[185], S.W. Lee[185], C. Madrid[185], A. Mankel[185], T. Peltola[185], I. Volobouev[185], E. Appelt[186], Y. Chen[186], S. Greene[186], A. Gurrola[186], W. Johns[186], R. Kunnawalkam Elayavalli[186], A. Melo[186], D. Rathjens[186], F. Romeo[186], P. Sheldon[186], S. Tuo[186], J. Velkovska[186], J. Viinikainen[186], B. Cardwell[187], H. Chung[187], B. Cox[187], J. Hakala[187], R. Hirosky[187], A. Ledovskoy[187], C. Mantilla[187], C. Neu[187], C. Ramón Álvarez[187], S. Bhattacharya[188], P.E. Karchin[188], A. Aravind[189], S. Banerjee[189], K. Black[189], T. Bose[189], E. Chavez[189],

JHEP04(2026)093

S. Dasu[189], P. Everaerts[189], C. Galloni[189], H. He[189], M. Herndon[189], A. Herve[189], C.K. Koraka[189], A. Lanaro[189], R. Loveless[189], J. Madhusudanan Sreekala[189], A. Mallampalli[189], A. Mohammadi[189], S. Mondal[189], G. Parida[189], D. Pinna[189], L. Pétré[189], A. Savin[189], V. Shang[189], V. Sharma[189], W.H. Smith[189], D. Teague[189], H.F. Tsoi[189], W. Vetens[189], A. Warden[189], S. Afanasiev[190], V. Alexakhin[190], Yu. Andreev[190], T. Aushev[190], D. Budkouski[190], A. Ershov[190], I. Golutvin[190,†], I. Gorbunov[190], V. Karjavine[190], V. Klyukhin[190,o], O. Kodolova[190,cs,cp], V. Korenkov[190], A. Lanev[190], A. Malakhov[190], V. Matveev[190,o], A. Nikitenko[190,ct,cu], V. Palichik[190], V. Perelygin[190], S. Petrushanko[190], M. Savina[190], V. Shalaev[190], S. Shmatov[190], S. Shulha[190], V. Smirnov[190], O. Teryaev[190], A. Toropin[190], N. Voytishin[190], B.S. Yuldashev[190,cv,†], A. Zarubin[190], I. Zhizhin[190], V. Andreev[191], M. Azarkin[191], A. Babaev[191], V. Blinov[191,o], E. Boos[191], V. Borshch[191], V. Bunichev[191], R. Chistov[191,o], M. Danilov[191,o], A. Dermenev[191], T. Dimova[191,o], D. Druzhkin[191], M. Dubinin[191,ch], L. Dudko[191], G. Gavrilov[191], V. Gavrilov[191], S. Gninenko[191], V. Golovtcov[191], N. Golubev[191], Y. Ivanov[191], K. Ivanov[191], V. Kachanov[191], A. Karneyeu[191], V. Kim[191,o], M. Kirakosyan[191], D. Kirpichnikov[191], M. Kirsanov[191], A. Kozyrev[191,o], N. Krasnikov[191], N. Lychkovskaya[191], V. Murzin[191], V. Oreshkin[191], M. Perfilov[191], S. Polikarpov[191,o], V. Popov[191], O. Radchenko[191,o], V. Savrin[191], Y. Skovpen[191,o], S. Slabospitskii[191], D. Sosnov[191], V. Sulimov[191], A. Terkulov[191], I. Tlisova[191], L. Uvarov[191], A. Uzunian[191], A. Vorobyev[191,†], G. Vorotnikov[191], A. Zhokin[191]

[1] *Yerevan Physics Institute, Yerevan, Armenia*
[2] *Institut für Hochenergiephysik, Vienna, Austria*
[3] *Universiteit Antwerpen, Antwerpen, Belgium*
[4] *Vrije Universiteit Brussel, Brussel, Belgium*
[5] *Université Libre de Bruxelles, Bruxelles, Belgium*
[6] *Ghent University, Ghent, Belgium*
[7] *Université Catholique de Louvain, Louvain-la-Neuve, Belgium*
[8] *Centro Brasileiro de Pesquisas Fisicas, Rio de Janeiro, Brazil*
[9] *Universidade do Estado do Rio de Janeiro, Rio de Janeiro, Brazil*
[10] *Universidade Estadual Paulista, Universidade Federal do ABC, São Paulo, Brazil*
[11] *Institute for Nuclear Research and Nuclear Energy, Bulgarian Academy of Sciences, Sofia, Bulgaria*
[12] *University of Sofia, Sofia, Bulgaria*
[13] *Instituto De Alta Investigación, Universidad de Tarapacá, Casilla 7 D, Arica, Chile*
[14] *Beihang University, Beijing, China*
[15] *Department of Physics, Tsinghua University, Beijing, China*
[16] *Institute of High Energy Physics, Beijing, China*
[17] *State Key Laboratory of Nuclear Physics and Technology, Peking University, Beijing, China*
[18] *Guangdong Provincial Key Laboratory of Nuclear Science and Guangdong-Hong Kong Joint Laboratory of Quantum Matter, South China Normal University, Guangzhou, China*
[19] *Sun Yat-Sen University, Guangzhou, China*
[20] *University of Science and Technology of China, Hefei, China*
[21] *Nanjing Normal University, Nanjing, China*
[22] *Institute of Modern Physics and Key Laboratory of Nuclear Physics and Ion-beam Application (MOE) — Fudan University, Shanghai, China*
[23] *Zhejiang University, Hangzhou, Zhejiang, China*
[24] *Universidad de Los Andes, Bogota, Colombia*
[25] *Universidad de Antioquia, Medellin, Colombia*

JHEP04(2026)093

[26] University of Split, Faculty of Electrical Engineering, Mechanical Engineering and Naval Architecture, Split, Croatia
[27] University of Split, Faculty of Science, Split, Croatia
[28] Institute Rudjer Boskovic, Zagreb, Croatia
[29] University of Cyprus, Nicosia, Cyprus
[30] Charles University, Prague, Czech Republic
[31] Escuela Politecnica Nacional, Quito, Ecuador
[32] Universidad San Francisco de Quito, Quito, Ecuador
[33] Academy of Scientific Research and Technology of the Arab Republic of Egypt, Egyptian Network of High Energy Physics, Cairo, Egypt
[34] Center for High Energy Physics (CHEP-FU), Fayoum University, El-Fayoum, Egypt
[35] National Institute of Chemical Physics and Biophysics, Tallinn, Estonia
[36] Department of Physics, University of Helsinki, Helsinki, Finland
[37] Helsinki Institute of Physics, Helsinki, Finland
[38] Lappeenranta-Lahti University of Technology, Lappeenranta, Finland
[39] IRFU, CEA, Université Paris-Saclay, Gif-sur-Yvette, France
[40] Laboratoire Leprince-Ringuet, CNRS/IN2P3, Ecole Polytechnique, Institut Polytechnique de Paris, Palaiseau, France
[41] Université de Strasbourg, CNRS, IPHC UMR 7178, Strasbourg, France
[42] Centre de Calcul de l'Institut National de Physique Nucleaire et de Physique des Particules, CNRS/IN2P3, Villeurbanne, France
[43] Institut de Physique des 2 Infinis de Lyon (IP2I), Villeurbanne, France
[44] Georgian Technical University, Tbilisi, Georgia
[45] RWTH Aachen University, I. Physikalisches Institut, Aachen, Germany
[46] RWTH Aachen University, III. Physikalisches Institut A, Aachen, Germany
[47] RWTH Aachen University, III. Physikalisches Institut B, Aachen, Germany
[48] Deutsches Elektronen-Synchrotron, Hamburg, Germany
[49] University of Hamburg, Hamburg, Germany
[50] Karlsruher Institut fuer Technologie, Karlsruhe, Germany
[51] Institute of Nuclear and Particle Physics (INPP), NCSR Demokritos, Aghia Paraskevi, Greece
[52] National and Kapodistrian University of Athens, Athens, Greece
[53] National Technical University of Athens, Athens, Greece
[54] University of Ioánnina, Ioánnina, Greece
[55] HUN-REN Wigner Research Centre for Physics, Budapest, Hungary
[56] MTA-ELTE Lendület CMS Particle and Nuclear Physics Group, Eötvös Loránd University, Budapest, Hungary
[57] Faculty of Informatics, University of Debrecen, Debrecen, Hungary
[58] HUN-REN ATOMKI — Institute of Nuclear Research, Debrecen, Hungary
[59] Karoly Robert Campus, MATE Institute of Technology, Gyongyos, Hungary
[60] Panjab University, Chandigarh, India
[61] University of Delhi, Delhi, India
[62] Indian Institute of Technology Kanpur, Kanpur, India
[63] Saha Institute of Nuclear Physics, HBNI, Kolkata, India
[64] Indian Institute of Technology Madras, Madras, India
[65] Tata Institute of Fundamental Research-A, Mumbai, India
[66] Tata Institute of Fundamental Research-B, Mumbai, India
[67] National Institute of Science Education and Research, An OCC of Homi Bhabha National Institute, Bhubaneswar, Odisha, India
[68] Indian Institute of Science Education and Research (IISER), Pune, India
[69] Isfahan University of Technology, Isfahan, Iran
[70] Institute for Research in Fundamental Sciences (IPM), Tehran, Iran
[71] University College Dublin, Dublin, Ireland
[72a] INFN Sezione di Bari, Bari, Italy

JHEP04(2026)093

[72b] *Università di Bari, Bari, Italy*
[72c] *Politecnico di Bari, Bari, Italy*
[73a] *INFN Sezione di Bologna, Bologna, Italy*
[73b] *Università di Bologna, Bologna, Italy*
[74a] *INFN Sezione di Catania, Catania, Italy*
[74b] *Università di Catania, Catania, Italy*
[75a] *INFN Sezione di Firenze, Firenze, Italy*
[75b] *Università di Firenze, Firenze, Italy*
[76] *INFN Laboratori Nazionali di Frascati, Frascati, Italy*
[77a] *INFN Sezione di Genova, Genova, Italy*
[77b] *Università di Genova, Genova, Italy*
[78a] *INFN Sezione di Milano-Bicocca, Milano, Italy*
[78b] *Università di Milano-Bicocca, Milano, Italy*
[79a] *INFN Sezione di Napoli, Napoli, Italy*
[79b] *Università di Napoli 'Federico II', Napoli, Italy*
[79c] *Università della Basilicata, Potenza, Italy*
[80a] *INFN Sezione di Padova, Padova, Italy*
[80b] *Università di Padova, Padova, Italy*
[81a] *INFN Sezione di Pavia, Pavia, Italy*
[81b] *Università di Pavia, Pavia, Italy*
[82a] *INFN Sezione di Perugia, Perugia, Italy*
[82b] *Università di Perugia, Perugia, Italy*
[83a] *INFN Sezione di Pisa, Pisa, Italy*
[83b] *Università di Pisa, Pisa, Italy*
[83c] *Scuola Normale Superiore di Pisa, Pisa, Italy*
[83d] *Università di Siena, Siena, Italy*
[84a] *INFN Sezione di Roma, Roma, Italy*
[84b] *Sapienza Università di Roma, Roma, Italy*
[85a] *INFN Sezione di Torino, Torino, Italy*
[85b] *Università di Torino, Torino, Italy*
[85c] *Università del Piemonte Orientale, Novara, Italy*
[86a] *INFN Sezione di Trieste, Trieste, Italy*
[86b] *Università di Trieste, Trieste, Italy*
[87] *Kyungpook National University, Daegu, Korea*
[88] *Department of Mathematics and Physics — GWNU, Gangneung, Korea*
[89] *Chonnam National University, Institute for Universe and Elementary Particles, Kwangju, Korea*
[90] *Hanyang University, Seoul, Korea*
[91] *Korea University, Seoul, Korea*
[92] *Kyung Hee University, Department of Physics, Seoul, Korea*
[93] *Sejong University, Seoul, Korea*
[94] *Seoul National University, Seoul, Korea*
[95] *University of Seoul, Seoul, Korea*
[96] *Yonsei University, Department of Physics, Seoul, Korea*
[97] *Sungkyunkwan University, Suwon, Korea*
[98] *College of Engineering and Technology, American University of the Middle East (AUM), Dasman, Kuwait*
[99] *Kuwait University — College of Science — Department of Physics, Safat, Kuwait*
[100] *Riga Technical University, Riga, Latvia*
[101] *University of Latvia (LU), Riga, Latvia*
[102] *Vilnius University, Vilnius, Lithuania*
[103] *National Centre for Particle Physics, Universiti Malaya, Kuala Lumpur, Malaysia*
[104] *Universidad de Sonora (UNISON), Hermosillo, Mexico*
[105] *Centro de Investigacion y de Estudios Avanzados del IPN, Mexico City, Mexico*
[106] *Universidad Iberoamericana, Mexico City, Mexico*

JHEP04(2026)093

[107] *Benemerita Universidad Autonoma de Puebla, Puebla, Mexico*
[108] *University of Montenegro, Podgorica, Montenegro*
[109] *University of Canterbury, Christchurch, New Zealand*
[110] *National Centre for Physics, Quaid-I-Azam University, Islamabad, Pakistan*
[111] *AGH University of Krakow, Krakow, Poland*
[112] *National Centre for Nuclear Research, Swierk, Poland*
[113] *Institute of Experimental Physics, Faculty of Physics, University of Warsaw, Warsaw, Poland*
[114] *Warsaw University of Technology, Warsaw, Poland*
[115] *Laboratório de Instrumentação e Física Experimental de Partículas, Lisboa, Portugal*
[116] *Faculty of Physics, University of Belgrade, Belgrade, Serbia*
[117] *VINCA Institute of Nuclear Sciences, University of Belgrade, Belgrade, Serbia*
[118] *Centro de Investigaciones Energéticas Medioambientales y Tecnológicas (CIEMAT), Madrid, Spain*
[119] *Universidad Autónoma de Madrid, Madrid, Spain*
[120] *Universidad de Oviedo, Instituto Universitario de Ciencias y Tecnologías Espaciales de Asturias (ICTEA), Oviedo, Spain*
[121] *Instituto de Física de Cantabria (IFCA), CSIC-Universidad de Cantabria, Santander, Spain*
[122] *University of Colombo, Colombo, Sri Lanka*
[123] *University of Ruhuna, Department of Physics, Matara, Sri Lanka*
[124] *CERN, European Organization for Nuclear Research, Geneva, Switzerland*
[125] *PSI Center for Neutron and Muon Sciences, Villigen, Switzerland*
[126] *ETH Zurich — Institute for Particle Physics and Astrophysics (IPA), Zurich, Switzerland*
[127] *Universität Zürich, Zurich, Switzerland*
[128] *National Central University, Chung-Li, Taiwan*
[129] *National Taiwan University (NTU), Taipei, Taiwan*
[130] *High Energy Physics Research Unit, Department of Physics, Faculty of Science, Chulalongkorn University, Bangkok, Thailand*
[131] *Tunis El Manar University, Tunis, Tunisia*
[132] *Çukurova University, Physics Department, Science and Art Faculty, Adana, Turkey*
[133] *Middle East Technical University, Physics Department, Ankara, Turkey*
[134] *Bogazici University, Istanbul, Turkey*
[135] *Istanbul Technical University, Istanbul, Turkey*
[136] *Istanbul University, Istanbul, Turkey*
[137] *Yildiz Technical University, Istanbul, Turkey*
[138] *Institute for Scintillation Materials of National Academy of Science of Ukraine, Kharkiv, Ukraine*
[139] *National Science Centre, Kharkiv Institute of Physics and Technology, Kharkiv, Ukraine*
[140] *University of Bristol, Bristol, U.K.*
[141] *Rutherford Appleton Laboratory, Didcot, U.K.*
[142] *Imperial College, London, U.K.*
[143] *Brunel University, Uxbridge, U.K.*
[144] *Baylor University, Waco, Texas, U.S.A.*
[145] *Catholic University of America, Washington, DC, U.S.A.*
[146] *The University of Alabama, Tuscaloosa, Alabama, U.S.A.*
[147] *Boston University, Boston, Massachusetts, U.S.A.*
[148] *Brown University, Providence, Rhode Island, U.S.A.*
[149] *University of California, Davis, Davis, California, U.S.A.*
[150] *University of California, Los Angeles, California, U.S.A.*
[151] *University of California, Riverside, Riverside, California, U.S.A.*
[152] *University of California, San Diego, La Jolla, California, U.S.A.*
[153] *University of California, Santa Barbara — Department of Physics, Santa Barbara, California, U.S.A.*
[154] *California Institute of Technology, Pasadena, California, U.S.A.*
[155] *Carnegie Mellon University, Pittsburgh, Pennsylvania, U.S.A.*
[156] *University of Colorado Boulder, Boulder, Colorado, U.S.A.*
[157] *Cornell University, Ithaca, New York, U.S.A.*

JHEP04(2026)093

[158] Fermi National Accelerator Laboratory, Batavia, Illinois, U.S.A.
[159] University of Florida, Gainesville, Florida, U.S.A.
[160] Florida State University, Tallahassee, Florida, U.S.A.
[161] Florida Institute of Technology, Melbourne, Florida, U.S.A.
[162] University of Illinois Chicago, Chicago, Illinois, U.S.A.
[163] The University of Iowa, Iowa City, Iowa, U.S.A.
[164] Johns Hopkins University, Baltimore, Maryland, U.S.A.
[165] The University of Kansas, Lawrence, Kansas, U.S.A.
[166] Kansas State University, Manhattan, Kansas, U.S.A.
[167] University of Maryland, College Park, Maryland, U.S.A.
[168] Massachusetts Institute of Technology, Cambridge, Massachusetts, U.S.A.
[169] University of Minnesota, Minneapolis, Minnesota, U.S.A.
[170] University of Nebraska-Lincoln, Lincoln, Nebraska, U.S.A.
[171] State University of New York at Buffalo, Buffalo, New York, U.S.A.
[172] Northeastern University, Boston, Massachusetts, U.S.A.
[173] Northwestern University, Evanston, Illinois, U.S.A.
[174] University of Notre Dame, Notre Dame, Indiana, U.S.A.
[175] The Ohio State University, Columbus, Ohio, U.S.A.
[176] Princeton University, Princeton, New Jersey, U.S.A.
[177] University of Puerto Rico, Mayaguez, Puerto Rico, U.S.A.
[178] Purdue University, West Lafayette, Indiana, U.S.A.
[179] Purdue University Northwest, Hammond, Indiana, U.S.A.
[180] Rice University, Houston, Texas, U.S.A.
[181] University of Rochester, Rochester, New York, U.S.A.
[182] Rutgers, The State University of New Jersey, Piscataway, New Jersey, U.S.A.
[183] University of Tennessee, Knoxville, Tennessee, U.S.A.
[184] Texas A&M University, College Station, Texas, U.S.A.
[185] Texas Tech University, Lubbock, Texas, U.S.A.
[186] Vanderbilt University, Nashville, Tennessee, U.S.A.
[187] University of Virginia, Charlottesville, Virginia, U.S.A.
[188] Wayne State University, Detroit, Michigan, U.S.A.
[189] University of Wisconsin — Madison, Madison, Wisconsin, U.S.A.
[190] An institute or international laboratory covered by a cooperation agreement with CERN
[191] An institute formerly covered by a cooperation agreement with CERN

[a] Also at Yerevan State University, Yerevan, Armenia
[b] Also at TU Wien, Vienna, Austria
[c] Also at Ghent University, Ghent, Belgium
[d] Also at Universidade do Estado do Rio de Janeiro, Rio de Janeiro, Brazil
[e] Also at FACAMP — Faculdades de Campinas, Sao Paulo, Brazil
[f] Also at Universidade Estadual de Campinas, Campinas, Brazil
[g] Also at Federal University of Rio Grande do Sul, Porto Alegre, Brazil
[h] Also at University of Chinese Academy of Sciences, Beijing, China
[i] Also at China Center of Advanced Science and Technology, Beijing, China
[j] Also at University of Chinese Academy of Sciences, Beijing, China
[k] Also at China Spallation Neutron Source, Guangdong, China
[l] Now at Henan Normal University, Xinxiang, China
[m] Also at University of Shanghai for Science and Technology, Shanghai, China
[n] Now at The University of Iowa, Iowa City, Iowa, U.S.A.
[o] Also at Another institute formerly covered by a cooperation agreement with CERN
[p] Also at Zewail City of Science and Technology, Zewail, Egypt
[q] Also at British University in Egypt, Cairo, Egypt
[r] Now at Ain Shams University, Cairo, Egypt

JHEP04(2026)093

[s] Also at Purdue University, West Lafayette, Indiana, U.S.A.
[t] Also at Université de Haute Alsace, Mulhouse, France
[u] Also at Istinye University, Istanbul, Turkey
[v] Also at Another institute or international laboratory covered by a cooperation agreement with CERN
[w] Also at The University of the State of Amazonas, Manaus, Brazil
[x] Also at University of Hamburg, Hamburg, Germany
[y] Also at RWTH Aachen University, III. Physikalisches Institut A, Aachen, Germany
[z] Also at Bergische University Wuppertal (BUW), Wuppertal, Germany
[aa] Also at Brandenburg University of Technology, Cottbus, Germany
[ab] Also at Forschungszentrum Jülich, Juelich, Germany
[ac] Now at RWTH Aachen University, III. Physikalisches Institut A, Aachen, Germany
[ad] Also at CERN, European Organization for Nuclear Research, Geneva, Switzerland
[ae] Also at HUN-REN ATOMKI — Institute of Nuclear Research, Debrecen, Hungary
[af] Now at Universitatea Babes-Bolyai — Facultatea de Fizica, Cluj-Napoca, Romania
[ag] Also at MTA-ELTE Lendület CMS Particle and Nuclear Physics Group, Eötvös Loránd University, Budapest, Hungary
[ah] Also at HUN-REN Wigner Research Centre for Physics, Budapest, Hungary
[ai] Also at Physics Department, Faculty of Science, Assiut University, Assiut, Egypt
[aj] Also at Punjab Agricultural University, Ludhiana, India
[ak] Also at University of Visva-Bharati, Santiniketan, India
[al] Also at Indian Institute of Science (IISc), Bangalore, India
[am] Also at Amity University Uttar Pradesh, Noida, India
[an] Also at UPES — University of Petroleum and Energy Studies, Dehradun, India
[ao] Also at IIT Bhubaneswar, Bhubaneswar, India
[ap] Also at Institute of Physics, Bhubaneswar, India
[aq] Also at University of Hyderabad, Hyderabad, India
[ar] Also at Deutsches Elektronen-Synchrotron, Hamburg, Germany
[as] Also at Isfahan University of Technology, Isfahan, Iran
[at] Also at Sharif University of Technology, Tehran, Iran
[au] Also at Department of Physics, University of Science and Technology of Mazandaran, Behshahr, Iran
[av] Also at Department of Physics, Faculty of Science, Arak University, ARAK, Iran
[aw] Also at Helwan University, Cairo, Egypt
[ax] Also at Italian National Agency for New Technologies, Energy and Sustainable Economic Development, Bologna, Italy
[ay] Also at Centro Siciliano di Fisica Nucleare e di Struttura Della Materia, Catania, Italy
[az] Also at Università degli Studi Guglielmo Marconi, Roma, Italy
[ba] Also at Scuola Superiore Meridionale, Università di Napoli 'Federico II', Napoli, Italy
[bb] Also at Fermi National Accelerator Laboratory, Batavia, Illinois, U.S.A.
[bc] Also at Lulea University of Technology, Lulea, Sweden
[bd] Also at Consiglio Nazionale delle Ricerche — Istituto Officina dei Materiali, Perugia, Italy
[be] Also at Institut de Physique des 2 Infinis de Lyon (IP2I), Villeurbanne, France
[bf] Also at Department of Applied Physics, Faculty of Science and Technology, Universiti Kebangsaan Malaysia, Bangi, Malaysia
[bg] Also at Consejo Nacional de Ciencia y Tecnología, Mexico City, Mexico
[bh] Also at Trincomalee Campus, Eastern University, Sri Lanka, Nilaveli, Sri Lanka
[bi] Also at Saegis Campus, Nugegoda, Sri Lanka
[bj] Also at National and Kapodistrian University of Athens, Athens, Greece
[bk] Also at Ecole Polytechnique Fédérale Lausanne, Lausanne, Switzerland
[bl] Also at Universität Zürich, Zurich, Switzerland
[bm] Also at Stefan Meyer Institute for Subatomic Physics, Vienna, Austria
[bn] Also at Laboratoire d'Annecy-le-Vieux de Physique des Particules, IN2P3-CNRS, Annecy-le-Vieux, France
[bo] Also at Near East University, Research Center of Experimental Health Science, Mersin, Turkey
[bp] Also at Konya Technical University, Konya, Turkey

JHEP04(2026)093

[bq] Also at Izmir Bakircay University, Izmir, Turkey
[br] Also at Adiyaman University, Adiyaman, Turkey
[bs] Also at Bozok Universitetesi Rektörlügü, Yozgat, Turkey
[bt] Also at Marmara University, Istanbul, Turkey
[bu] Also at Milli Savunma University, Istanbul, Turkey
[bv] Also at Kafkas University, Kars, Turkey
[bw] Now at Istanbul Okan University, Istanbul, Turkey
[bx] Also at Hacettepe University, Ankara, Turkey
[by] Also at Erzincan Binali Yildirim University, Erzincan, Turkey
[bz] Also at Istanbul University — Cerrahpasa, Faculty of Engineering, Istanbul, Turkey
[ca] Also at Yildiz Technical University, Istanbul, Turkey
[cb] Also at School of Physics and Astronomy, University of Southampton, Southampton, U.K.
[cc] Also at IPPP Durham University, Durham, U.K.
[cd] Also at Monash University, Faculty of Science, Clayton, Australia
[ce] Also at Università di Torino, Torino, Italy
[cf] Also at Bethel University, St. Paul, Minnesota, U.S.A.
[cg] Also at Karamanoğlu Mehmetbey University, Karaman, Turkey
[ch] Also at California Institute of Technology, Pasadena, California, U.S.A.
[ci] Also at United States Naval Academy, Annapolis, Maryland, U.S.A.
[cj] Also at Ain Shams University, Cairo, Egypt
[ck] Also at Bingol University, Bingol, Turkey
[cl] Also at Georgian Technical University, Tbilisi, Georgia
[cm] Also at Sinop University, Sinop, Turkey
[cn] Also at Erciyes University, Kayseri, Turkey
[co] Also at Horia Hulubei National Institute of Physics and Nuclear Engineering (IFIN-HH), Bucharest, Romania
[cp] Now at Another institute formerly covered by a cooperation agreement with CERN
[cq] Also at Texas A&M University at Qatar, Doha, Qatar
[cr] Also at Kyungpook National University, Daegu, Korea
[cs] Also at Yerevan Physics Institute, Yerevan, Armenia
[ct] Also at Imperial College, London, U.K.
[cu] Now at Yerevan Physics Institute, Yerevan, Armenia
[cv] Also at Institute of Nuclear Physics of the Uzbekistan Academy of Sciences, Tashkent, Uzbekistan
[†] Deceased

JHEP04(2026)093